MONOLITHIC CATALYST BEDS FOR HYDRAZINE REACTORS

FINAL REPORT

November 12, 1969, through February 28, 1973

73-R-360
Contract NAS 7-755

Prepared by:
Rocket Research Corporation
Redmond, Washington 98052

For:
National Aeronautics and Space Administration
Ames Research Center, Moffett Field, California

and

Jet Propulsion Laboratory
Pasadena, California

May 2, 1973

TABLE OF CONTENTS

LIST OF FIGURES

LIST OF FIGURES (Concluded)

LIST OF TABLES

FOREWORD

This report summarizes results obtained under Contract NAS 7-755 during the period November 12, 1969, through February 28, 1973. The work was conducted for the Jet Propulsion Laboratory, Pasadena, with Theodore W. Price, Gregory J. Nunz, and Robert W. Riebling as JPL technical managers and with Frank E. Compitello and William Cohen as NASA program managers.

Rocket Research Corporation personnel contributing were Bruce W. Schmitz and Don L. Emmons as program managers, Dr. Eckart W. Schmidt as principal investigator, Tom A. Groudle and Bruce Walker as research engineers, and J. Warren Krug as research chemist. The tungsten foam material was made by Astro-Met Associates, Incorporated, of Cincinnati, Ohio, under the direction of John W. Graham, president.

SUMMARY

Rocket Research Corporation (RRC), under NASA Contract NAS 7-755, has evaluated a monolithic catalyst bed for monopropellant hydrazine decomposition. The program involved the evaluation of a new hydrazine catalyst concept wherein open-celled foamed materials are used as supports for the active catalysts. A high-surface-area material is deposited upon the open-celled foamed material and is then coated with an active metal to provide a spontaneous catalyst. Only a fraction of the amount of expensive active metal used in currently available catalysts is needed to promote monolithic catalyst.

Numerous parameters were evaluated during the program, and the importance of additional parameters became obvious only while the program was in progress. A demonstration firing at the end of the initial contract (using a 2.2-Newton (N) (0.5-lbf) reactor) successfully accumulated 7,700 seconds of firing time and 16 ambient temperature starts without degradation. Results obtained during the initial contract were reported in an interim report entitled *Monolithic Catalyst Beds for Hydrazine Reactors* 71-R-259, and submitted to NASA Ames Research Center for the Jet Propulsion Laboratory on May 1, 1971. A summary of results obtained during this initial contract is also included herein. The results were encouraging, and a second contract increment was funded and conducted between July 27, 1971, and February 28, 1973, to resolve remaining problem areas discovered during the initial contract and to improve durability of the monolithic catalyst.

The objective of the follow-on effort was to evaluate alternate substrate materials and nitridation resistant protective coatings, to develop methods of surface preparation prior to depositing a ceramic coating, and to improve adherence of the coating. It included a series of thruster firings to test the most promising concepts evolved from previous evaluation and to define parameters to be used in the parametric test matrix. The most successful catalyst configuration resulting from the parametric test matrix was then life tested to a JPL-specified duty cycle. Finally, monolithic foam samples were delivered to JPL for testing in a 0.44-N and a 44-N reactor. During this program, open-celled tungsten foam was found to be the optimum monolithic bed substrate material. Nitridation resistant protective coatings for other foam materials were considered and discarded. Surface preparation of the foam metal prior to applying ceramic was found to be a critical step in having the ceramic coating adhere properly to the foam surface. A foam surface roughening technique involving the dusting-on of tungsten powder was developed. The ligaments of the foam were coated with a high surface area alumina ceramic and iridium as active metal. The concentration of iridium in the active material (ceramic plus active metal) is the same as in the Shell 405 catalyst. For a given reactor volume, only a fraction of the expensive iridium present in a reactor filled with Shell 405 is used. Consequently, the overall reactivity is somewhat lower than that of Shell 405, but the catalyst has a long-life potential in that it is not susceptible to void formation and attrition commonly found in granular packed beds. Loading a piece of monolithic catalyst into a reactor involves less complexity so that uniformity in performance is more easily maintained between reactors.

In spite of the fact that the monolithic catalyst uses only about one-third the amount of the expensive active metal, iridium (compared to an equivalent volume of Shell 405 catalyst), it has many performance characteristics equivalent to Shell 405 catalyst. A comparison of steady-state performance data is given in Figure 1. As shown in this chart, C* and I_{sp} performance exceed that of Shell 405. The only disadvantage shown by the monolithic catalyst when compared to Shell 405 catalyst was the slower response times when firing pulse-mode duty cycles. The demonstrated life of the monolithic catalyst in the pulse-mode duty cycle included 2,460 seconds total on-time, 133 cold starts, and 5,132 pulses at a duty cycle of 0.1 second on/0.9 second off. This duty cycle and the duration of the life test had been prescribed by the Jet Propulsion Laboratory. Steady-state and pulse-mode performance at the end of this required life demonstration had not deteriorated significantly, and it would have been desirable to extend the life test to demonstrate margin and test the real life capability of monolithic catalysts for this specific duty cycle. Schedule and budget limitations prevented extending the life test firings of the monolithic bed to the point of substantial degradation.

Based on the excellent results obtained throughout the program and the demonstrated life capability of the monolithic foam, it is recommended that additional studies be conducted to further exploit the advantages of this concept.

11062-72A

iii

COMPARISON OF SHELL 405 CATALYST (TEST FIRING #154) TO #1 RATED MONOLITHIC CATALYST (TEST FIRING #149)

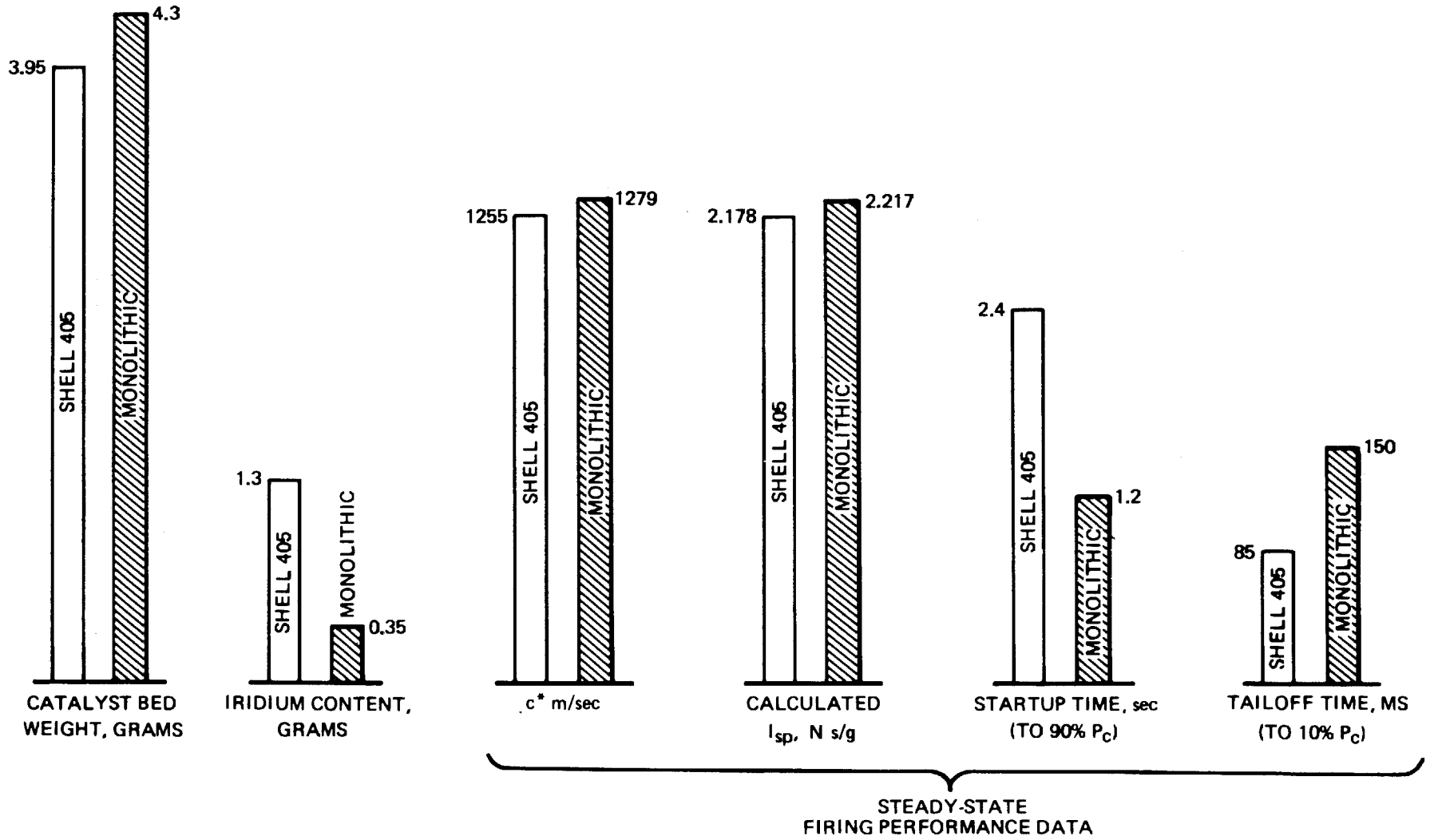

Figure 1

1.0 INTRODUCTION

1.1 GENERAL

Rocket Research Corporation, under NASA Contract NAS 7-755, has evaluated and continued development of a monolithic catalyst for monopropellant hydrazine decomposition. The monolithic catalyst offers a single-piece catalyst bed as opposed to current catalysts which are packed into the reactor in granular form. It is postulated that the monolithic nature of the catalyst will result in reduced catalyst attrition as compared to present granular catalyst beds. Additionally, the monolithic catalyst offers the potential of increased bed thermal conductivity, lower bed pressure drop, and simplified reactor assembly procedures. The overall program involved the evaluation of a new hydrazine catalyst concept wherein open-celled foamed materials are used as supports for the active catalysts. A high-surface-area material is deposited upon the open-celled material and is then coated with an active metal to provide a spontaneous catalyst.

This final technical report covers work performed during the period from July 27, 1971, to February 28, 1973. Also included is a summary of work performed during the previous contract conducted during the period from November 12, 1969, to April 12, 1971. A detailed report covering the results of the initial program was issued as interim report 71-R-259.

1.2 SCOPE OF THE PROGRAM

The overall program was divided into six major phases of effort with the first three phases conducted during the initial contract (see Figure 1-1). Phase I – laboratory evaluation – was a screening of the various foam materials, ceramic coatings, and techniques of active metal deposition. Based on the results of these studies, catalyst samples found to exhibit sufficient activity and promising life characteristics were subjected to test firings in a 2.2-N (0.5 lbf) rocket engine (Phase II – reactor test firings). Phase III – catalyst delivery – was originally planned to include the delivery of catalyst to NASA-JPL at the conclusion of the program. As the result of the program extension, this task was not completed during the initial contract but was completed during Phase VI at the end of the follow-on program.

Based on encouraging results obtained during the initial contract, the program was extended to further optimize the catalyst processing techniques and to improve durability of the monolithic catalyst. The objectives of the follow-on program were as follows:

a. Obtain a metal foam substrate resistant to attack from hydrazine decomposition gases.

b. Develop suitable substrate surface preparation techniques to ensure adhesion of the aluminum oxide on the metal foam substrate.

c. Select an optimum catalyst formulation and select a suitable geometry.

d. Evaluate life of the finally developed catalyst for the selected geometry.

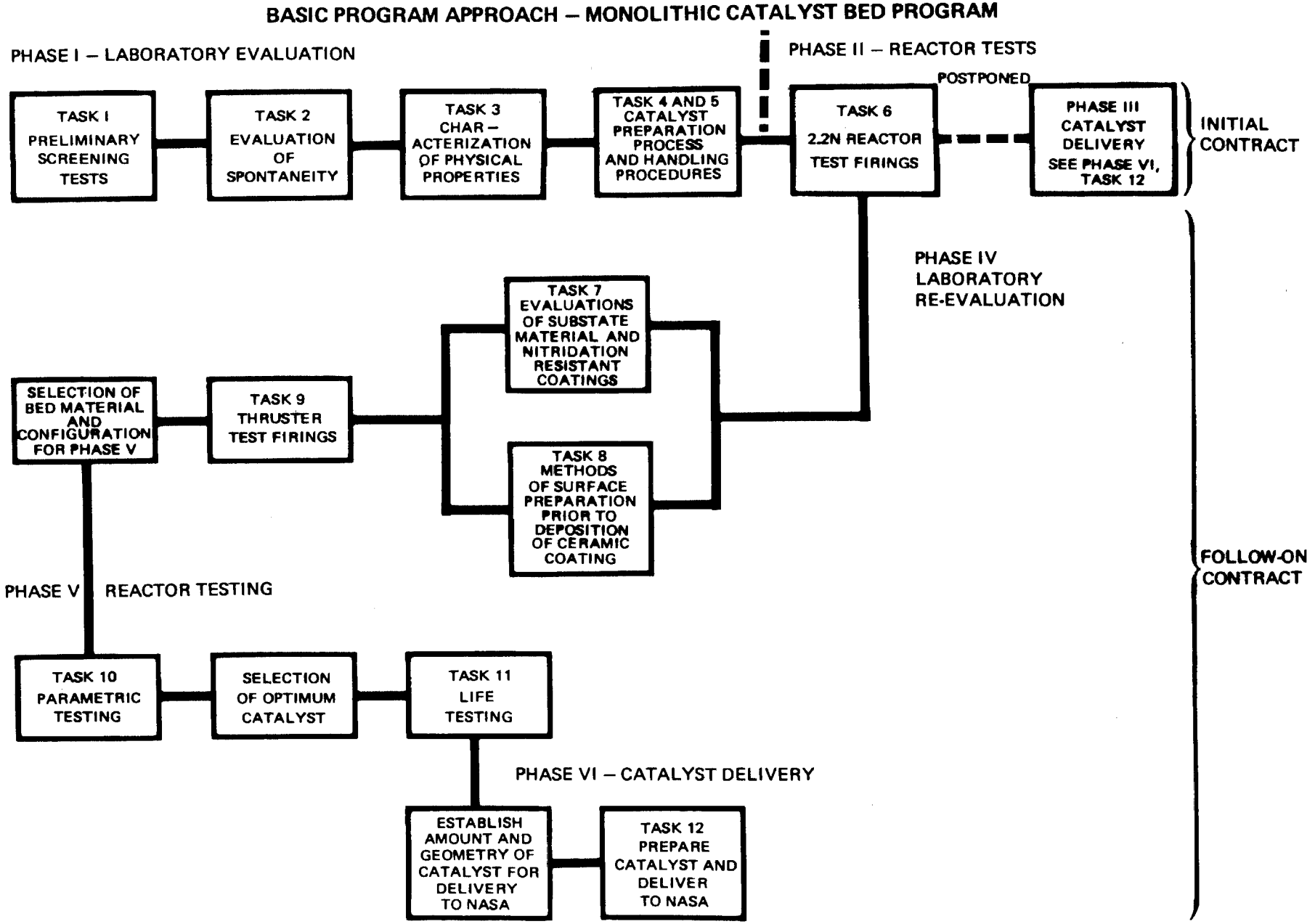

11064-75A

Figure 1-1

The follow-on program consisted of Phases IV, V, and VI. The basic approach to the follow-on portion of the program is included in Figure 1-1.

During Phase IV – laboratory evaluation – parallel laboratory studies were conducted to 1) prepare the foam surface before applying the activated alumina coating to the substrate metal and 2) establish a technique for achieving a foam metal substrate resistant to nitriding and hydrogen embrittlement. After selecting a foam metal and coating technique from these parallel studies (Tasks 7 and 8) several bed configurations were prepared and test fired at the 2.2-N (0.5-lbf) thrust level during Task 9.

Upon completion of Tasks 7 through 9, an abbreviated parametric test series (Task 10) was conducted during Phase V to determine the optimum pore size, bed length, and bed loading for optimum performance of the 2.2-N reactor. The optimum foam and operating conditions were then selected for the Task 11 life demonstration tests. The goal of the life tests was to 1) demonstrate pulsing and steady-state performance capability and 2) demonstrate cold-start capability.

Phase VI – catalyst delivery – was completed in accordance with requirements received from NASA-JPL. A total of nine foam catalyst samples was delivered for test evaluation at JPL.

Presented in the following sections is a detailed discussion of the various tasks conducted during the program.

2.0 MONOLITHIC CATALYST PROPERTIES CONSIDERATIONS

The monolithic catalyst bed concept involves a large number of variables which had to be explored to obtain a satisfactory catalyst. The major mechanical and chemical characteristics that influence the overall performance of such catalysts include:

a. Foam void volume including pore size, pore size distribution, foam ligament thickness, ligament surface area, and ligament porosity

b. Foam material properties including thermal conductivity, heat capacity, melting point, coefficient of thermal expansion, chemical inertness, and crush strength

c. Surface coating characteristics including surface area, adherence to metal matrix, and surface area degradation at high temperatures

d. Active metal coating including the chemical nature of the active metal, quantity of active metal deposited, method of active metal deposition, and hydrogen chemisorption value of the final catalyst.

The various foam bed properties have already been discussed in detail in the interim report. A summary of the more important properties which were used in selecting the ultimate foam configuration follows.

2.1 FOAM MATERIALS

2.1.1 Structure of the Foam Matrix

The substratum for deposition of an active surface area coating and active metal is an open-celled, hollow ligament, metal foam. A photomicrograph of typical foam structures with two different pore sizes prior to application of any coating is shown in Figure 2-1. The repeating unit in this structure, the cell unit, is that of a dodecahedron with pentagonal windows and is shown as an insert in Figure 2-1. The strands, or ligaments, connecting the nodes typically have a triangular cross section and are hollow.

The foam structure is generally described by two numbers: the average pore diameter and the percent void contained in a unit volume. More frequently, the percent density is used which is equal to 100% minus percent void volume. Typical pore diameters used in the monolithic catalyst program were 500 μm (0.020 inch) to 250 μm (0.010 inch). Densities ranged from 3 to 10%. Metal foams are also frequently characterized by giving the number of geometrical pores per inch instead of the pore diameter. It is important to emphasize that the macroporosity of the foam must not be confused with the micropores in the high surface area ceramic coating (alumina).

An important requirement for monolithic catalysts is the uniformity of the foam structure. Closed pores or variations in density or pore size can cause the flow to channel along the path of lower resistance. Uniformity of foam samples was inspected by two methods, including 1) sectioning

COMPARISON OF 10 MIL (LEFT)
AND 20 MIL (RIGHT) PORE SIZE TUNGSTEN FOAM

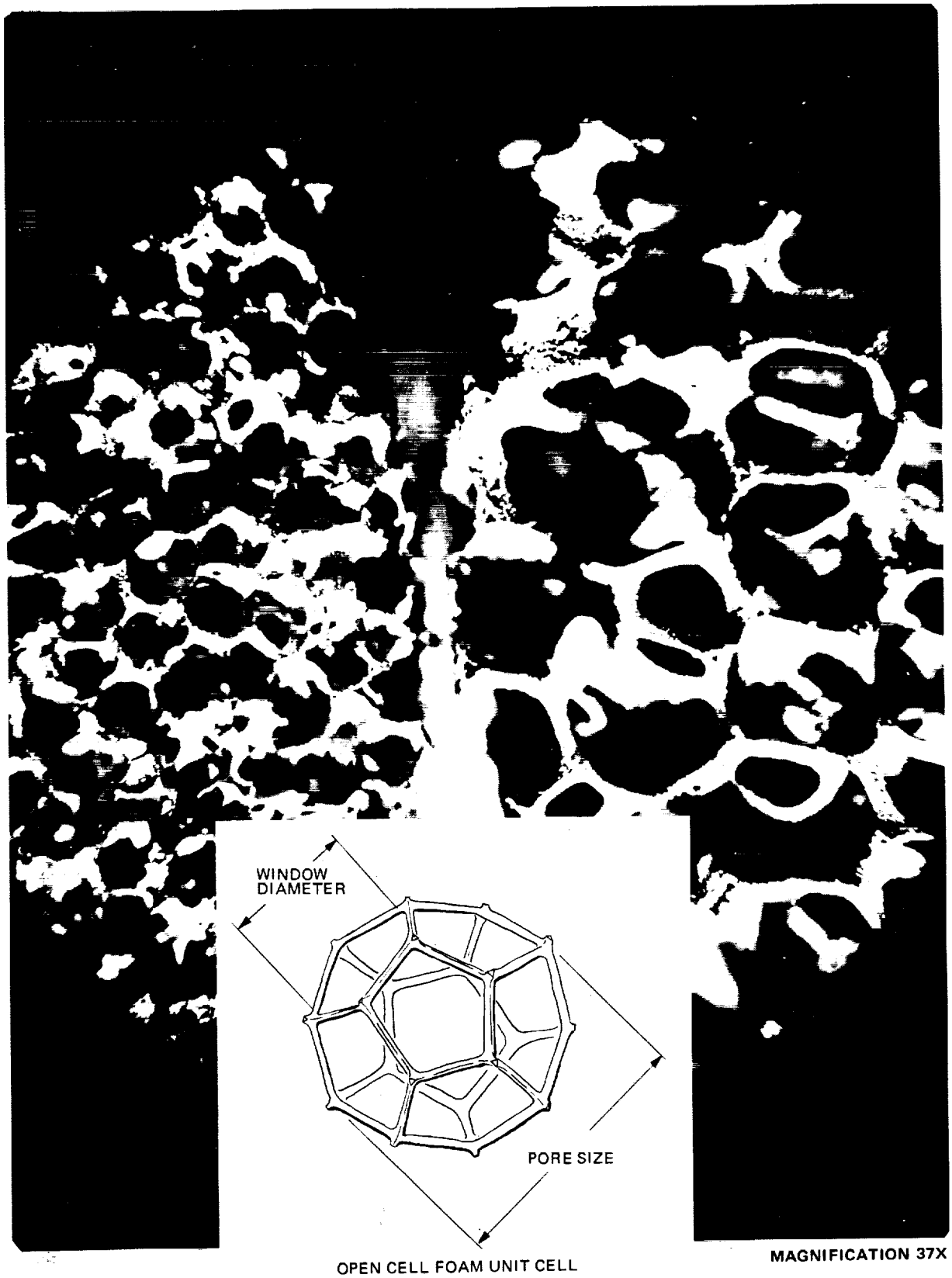

OPEN CELL FOAM UNIT CELL

MAGNIFICATION 37X

followed by visual examination or weighing and 2) taking X-ray photographs. In a few instances irregularities of the foam structure, such as closed pores, were noted when block specimens were machined to size. These solid metal nodules were also clearly visible when X-ray shadowgraphs were taken. However, it is more difficult to obtain X-ray penetration through tungsten than through nickel-base alloys. The sectioning and visual examination technique was mostly applied to post-firing samples. Whereas previously the samples were cut dry, it is now preferred to fill them with a white contrast material (e.g. Ti 0_2 in epoxy) and cure the polymer prior to sectioning, polishing, and microscopic examination.

2.1.2 Scanning Electron Microscope Investigation of Foam Structure

The scanning electron microscope (SEM) proved to be a very useful tool to study the structure and ligament surface characteristics of bare metal foam as well as finished catalysts. The prime objective of the SEM study was to find a method of surface preparation which would lead to improved ceramic coating adherence (discussed in paragraph 3.3). Another discovery was the presence of a "mud cracking" pattern on finished catalysts which was later traced to local overdeposition of active metal (see paragraph 3.5).

Throughout the initial series where Hastelloy-X foam was being used, satisfactory adherence of the promoted ceramic coating had been achieved. Only after Hastelloy-X foams had been abandoned because of nitridation damage and tungsten foam was used instead, flaking and excessive loss of active material (ceramic plus iridium, as opposed to inactive material = tungsten foam) was noted.

The visual appearance of the first batch of tungsten foam received (lot number 32-144), namely its shiny appearance, suggested that the surface of the ligaments was very smooth as opposed to Hastelloy-X with a grey dull appearance. This was then confirmed by taking a series of SEM photomicrographs of the two materials at different magnifications (see Figures 2-2 through 2-5). The Hastelloy-X foam (Figure 2-2) has a very porous structure, whereas the ligaments of tungsten (Figure 2-3) have a very smooth surface. This is more clearly illustrated by the photomicrographs taken at increased magnification (Figures 2-4 and 2-5). In order to aid in locating the features shown at increased magnification, the area covered by those later photomicrographs is marked by a little rectangle on Figures 2-2 and 2-3.

It is quite obvious that the porosity seen in the Hastelloy-X foam is very desirable in that it allows the ceramic to penetrate and anchor itself into the ligaments. Very poor adherence must be expected when a material is used with as smooth a surface as shown in Figure 2-5. The smooth surface is the result of higher sintering temperatures required for making the higher melting tungsten foam.

At RRC's specific request the manufacturer of tungsten foam* has prepared foam samples at lower sintering temperatures in order to maintain some surface roughness. However, foams produced at

*Astro-Met Associates, Cincinnati, Ohio

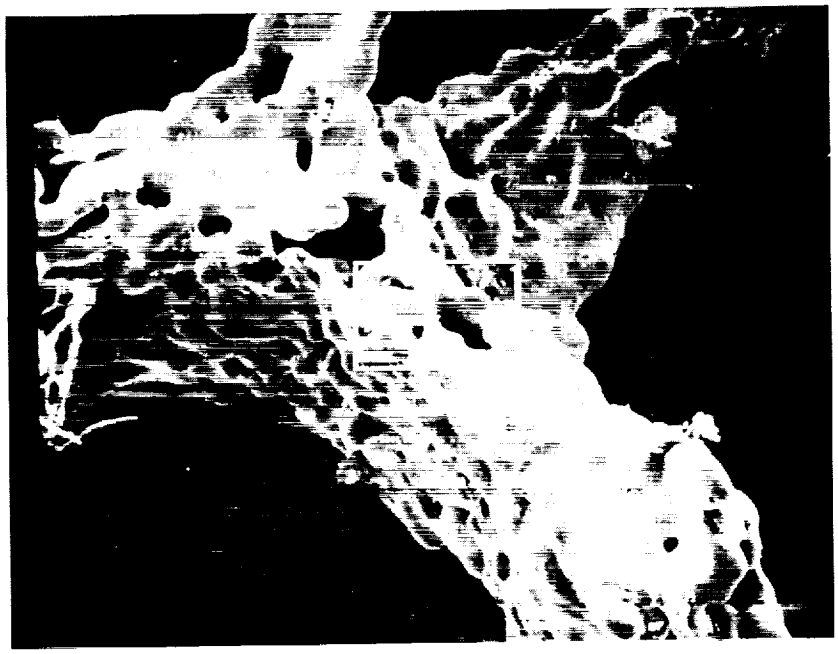

Figure 2-2 SEM PHOTOMICROGRAPH OF HASTELLOY X FOAM, 300X

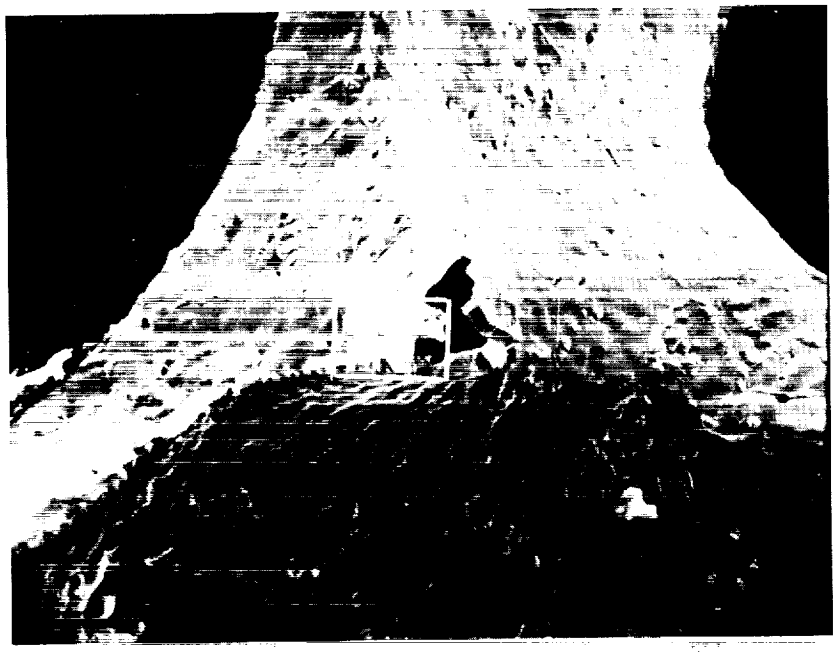

Figure 2-3 SEM PHOTOMICROGRAPH OF TUNGSTEN FOAM, 300X

Figure 2-4 SEM PHOTOMICROGRAPH OF HASTELLOY-X FOAM, 1500X

Figure 2-5 SEM PHOTOMICROGRAPH OF TUNGSTEN FOAM, 3000X

the lower sintering temperature (lot numbers 32-244 and 32-254) had insufficient crush strength (see paragraph 2.1.3.1) and collapsed during reactor testing. The compromise between desired surface roughness and sufficient mechanical strength was therefore not achieved. For this reason methods of surface modification have been studied and are described in paragraph 3.3.

2.1.3 Foam Metal Properties

The usefulness of foam metals for monolithic catalyst preparation is determined by their mechanical, thermal, and chemical properties. Candidate metals were surveyed for their applicability to hydrazine catalysts during the initial contract, and applicable data were summarized in the interim report. Under Task 7 of Phase IV of the follow-on contract, alternate nitridation resistant substrates were sought. The main candidate as an alternate for tungsten was rhenium, and results of a literature study on rhenium and rhenium alloys are included in this report.

2.1.3.1 Mechanical Properties

Mechanical properties of importance for monolithic catalyst beds are crushing strength and pressure drop.

Crushing strength had previously been determined in a hydraulic press under static conditions with the load being increased in increments. During the second phase of the contract, a more sophisticated instrument, an INSTRON tester was used which also gave deflection versus load curves under dynamic conditions. The cylindrical samples used in the INSTRON tester were identical to half-length foam samples used in composite bed tests (12.7-millimeter diameter by 10-millimeter length). The crushing load was applied in the axial direction. The samples were very carefully EDM machined to ensure that the ends of the cylinders were flat and parallel. Nevertheless, graphite hemispheres were used with one of the later test series to eliminate effects of misalignment of the end surfaces.

The crushing behavior of monolithic samples is different from granular materials. The initial deformation at low loads is caused mainly by breakage of single ligaments protruding from each end of the sample. This end effect is more pronounced with large cell size foam where only few ligaments per unit area exist. Tungsten foam is very brittle and yields abruptly once a certain crushing load is exceeded. A typical series of curves obtained on an INSTRON tester is shown in Figure 2-6. The range of the load cell had to be increased three times before the sample crushed. The sample behaved elastically in the lower load ranges, and the deflection (strain) returned to the starting line when the load was taken off the sample to change the setting on the load cell. The sample crushed at 0.33 kN, which is equivalent to a load at failure of 2,632 kN/m^2.*

*An error was discovered in the crush strength data reported in the interim report. The load scales in Figures 2-8 and 2-9 of the interim report and all data reported there in kN/m^2 should be multiplied by 100 to obtain the correct values.

LOAD/DEFLECTION CURVE OF 500μm PORE SIZE TUNGSTEN FOAM SAMPLE

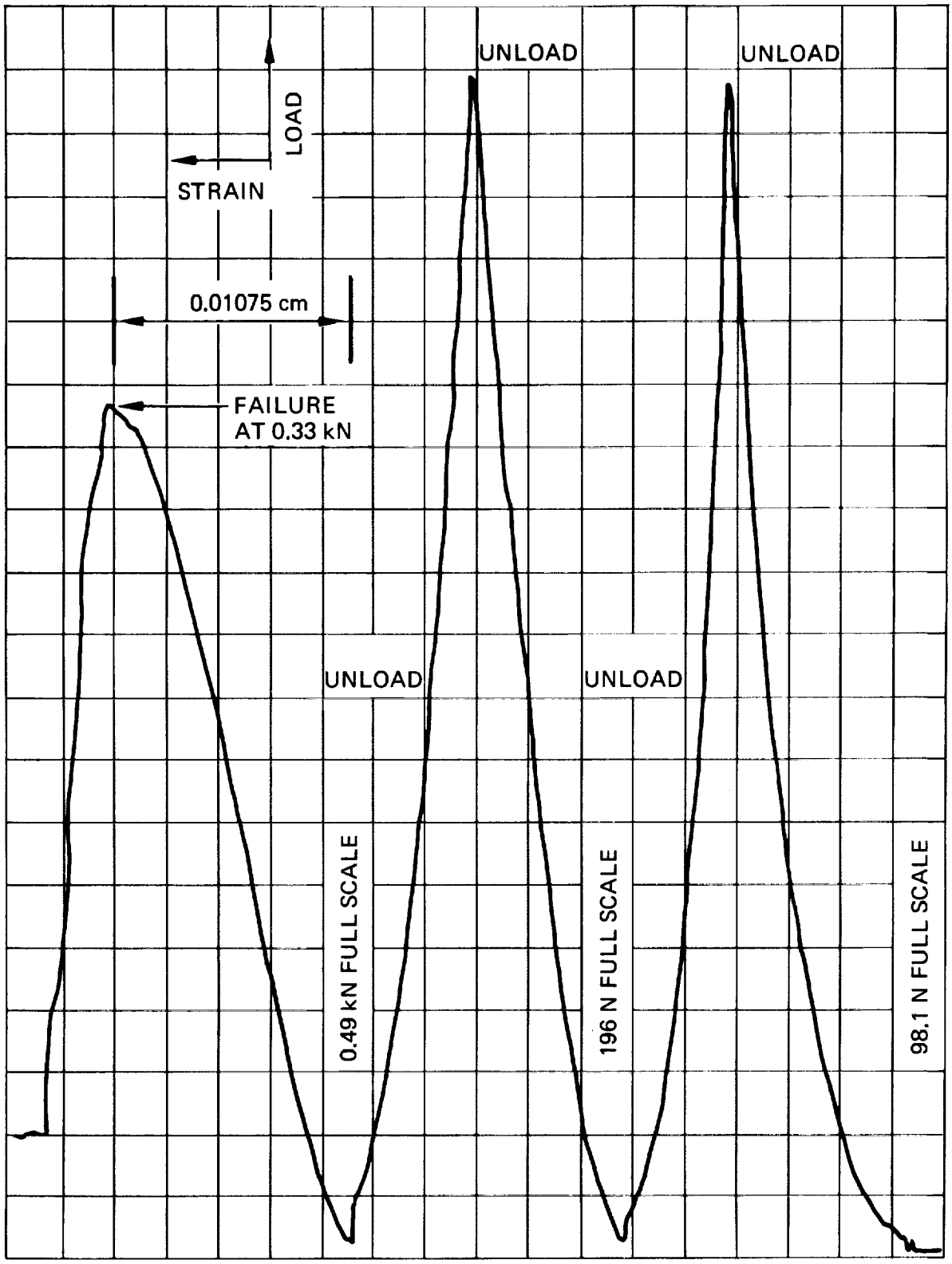

Figure 2-6

Crush strength depends on the density of the material and the quality of particle-to-particle bonding achieved in the powder metallurgical sintering process. Crush strength was used mainly as an acceptance criterion for tungsten foam after some samples had failed in the reactor during test firing. A summary of crush strength data is given in Table 2-1. The minimum crush strength requirements are probably different for the two different pore sizes. The small pore size foam typically has a higher pressure drop and requires a higher crush strength. Samples which were machined from the same block and which collapsed in the reactor are marked with an asterisk in Table 2-1. It appears that approximately 800 kN/m^2 is a minimum crush strength required for monolithic catalysts. Properly sintered foam samples with nominal 7% density had crush strengths up to 2,700 kN/m^2.

Crush strength data were provided to the foam manufacturer to help select a furnace temperature cycle which would give sufficient crush strength while simultaneously retaining some desirable surface roughness.

Crush tests were also conducted to determine a possible adverse effect of surface roughening by oxidation/reduction on mechanical integrity. However, samples superficially oxidized under carefully controlled conditions had a crush strength identical to that of untreated samples.

All crushing tests were conducted with bare metal foams only. It is not expected that the ceramic and the active metal will contribute significantly to the crush strength of a finished sample.

Besides high crush strength, another desirable foam metal property is ductility. Tungsten is very brittle and tungsten foam samples have to be handled with care to avoid breaking the protruding ligaments. An alternate material evaluation was therefore conducted under Task 7. Several approaches were considered: a protective coating for Hastelloy-X and foams made from metals other than tungsten or molybdenum. The compatibility aspects of this metal selection study are discussed in paragraph 2.1.3.3. As far as ductility is concerned, a rhenium or a rhenium/tungsten alloy foam would most likely exhibit good ductility and improved handling characteristics. However, rhenium foam has never been made before and the metal is 400 times more expensive than tungsten ($3,300/kg rhenium).

Pressure drop is important for the overall system and reactor operating conditions. If the reactor had too high a pressure drop, a more bulky propellant feed system and higher feed pressure would be required. One of the advantages of monolithic catalyst is its low pressure drop when compared to 25- to 30-mesh Shell 405 commonly used in the same size 2.2-N thruster.

Throughout the multistep preparation of monolithic catalyst beds, the pressure drop was monitored to ensure that none of the samples was inadvertently plugged. A typical pressure drop history of a sample as it underwent the various steps of ceramic coating, and active metal deposition, is illustrated in Figure 2-7. The pressure drop as defined in Figure 2-7 is expressed in dimensionless units as pressure drop modulus and plotted versus the dimensionless effective Reynolds number. This makes comparison easier.

Table 2-1

CRUSH STRENGTH OF TUNGSTEN FOAMS

Lot No.	Sample No.	Pore Size (μm)	Density (%)	Stress at Failure		Foam of Same Lot Used in Test Firing Nr.	Remarks
				Reading	Average		
				kN/m2	kN/m2		
32-196	11	250	7.0	1,270		078–080, 111–113, 114–124, 129–130	Different furnace cycle than lot 32-197A
32-254	AE4		6.0	310	284	081–083*	Lower sintering temperature, lower density
32-254	AE5		6.4	271			
32-254	AE6		5.7	271			
32-254	AE3		6.3	341			Surface modified by oxidation and reduction
39-11	AB8		5.3	627	459		Supposed to be identical with 32-196
39-11	AB9		5.5	464			Lower density sample (leftover)
39-11	AB10		4.3	286			
32-144	9a	500	5.0	519		038–040, 059, 060	Shiny surface; adherence problem
32-197A	6a		7.3	2,632		061–077, 084–099, 100–110, 131–137	Powder dusted, additional furnace cycle
39-11C	9		7.3	2,632	1,983		Second shipment similar to 32-197A
39-11C	10		5.9	1,335			
32-244	BE2		5.2	348	699	139–142*	Too low density sample
32-244	BE5		6.4	913			Lower sintering temperature to increase surface roughness
32-244	BE6		5.7	836			
32-244	BE1		5.2	371			Surface modified by oxidation and reduction
35-16A	37		6.7	2,740			Oxidation roughened only
35-16A	38		6.0	1,842			Oxidation roughened only
35-16A	39		5.9	2,438		163–169	Control
35-16A	40		5.6	2,129		156–163	Control
35-16A	41		6.7	1,796			Oxidation roughened and W-dusted
35-16A	42		6.6	1,627			Oxidation roughened and W-dusted

*Collapsed in reactor

PRESSURE DROP OF MONOLITHIC CATALYST AT VARIOUS STAGES OF TESTING

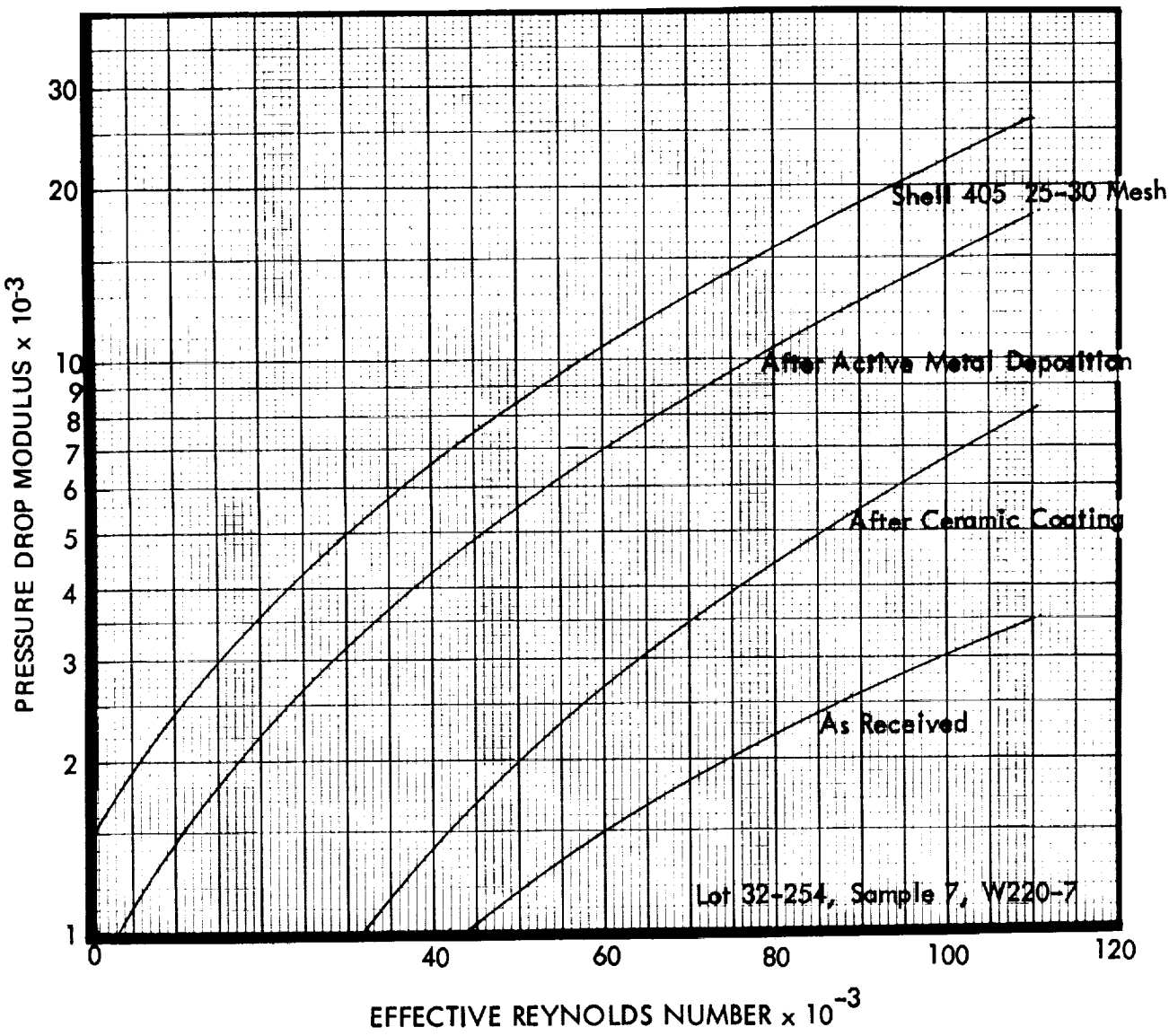

$$N_{PD} = \frac{g_c \rho\, d^3\, \Delta P}{\mu^2\, L_B} \qquad N_{Re} = \frac{4\,\dot{w}}{\pi\, d \mu}$$

NOMENCLATURE – SEE APPENDIX C

Pressure drop is measured across the sample with a U-tube filled with water or mercury and nitrogen gas exhausting at ambient pressure. The undesirable increase in pressure drop limits the amount of ceramic which can be deposited on the foam. The steep increase of pressure drop beyond a ceramic loading of 0.4 g/cm^3 as shown in Figure 2-8 is an indication of incipient plugging of macropores. For this and other reasons a ceramic loading of nominal 0.3 g/cm^3 has been chosen as optimum. The small pore size foam is more sensitive to this threshold than the larger pore size 500μm foam.

2.1.3.2 Thermal Properties

Thermal properties include melting point, coefficient of thermal expansion, heat capacity, and thermal conductivity. Melting point and coefficient of thermal expansion considerations were already discussed in the interim report and no new aspects were discovered. Only few metals have a high enough melting point and maintain sufficient strength at reactor operating temperatures to become eligible for monolithic catalyst application. Because of its melting point and also because of its low thermal expansion, which closely matches that of aluminum oxide, tungsten is a preferred material.

Another evaluation criterion is thermal conductivity. Thermal conductivity is generally considered to be of importance for both catalytic and thermal bed applications. In contrast to conventional catalyst beds where particles are in only loose contact with each other, the foam provides an unbroken thermal path between the hot decomposition zone and the injector area, where heat is needed for fast vaporization of injected liquid propellant. Thermal conductivities of a number of candidate materials are listed in Table 2-2 in the order of decreasing conductivity. Next to copper, which cannot be used because of its low melting point, tungsten is the preferred material with respect to high thermal conductivity.

Another thermal property which may be of particular importance for monolithic beds is the volume specific heat capacity. If foams of equal percent density are compared on this basis, the number shows the amount of heat lost to heat the foam structure of a given unit volume. Tungsten compares favorably on this scale as well as on the thermal diffusivity scale shown in the last column of Table 2-2. Materials with high diffusivity are more efficient in conducting heat from one place to another during transient heatup conditions such as those occurring during pulse-mode operation.

2.1.3.3 Compatibility

Early in the program a change had to be made from previously used Haynes-25 and Hastelloy-X foam materials to a nitridation resistant metal. Hastelloy-X foams were found to be badly nitrided and became brittle after 3,000 seconds of firing time. Even though reactor bodies and bed plates can be made from Haynes-25 or Hastelloy-X without significant nitridation damage, the thin ligaments of foam are more susceptible to nitridation damage, in particular because attack occurs from both sides of the porous hollow ligaments (see Figure 2-2).

Under Task 7 of the follow-on contract, alternate foam metals and methods to deposit a protective nitrogen-impermeable coating on Hastelloy-X have been evaluated. Of all alternate metals considered, tungsten is one which combines compatibility with a number of other desirable

PRESSURE DROP AS FUNCTION OF CERAMIC LOADING

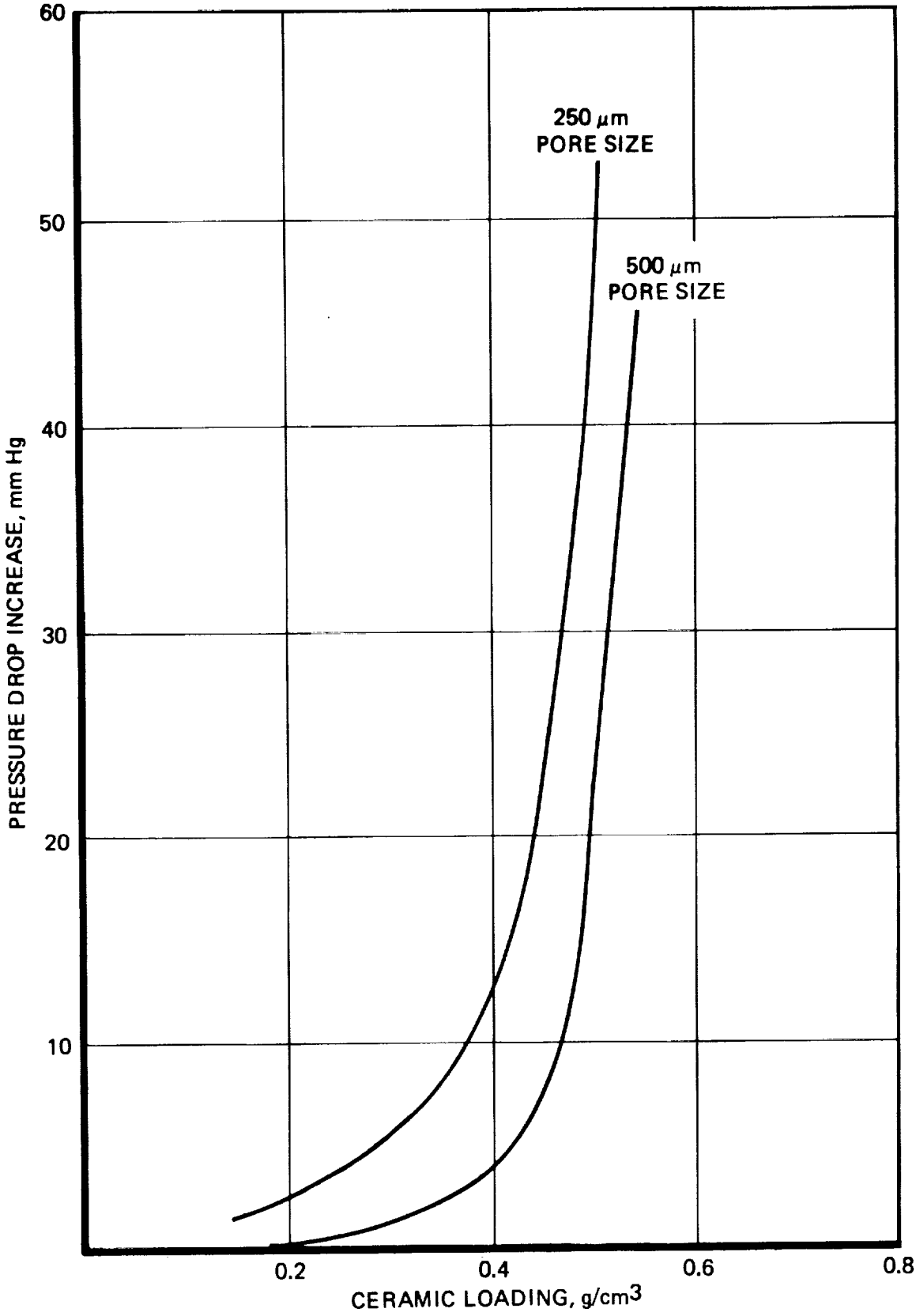

Table 2-2

THERMAL PROPERTIES OF CANDIDATE FOAM MATERIALS

	Thermal Conductivity		Heat Capacity at 294°K	Volume-Specific Heat Capacity	Thermal Diffusivity
	*cal/cm sec °K	at °K	cal/g °K	cal/cm^3 °K	cm^2/sec °K
Copper	0.93	293	0.092	0.819	1.129
Tungsten	0.40	373	0.034	0.656	0.606
Molybdenum	0.35	373	0.065	0.663	0.528
Rhodium	0.21	373	0.058	0.722	0.292
Platinum	0.17	373	0.032	0.686	0.247
Cobalt	0.15	293	0.091	0.810	0.186
Nickel	0.15	293	0.109	0.965	0.154
Iridium	0.14	373	0.032	0.717	0.194
Niobium (columbium)	0.13	373	0.064	0.691	0.188
Rhenium	0.087	473	0.032	0.673	0.129
Haynes-25	0.05	973	0.09	0.823	0.061
Hastelloy-X	0.05	863	0.10	0.823	0.061
Titanium	0.04	298	0.124	0.558	0.068
Zirconium	0.04	373	0.067	0.431	0.090
Aluminum oxide	0.01	1,173	0.19	0.731	0.014
Zirconium oxide	0.002	293	0.13	0.507	0.004
Beryllium oxide	0.57	298	0.240	1.624	0.833

*Cal = calorie = 4.1868 Joule

properties. Rhenium and tungsten/rhenium alloys would also be compatible with the hydrazine decomposition products environment. However, rhenium and tungsten/rhenium alloy foams are not available and the cost of rhenium metal is prohibitive. An additional benefit which might be derived from the presence of rhenium in the reactor is the fact that rhenium catalyzes the hydrazine decomposition reaction in a manner similar to noble metals.

Noble metals were considered as protective coatings for Hastelloy-X and similar otherwise nitridation susceptible foam materials. However, it was concluded that it would be extremely difficult to achieve uniform penetration into the porous foam structure by conventional plating methods. The hollow ligaments would have to be plated not only from the outside, but also from the inside to achieve the desired protective effect.

Furthermore, the noble metal would have to be plated to a substantial thickness to prevent diffusion of nitrogen through the film. In the course of high-temperature operation, the film would also alloy with the base metal and diffuse. Some protection of fine-mesh screens in hydrazine reactors has been achieved by rhodium plating. However, these screens do not have to bear a load like the monolithic catalyst structure would. It was concluded that a protective coating is not feasible at the present time and foams must be fabricated from a metal which is resistant to nitridation.

2.1.4 Optimum Foam Metal Selection

In the preceding paragraphs and in corresponding paragraphs of the interim report, the various considerations leading to an optimum foam substrate have been discussed in detail. The properties to be considered are summarized in the evaluation matrix of Table 2-3, which shows tungsten to be a prime choice, with rhenium alloys a second-choice alternate.

Table 2-3
SUBSTRATE EVALUATION MATRIX

Property	Maximum Points	Tungsten	Molybdenum	Rhenium	Tungsten–25% Rhenium
High temperature strength	10	10	8	10	10
Ductility	6	0	0	6	5
Density	6	4	6	2	3
Nitridation resistance	4	4	3	4	4
Cost	10	10	10	0	7
Thermal conductivity	6	6	4	1	3
Thermal expansion (match with Al_2O_3)	4	4	2	3	1
Heat capacity	4	4	2	4	3
	50	42	35	30	36
Rating		1	3	4	2

2.2 CERAMIC COATINGS

Prior to contract award, initial tests of the monolithic catalyst approach were conducted with the active metal deposited directly on the foam substratum. When these tests showed low catalyst activity, further tests were performed with a high active surface area material deposited. The prime candidate for this ceramic coating was aluminum oxide, because it maintains high surface area up to very high temperatures.

Sufficient experience with aluminum oxide as a catalyst carrier was available to extrapolate to its use in monolithic catalysts. As with granular and pelletized catalyst, undesirable shrinkage and subsequent flaking of ceramic coating due to phase changes have to be considered.

2.2.1 Ceramic Composition

Throughout the program the composition of the ceramic coating slip had to be changed twice because the manufacture of key ingredients had been discontinued, and Baymal(R), an aluminum oxide sol and Ludox(R) SM-15 were no longer available on the market. The ceramic coating is now made by use of Ludox SM-30 which is a more concentrated modification of Ludox SM-15.

The following parameters are of importance in evaluating ceramic coatings:

a. Adherence
b. Active surface area
c. Sintering characteristics
d. Chemical composition

Adherence was evaluated in one test by vibrating ceramic-coated foam samples before and after subjecting them to 10 thermal shock cycles. While this test is no substitute for adherence testing under reactor conditions, it gave preliminary indication of the adherence which can be achieved with and without surface preparation.

The adherence of the ceramic coating can be improved by an increase of the sintering temperature. However, a compromise has to be made between increased sintering temperature and loss of active surface area. A considerable portion of the ceramic active surface area is lost while it is being baked in place. The active surface area is a prerequisite for an active catalyst and must be carefully monitored if the sintering temperature is increased. In the course of the program, the sintering temperature was actually increased from 873 to 973°K with only moderate loss in active surface area (204 m^2/g down to 173 m^2/g).

Another method to evaluate ceramic coatings was to cast 1/8- by 1/8-inch cylindrical pellets and subject them to the same calcining conditions as those to which ceramic coating would be subjected. Pellets were then tested in a Stokes hardness tester for crushing strength and compared to commercially available pellets such as Harshaw Al 1404. The crushing strength of pellets made from RRC ceramic coating slip, but sintered at 1,253°K for 1 hour, was in some instances superior to that of Al 1404 used for AAT-type Shell 405 catalyst. Even after changing from Ludox SM-15 to Ludox SM-30, the chemical composition of the calcined ceramic coating remained the same (94.5% Al_2O_3, 5.5% SiO_2).

2.2.2 Optimization of Ceramic Loading

The BET* total surface area available in a monolithic reactor is only a fraction of that available with granular Shell 405 and may explain differences in activity which will be discussed in more detail in the section on hydrogen chemisorption. It is desirable to include as much ceramic material as possible in a monolithic reactor to provide sufficient active surface area onto which the active metal will be deposited. The amount of ceramic is limited by the thickness to which the ceramic coating can be deposited without cracking upon sintering. Furthermore it is limited by the increase in pressure drop already discussed in paragraph 2.1.3.1. The ceramic loading in a catalytic reactor should also be such that a maximum geometrical, macrophysical surface area is exposed to the incoming reactants. It is for this reason that 25- to 30-mesh granular Shell 405, for instance, is preferred in the upstream portion of reactors, even though on a weight basis 14- to 18-mesh granules would have the same BET surface area. However, this area is hidden inside the granules and not as readily accessible except by slow diffusion processes. In order to optimize the ceramic loading, an analytical study was conducted; and formulas were derived by which the exposed macroscopic surface area on the triangular ligaments could be calculated as a function of foam pore size, foam density, ceramic specific weight, and ceramic loading expressed in g/cm^3.

The optimization assumed a foam model comprising a dodecahedron with pentagonal windows and triangular ligament cross section. The geometrical surface area of these ligaments increases as more and more ceramic is deposited, until further growth is restricted by neighboring ligaments growing in the opposite direction. Obviously, if the entire dodecahedron was filled with ceramic, the geometrical surface area would be zero. A number of simplifying assumptions had to be made in the analysis, and the model could be refined and computerized if need be. The preliminary optimization for a 7% density foam showed that an optimum ceramic loading is at 0.22 g/cm^3 and that it is independent of foam pore size. The distribution about the maximum at 0.22 g/cm^3 is very flat and deviations of ± 0.1 g/cm^3 can be tolerated and result in only 7% loss of optimum surface area. The selected optimum ceramic loading of 0.3 g/cm^3 is thus well within the range confirmed by the analytical model.

2.3 ACTIVE METAL PROPERTIES

The most promising active metal for monolithic catalysts continues to be iridium. Ruthenium had undergone limited testing in the first phase of the program; but on the basis of other efforts to find a substitute for Shell 405, it is concluded that ruthenium-promoted monolithic catalysts will not have the same life potential as iridium catalysts.

2.4 EVALUATION OF CATALYST SAMPLES

During the development phase when various catalyst supports and methods of promoting the catalysts were screened, spot plate activity and ignition delay tests and hydrogen chemisorption were used to evaluate finished catalysts before more costly reactor firings were made.

*Brunauer, Emmett, and Teller, J. Am. Chem. Soc. 60, 309-19 (1938)

The spontaneity of catalyst samples was tested with a versatile laboratory tool, the RRC ignition delay tester. With this instrument, the delay between the contact of propellant with the catalyst and the first release of heat (exotherm) can be measured.

2.4.1 Ignition Delay Tester

The ignition delay of monopropellant reactors is a very important evaluation criterion where short response times are required (attitude control, trajectory correction, orbit insertion). For the data compared herein, ignition delay is defined as time lapse between valve open signal and 1% of steady-state chamber pressure. Unfortunately, this delay is composed of a mechanical delay (valve opening time, time for propellant flow to reach catalyst) and a chemical delay. The mechanical delay is not always constant and may vary with test conditions. It is not possible on the basis of reactor firing data alone to differentiate between mechanical and chemical delay. The ignition delay tester used in this study measures the chemical delay only. This method has proven to be valuable in studying the effects of numerous variables (catalyst activity, catalyst pretreatment, catalyst poisons, adsorbed gases, temperature, pressure) on the ignition delay. With this improved system, not only an exotherm as such, but also the magnitude of an exotherm and the rate of temperature increase could be used in defining the ignition delay.

A reasonably good correlation of ignition delay data with those reported by Shell Development Company was obtained when both data were plotted together on the same sheet. This confirms that both methods basically measure the same phenomenon. The apparatus was depicted in the interim report.

The central part of the ignition delay test apparatus is a ceramic or quartz crucible which holds the catalyst sample and rests on a sensitive piezoelectric crystal microphone. The microphone picks up the momentum of propellant impact when it hits the catalyst surface. The reaction noise is recorded on the same oscillograph trace. The crucible and the microphone are mounted in a temperature conditioned beaker. A thermopile arrangement was so sensitive that even the heat of wetting of the bare carrier material, Harshaw 1404 or Reynolds RA-1, could be recorded, although it was several orders of magnitude smaller than the heat evolved during hydrazine decomposition on active catalyst.

Unshielded thermocouples gave the fastest response because of the small heat capacity of the welded joint bead. Even better response was expected by the use of surface thermocouples where the thickness of the hot junction has been decreased by grinding down to 0.001 inch. However, it was not possible to use a thermopile arrangement with the metal foam catalyst samples as the electrically conductive foam shorted the thermopile output. Insulating the thermocouples from the foam sample would have drastically increased the response time. Two calibrated, redundant surface thermocouples were used for metal foam catalyst samples instead. For optimum response, the thermocouples were implanted into the monolithic catalyst sample. A 1.5-millimeter (0.05-inch) diameter hole was drilled radially through the sample to hold one thermocouple on each side. Both the microphone and the thermocouple or thermopile outputs were recorded on a Honeywell Visicorder high-speed oscillograph operating at a speed of 20 in./sec with a timing of 10 milliseconds. The best obtainable time resolution was 2 milliseconds (estimated).

With the currently used ignition delay tester, the propellant was injected from a temperature-conditioned feed line through a Parker microvalve. The microvalve was operated via a variable micropulser which allowed pulse widths as low as 10 milliseconds. At 25-psig feed pressure, a 60-millisecond pulse resulted in the ejection of 0.3 milliliter hydrazine per pulse. The use of a valve instead of a pipette enabled the ignition delay tester to operate under vacuum conditions as well. The holdup volume of the downstream end of the valve was extremely small. For best results, the valve and the injector were placed as close to the catalyst sample as possible.

The propellant and the catalyst thermal conditioning jackets were connected to a constant temperature circulator by which the temperature could be varied between 255.2°K (0°F) and 344°K (+160°F). All testing was performed at 298°K (77°F), and the calibrated thermocouples in contact with the catalyst were used to monitor the initial catalyst temperature before each test.

The ignition delay system was contained in a T-shaped vacuum vessel with O-ring sealed flanges, which provided excellent accessibility to the system from all sides. The T-shaped vacuum vessel could be alternately evacuated and filled with inert gas, argon or nitrogen. All ignition delay tests were performed under argon. The argon was passed through a cartridge with hydrogen-loaded Shell 405 catalyst which served as an oxygen scavenger to remove last traces of oxygen from the inert gas. Oxygen present as a trace contaminant (10 ppm) had a very pronounced effect on measured ignition delays.

As a general trend with all samples tested, the ignition delay increases with increasing numbers of cold starts. This increase is also observed with Shell 405 catalyst and may be attributed to the following effects:

a. Loss of active oxygen after the first reaction with hydrazine
b. Active sites on the catalyst blocked by adsorbed gases (ammonia, hydrogen)
c. Active sites on the catalyst poisoned by propellant contaminants (aniline)
d. Loss of active material.

Some catalysts recover after air is readmitted to the catalyst, causing the adsorbed hydrazine decomposition products and the catalyst surface to become oxidized. During the early testing of monolithic catalyst samples, air was occasionally admitted for a last test. However, this did generally not improve catalyst performance. Consequently, the loss of activity was most likely due to mechanical loss of active material.

One of the main purposes of the spontaneity testing was to establish the required active metal concentration. The considerations leading to the selection of the optimum active metal concentration are outlined in paragraph 3.6. The ignition delay tester was a useful laboratory tool in the early evaluation of catalyst samples before proceeding with more extensive reactor testing such as that conducted under Tasks 9 and 10 of the follow-on contract.

2.4.2 Hydrogen Chemisorption

The measurement of hydrogen chemisorption is a very useful tool in evaluating catalyst activity. Hydrogen chemisorption depends on both a high active surface area and the presence of finely dispersed active metal. Bulk active metals show hardly any hydrogen chemisorption. Hydrogen chemisorption was measured by a thermal conductivity method with 99% argon/1% hydrogen and a gas chromatograph. The samples were degassed at 773°K and then rapidly cooled to 273°K in the Ar/H_2 stream. The recorded peak area was proportional to the adsorbed hydrogen.

The results summarized in Table 2-4 show that hydrogen chemisorption of monolithic catalysts on a total weight basis is lower than for Shell 405 catalyst. This must be expected because most of the monolithic catalyst is metal foam which does not significantly contribute to the surface area. In order to evaluate the active metal deposition, the μ moles hydrogen chemisorbed should be related to the amount of active material, i.e., the active metal plus ceramic only. The numbers thus obtained are in the same order of magnitude as for Shell 405. This confirms that good active metal dispersion is achieved by the RRC-developed active metal deposition process.

Because the hydrogen chemisorption measurement alters the properties of the catalyst, no post-hydrogen chemisorption samples could be used for test firings. Instead, control samples were prepared under exactly identical conditions along with samples intended for reactor firings.

Decrease of hydrogen chemisorption with firing time was measured for eight post-firing samples. The decrease is no greater than for Shell 405 catalyst. The record sample with 7,700 seconds accumulated burn time which was tested during the initial phase of the contract exhibited a reasonably high residual hydrogen chemisorption after the firings.

If one considers the amount of iridium present in a given reactor volume, the monolithic catalysts contain less than half as much active metal surface area per reactor volume as Shell 405. This results in a slightly slower startup in some cases but constitutes a significant reduction in the amount of expensive iridium required to use a reactor of a given thrust level and chamber volume.

Table 2-4

HYDROGEN CHEMISORPTION OF MONOLITHIC CATALYSTS AT 273°K

Lot No.	Sample No.	Iridium, % by Weight in Al_2O_3 + Ir	Hydrogen Chemisorption		Remarks
			μ Moles per gram Al_2O_3 + Ir	μ Moles per cm^3 Reactor Volume	
32-144	1	28.7	122	41	Post-firing, 700 seconds
34-210	5D	33.5	90	—	NH_3 added to active metal solution
32-171	3B	37.1	233	127	Control sample for W32-196 #5 and #8
32-197A	1	34.0	102	47	Post-firing, 7,700 seconds steady state
32-196	5	36.4	161	93	Post-firing, 470 seconds
32-196	6	33.0	155	106	Post-firing, 2,400 seconds
32-198	7	34.6	146	100	Post-firing, 2,600 seconds
32-198	8	34.0	147	90	Post-firing, 3,600 seconds
32-196	8	36.8	190	111	Unfired
32-196	1	33.5	201	160	Unfired
32-254AD	10	38.9	163	74	Post-firing, 120 seconds
32-197A	2	34.8	104	40	Post-firing, 140 seconds, contaminated?
For comparison					
Shell 405 ABSG		32	287	210	As received

3.0 PREPARATION OF MONOLITHIC CATALYST SAMPLES

The preparation of monolithic catalyst samples is a multistep procedure. It consists of selection and characterization of a foam material, machining it to size, coating with active surface area ceramic, and promoting with active metal. The various steps are best illustrated in Figure 3-1 where monolithic catalyst samples for a 2.2-N (0.5-lbf) reactor are shown at various steps in the preparation.

3.1 ACCEPTANCE CRITERIA OF FOAM SAMPLES FOR MONOLITHIC CATALYSTS

Rocket Research Corporation Specification MS-0122 was intended to be used to control and purchase foam metal under the contract. However, because of development difficulties in this recently developed tungsten foam material, the sole-source supplier could not ensure reproducible delivery to this specification. Also, some requirements were still changing as the program was in progress. So far, tungsten foam was prepared on a best-effort basis, and each batch had to be qualified by receiving inspection at RRC. A copy of Material Specification MS-0122, recommended for future procurement, is contained in Appendix A to this report.

3.2 MACHINING OF FOAM SAMPLES

Foam materials which are received as bulk samples had to be machined by electric discharge (EDM). This was easily done for Hastelloy X foam. However, tungsten foam required extreme care and skill by the EDM machinist not to crush samples in the process and to achieve a smooth surface. Initial attempts to EDM machine tungsten foam were unsuccessful; and for the first year after tungsten foams became available, the samples were machined by the foam manufacturer on a lathe after filling them with wax. The wax then had to be removed in a high-temperature vacuum furnace at 2,300°F. The tolerances which could be achieved by this process were unacceptably wide, resulting in poor fit into the 2.2 N reactor. This allowed flow to channel along the wall and bypass the catalyst. Void volumes in the injector area are frequently the cause of excessive chamber pressure fluctuations. Suitable EDM operating conditions were established for tungsten foams only after repeated attempts, and most of the samples used in the second increment of the contract were machined to close tolerances by EDM.

3.3 METAL FOAM SURFACE PREPARATION

Throughout the period when nickel, Haynes 25, and Hastelloy X foams were used, foam metals were coated after degreasing and cleaning the samples without further surface preparation. Because these foams usually have a very rough and sometimes porous ligament surface, good adherence of the ceramic coating was achieved. Some adherence problems were encountered with the first tungsten foam samples for reactor firings, which had a very shiny and "too-perfect" surface. One of these shiny, uncoated samples is shown on Figure 3-1.

MONOLITHIC CATALYST SAMPLES AT VARIOUS STAGES OF TESTING

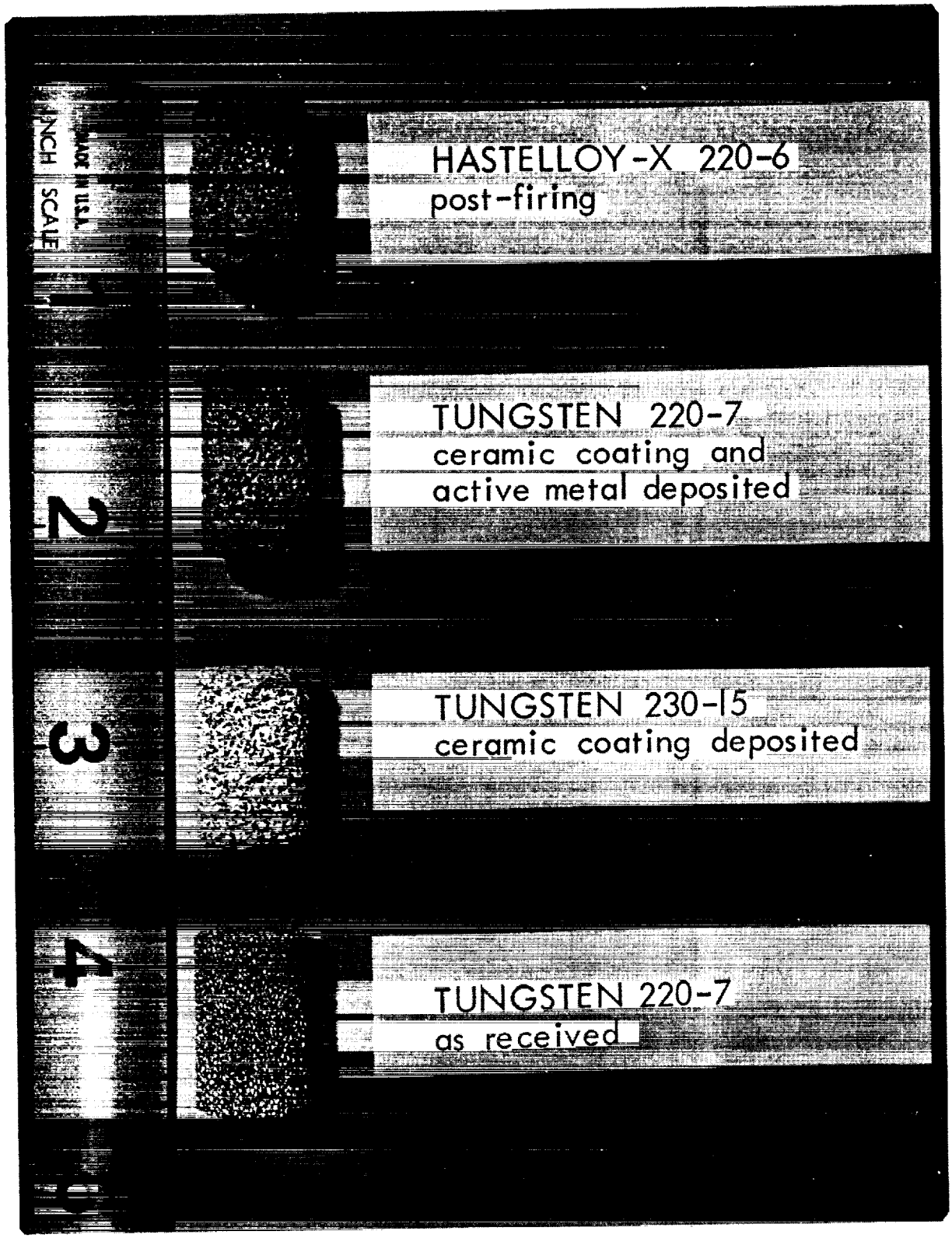

56000-39

Figure 3-1

In order to improve adherence to tungsten foams, a surface preparation study was initiated as Task 8 under the follow-on effort. Methods of surface preparation to be studied were 1) dusting on of additional tungsten powder, 2) controlled oxidation of the tungsten surface followed by reduction, 3) chemical etching, 4) chemical etching after preceding aluminiding of the surface, and 5) anodic electrolytic etching.

3.3.1 Dust-On of Tungsten Powder

The most promising approach to achieve sufficient surface roughness and good ceramic adhesion while simultaneously maintaining crush strength consisted of a two-step process. First, the manufacturer prepared a shiny, strong foam of the type received under lot number 32-144. Then samples were EDM machined to size from this raw material and returned to the manufacturer for receiving an additional tungsten coating. In this second step, the furnace cycle in the high-temperature vacuum furnace would be selected so that the tungsten particles would adhere to, but not fuse into, the ligament surface. A SEM photomicrograph of a foam modified in this manner is shown in Figure 3-2. Satisfactory ceramic adherence has been achieved with a surface of this structure, and samples prepared for evaluation matrix Task 10 and life test Task 11 were roughened in this fashion.

The dust-on process cannot yet be applied to foam samples with diameters in excess of 1 inch, and additional foam technology development will be required for scaling up this procedure.

3.3.2 Surface Roughening by Oxidation

Surface roughening by oxidation had previously been attempted when the adherence problem was first discovered. Initial attempts apparently resulted in excessive oxidation and thus weakened the foam structure. A controlled oxidation process was developed during the second increment of the contract which resulted in reproducible surface roughening without weakening the foam structure. This was confirmed by crush tests, the results of which were included in Table 2-1.

As became apparent when taking SEM photomicrographs, the initial oxidation procedure was too strong, leaving only 50% unoxidized metal behind. The oxidation temperature was then decreased and desirable surface roughness without weakening the metal foam structure was obtained, as shown in Figure 3-3.

3.3.3 Other Methods of Surface Preparation

None of the other methods of surface preparation gave promising results. Chemical etchants, such as hydrofluoric acid in nitric acid, removed a uniform layer of material. These studies were conducted with tungsten sheet metal coupons, where the surface to be roughened was more accessible to observation than in a foam. Aluminiding efforts were hampered by inability to achieve temperatures high enough to cause migration and diffusion of aluminum into tungsten at reasonable rates. Anodizing was rejected because only the periphery of the foam sample could be attacked by electrolytic methods.

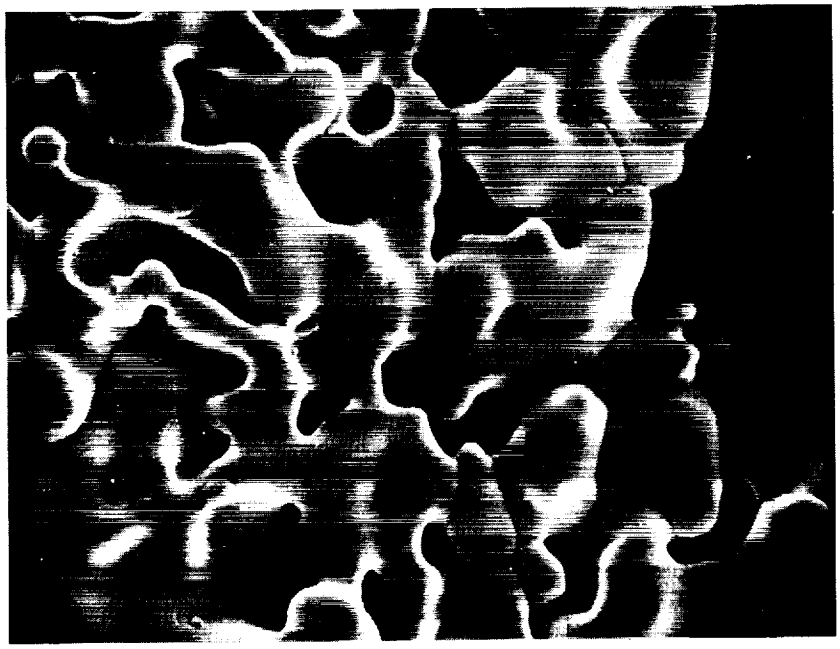

Figure 3-2 TUNGSTEN FOAM SURFACE ROUGHENED BY DEPOSITION OF ADDITIONAL TUNGSTEN POWDER, 3000X

Figure 3-3 TUNGSTEN FOAM SURFACE ROUGHENED BY OXIDATION REDUCTION, 3000X

3.4 CERAMIC COATING

The weighed and cleaned foam samples were placed on a Petri dish and identified. In a typical process, a ceramic coating slip was made from 181 grams of submicron-size alumina RA-1, 74 grams of water, 44 grams of silica colloid Ludox SM-30, and one drop of a wetting agent. The mixture was thoroughly stirred to remove all lumps and allowed to stand for 5 minutes to allow coarser particles to settle. The dispersion was then decanted and the viscosity measured with a Brookfield viscometer. The viscosity of the coating slip was typically in the range of 400 to 600 centipoise.

The foam sample was then submerged in the mixture, and vacuum was applied three times to aid penetration. The sample was then taken out of the mixture, and the excess coating was blown out with moisture-saturated air. The samples were allowed to air dry for at least 3 hours and then dried at 393°K for at least 12 hours. Calcining was achieved by heating them in a quartz tube under hydrogen for 1 hour at 973°K. The samples were allowed to cool off under hydrogen to between 373 and 423°K and finally cool to ambient in a desiccator. The weight gain was determined and the percent ceramic calculated. All samples were then retested for pressure drop, and a new ΔP curve was plotted on the chart accompanying each sample. From this increase in ΔP, it could be determined whether or not an excessive number of pores had been inadvertently plugged with ceramic.

3.5 ACTIVE METAL DEPOSITION

Details of the active metal deposition process are classified confidential and are contained in a classified addendum to the interim report RRC 71-R-259. No major changes were made during the follow-on period to this active metal deposition process.

In an effort to minimize the number of temperature cycles, which were suspected to weaken the ceramic, some samples were prepared by a modified method. However, this did not result in the expected improvement in ceramic adherence, and all samples for Tasks 10 and 11 were prepared with the standard method described in the classified addendum to 71-R-259.

When inspecting SEM photomicrographs taken from promoted samples, a mud-cracking pattern was observed. This type of surface texture is highly undesirable because the pieces comprising the crack pattern are liable to flake off. The mud-crack pattern was then traced to local overdeposition of iridium metal on the surface of the monolithic sample. No such mud cracking could be observed in the interior of the foam grain after it was sectioned. The occurrence of mud cracking can be avoided by forcing the active metal solution rapidly into the ceramic-coated foam grain, rather than allowing it to wick in by itself.

Later, the percent active metal in the activated ceramic coating was optimized to avoid overloading the active surface area and plugging micropores, but still making maximum use of the available surface area on the ceramic. Typical active metal contents are now 33% in the ceramic, which is also representative for commercially available hydrazine decomposition catalysts like Shell 405.

It must be emphasized that for a given reactor volume, typical monolithic catalysts contain only one-third to one-half the amount of expensive iridium which the reactor would otherwise hold with Shell 405. This can result in substantial savings of expensive noble metals in addition to the other benefits of monolithic catalysts.

During the initial increment of the program, too many parameters were varied; and reproducibility in reactor performance for supposedly identical samples was not yet demonstrated. After some manual skill was developed and all parameters were carefully controlled, catalyst samples with reproducible properties could be prepared. The major variable is the amount of ceramic material deposited. With four W 220-7 samples in two batches, ceramic loading varied from 18.9 to 21.8%. Active metal content in the activated coating varied from 31.3 to 31.7% for a series of three samples in the same batch (nominal 32% iridium).

3.6 RANGE OF PARAMETERS STUDIED

In total, 14 parameters can be varied in order to arrive at an optimal monolithic catalyst bed. Obviously not all of these parameters could be included in the test matrix. This restriction existed not only because of lack of time, but also because the significance of some additional parameters became apparent only during the test program. Table 3-1 shows a summary of the more important parameters.

Initial testing was limited to 500 μm (20-mil) pore-size foam materials. Two hundred fifty μm (10-mil) pore-size materials, in particular for refractory metals, were more difficult to manufacture and became available only toward the end of the initial contract as the foam technology advanced. When small pore-size foams were being made, the risk of accidentally plugging pores or leaving membranes across windows was higher than with large pore sizes. Small pore sizes were desirable because the fuel entering the bed was more finely dispersed and exposed to more surface area than with coarse foam. This resulted in faster response and smoother reactor operation.

However, as the volume and temperature of the decomposition gases increases, a coarser foam is desirable for the lower portion of the bed to reduce the pressure drop found with 10-mil pore-size foam samples. This is possible by sandwiching or by stacking up samples of different pore sizes in a composite bed. Some tests were made in this composite bed mode, which is more promising for large reactors rather than small 2.2-N reactors.

The density of a foam matrix influences its strength and its weight. Sufficient strength to withstand the reactor environment is certainly a prerequisite. Typical foam densities used were approximately 7%. Samples with higher foam densities were very heavy with the result that too much inert material had to be heated up during the start period. This resulted in a long transient, a stepwise chamber pressure increase, and flame front shifts during the early phase of reactor tests. The time to reach 90% P_C was longer than with lower density samples.

The ceramic coating parameter studied was the type of coating and mode of deposition. Adherence was a very important criterion, and improvements are still possible in this particular area. The

Table 3-1

RANGE OF PARAMETERS STUDIED FOR MONOLITHIC CATALYST BED EVALUATION

Parameter	Range	Important For
Foam Parameters		
Pore size	10 to 30 mil	Pressure drop, response, P_c roughness
Density	3.5 to 15%	Mechanical strength, response
Type of foam metal	Hastelloy-X, tungsten, molybdenum	Exhaust compatibility, strength, catalyst durability
Surface roughness	Smooth, roughened, oxidized	Ceramic adherence
Ceramic Coating		
Active surface area coating	SiO_2, Al_2O_3 composition	Catalyst activity
Sintering temperature	600 to 700°C	Adherence versus activity
BET surface area	60 to 240 m^2/g	Catalyst activity
Ceramic loading	4 to 40% by weight	Catalyst activity, pressure drop
Active Metal		
Active metal	Iridium, ruthenium	Catalyst activity, cost
Active metal loading	4 to 17% by weight 0.05 to 0.3 g Ir/cm^3 15 to 50% in activated coating	Catalyst activity
Hydrogen chemisorption	100 to 240 μ moles/g	Catalyst activity

ceramic loading was limited by the danger of plugging pores and unduly increasing pressure drop of the sample. Also, thick layers of ceramic are more susceptible to cracking and flaking. The BET surface area was used as a guideline to evaluate different ceramic coatings and methods of ceramic coating application.

The range of active metals studied was limited to iridium and ruthenium. The amount of active metal in the catalyst, another important parameter, can be expressed in three different ways: percent by weight in the overall sample, volume-specific loading of the overall sample, and percent by weight active metal in the activated ceramic coating. This sequence is also the chronological order in which the three parameters were used to optimize active metal loading. Initially, percent by weight active metal was used, but then it became difficult to compare Hastelloy X with tungsten. Therefore, the volume specific loading was used instead, which is independent of the foam metal.

The most important parameters to be included in the Task 10 parametric test matrix included two foam-related and two engine-related parameters. Foam samples were prepared with either 250 or 500μm pore size and with either 33 or 48% by weight iridium in the active material, which consists of alumina and iridium. The engine parameters varied were the bed length and the bed loading.

Tests with composite bed configurations (250 μm upstream, 500 μm pore-size foam downstream) were initially considered for the Task 10 test matrix, but it is felt that the advantages of composite beds can only be realized in larger reactors. For instance, the RRC 2.2 N reactor, MR-6A, uses one uniform granulation of Shell 405, whereas the 22 N reactor, MR-50A, uses a composite bed with advantage.

4.0 REACTOR TEST FIRING RESULTS

4.1 TEST HARDWARE

Monolithic catalyst test firings were conducted with a 2.2 N (0.5-lbf) thrust reactor originally developed for Shell 405 catalyst. The reactor is shown in Figure 4-1 and a summary of the nominal operating conditions and dimensions is presented in Table 4-1.

Table 4-1
MONOLITHIC REACTOR OPERATING CHARACTERISTICS

	Bed Loading, kg/m^2 sec		
	8	5	3
Vacuum thrust, N (lbf)	2.2 (0.5)	1.3 (0.3)	0.8 (0.2)
Propellant feed pressure, kN/m^2 (psia)	2,750 (400)	2,750 (400)	2,750 (400)
Chamber pressure, kN/m^2 (psia)	1,375 (200)	1,375 (200)	1,375 (200)
Throat diameter, mm (in.)	1.09 (0.043)	0.86 (0.034)	0.67 (0.026)
Catalyst bed diameter, cm (in.)	1.265 (0.500)		
Catalyst bed length, cm (in.)	2.00 (0.785)		
Materials:			
Thrust chamber	347 stainless steel		
Injector	347 stainless steel		
Capillary feed tube	Inconel 600		
Thermal standoffs	AM 355		

As shown in Figure 4-1, the injector assembly is flanged to the chamber body to permit easy inspection and replacement of the catalyst bed. Sealing of the injector to the chamber is accomplished by an asbestos-filled, copper-jacketed gasket. The injector consists of two flanges separated and held together by three tubular thermal standoffs and a capillary feed tube. The propellant valve screws into the modified AN fitting at the upper injector flange. An orifice is also contained in the injector inlet flange. The capillary feed tube injects the propellant into the catalyst bed. The inner walls of the thrust chamber are coated with a 0.05 centimeter (0.020 inch) thick Rockide Z (zirconium oxide) coating to minimize heat losses. The catalyst bed is retained on the downstream end by a perforated bed plate and a 50 by 50 wire mesh screen. A 100 by 100 wire mesh screen is placed between the injector orifice and the catalyst bed.

EXPLODED VIEW OF 2.2 N (0.5 lbf) REACTOR
WITH MONOLITHIC CATALYST AND INJECTOR HEAD

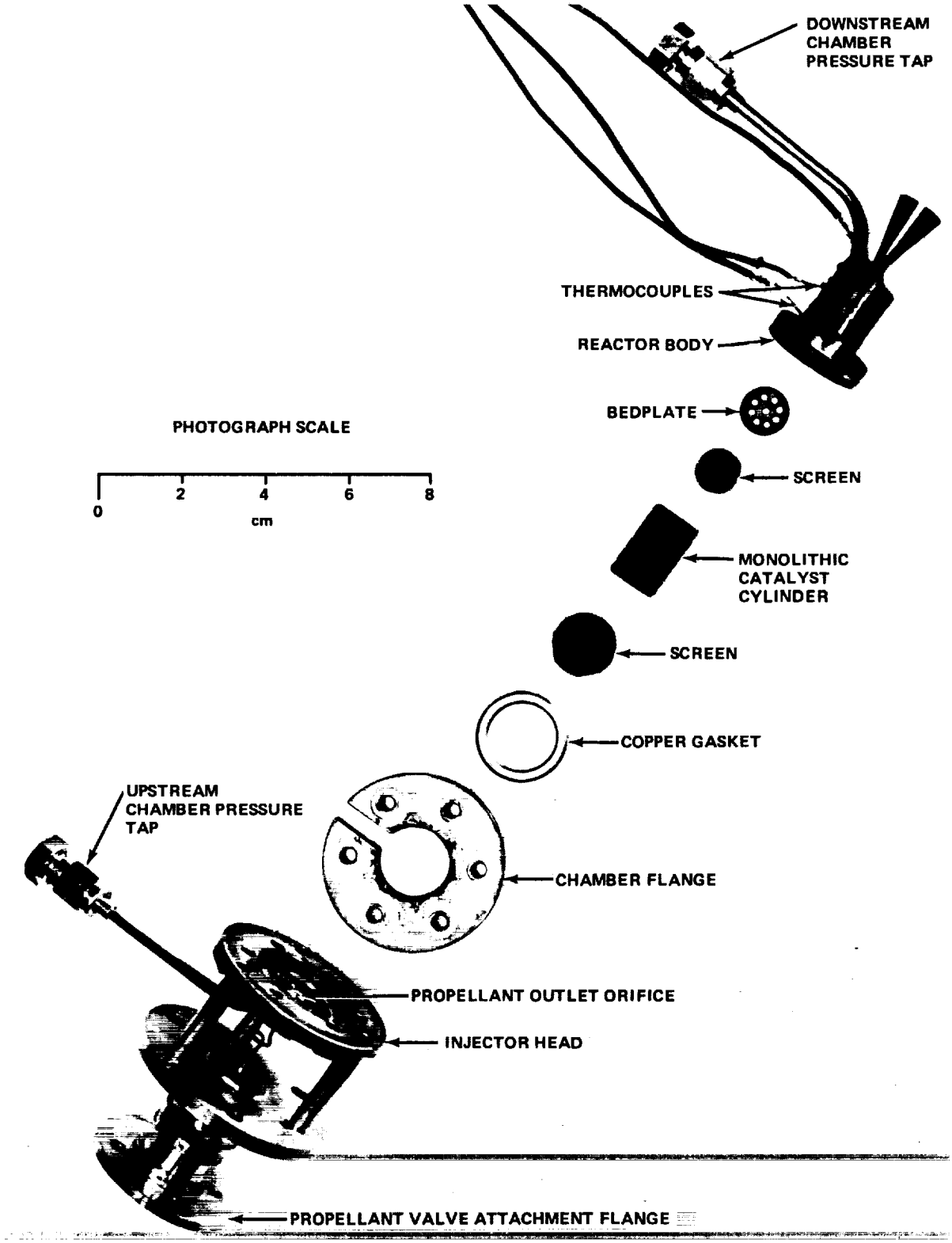

56000-38A

Figure 4-1

The monolithic bed foam cylinder diameters were electrical-discharge machined to fit tightly inside the reaction chamber. It was anticipated that the close-tolerance fit would not allow hydrazine to bypass the catalyst bed by wicking down the chamber wall around the catalyst cylinder. The maximum diametral clearance allowed between the foam catalyst cylinder and inside diameter of the chamber was 0.1 millimeter (0.005 inch).

4.2 FOAM EVALUATION TEST FIRINGS

Test firings of several monolithic foam catalysts were conducted in the reactor described above. A summary of all the steady-state firings made throughout the monolithic catalyst program is presented in Appendix B.

Test firings 1 through 77 were conducted early in the program and were discussed in detail in Section 4.0 of interim report 71-R-259. In summary, based on the results of the early tests it was concluded that:

a. Hastelloy X foam was susceptible to nitridation damage – the foam broke up after 3,000 to 4,000 seconds of firing time.

b. Optimum ceramic loading was 0.3 g/cm^3 of bed volume.

c. The ceramic coating adhered only to a properly roughened foam surface.

d. Tungsten foam, in 20-mil pore size, gave satisfactory steady-state firing performance of up to 7,700 seconds. (Pulse-mode performance was not evaluated.) A larger pore size foam (30 mil) did not sustain hydrazine decomposition.

e. Iridium was the best active metal to use for monolithic catalyst.

Test firings 78 through 130 (Task 9) were conducted to evaluate the more promising catalysts developed during Tasks 7 and 8. The goal of these tests was to screen the foam-processing variables and to select the catalyst(s) and operating variables for the Task 10 parametric tests. Results and conclusions of the Task 9 tests are as follows:

a. Tungsten foam surface preparation (roughening) prior to applying ceramic coatings is best accomplished by "dusting on" powdered tungsten. The alternate surface preparation method – lower sintering temperatures – resulted in reduced crush strength foam which collapsed during test firings. The resulting chamber void allowed hydrazine accumulation with subsequent severe chamber pressure oscillations.

b. The reactor bed loadings used during these test firings, 9 to 11 kg/m^2 sec, were marginally high. The higher bed loadings caused the hydrazine decomposition flame front to move downstream in the catalyst bed, causing incomplete hydrazine decomposition; and low performance was observed intermittently throughout these steady-state firings.

c. It was postulated that the catalyst bed length of 2 centimeters used throughout these tests was insufficient to allow complete hydrazine decomposition when using monolithic catalysts having less activity than Shell 405. Bed lengths greater than 2 centimeters were therefore planned for the Task 10 studies.

d. Substituting a rigimesh injector for the single orifice injector improved reactor response times and c* performance (see Appendix B, test data for run number 134, using a 12- by 64-mesh rigimesh injector, and run number 136, using a 50- by 250-mesh rigimesh injector). However, excessive chamber pressure roughness soon developed in these tests, resulting in short catalyst bed life.

e. Tungsten foam having 10-mil (250 μm) pore size was test fired for the first time in this test series. Five different 10-mil foam samples were test fired. Two of the foam beds collapsed during test firing – the result of inadequate crush strength. Marginal performance was experienced in the other 10-mil foam test firings, as chamber pressures occasionally dropped to 50% of the nominal value briefly during a test and then recovered to the nominal value. It was postulated that inconsistent foam coating techniques were responsible for the marginal reactor performance.

f. Pulse-mode data obtained during the Task 9 test series indicated low performance. Pulse trains having 0.20 second on time and 0.80 seconds off time were fired with various foam catalyst bed samples. Approximately 400 pulses were generally required to warm the reactor to sufficiently high temperatures to achieve high performance.

4.3 TASK 10 PARAMETRIC EVALUATION TESTS

After completion of the Task 9 reactor firings, an abbreviated parametric test series was conducted to determine optimum pore size, bed length, bed loading,and active metal content. The reactor was fired from ambient startup temperatures to evaluate both steady-state and pulse-mode performance. The pulse mode consisted of 100 pulses having 0.100 second on time and 0.900 second off time. The goal of this task was to select the optimum catalyst and operating condition for the Task 11 useful life evaluation tests.

4.3.1 Task 10 Test Matrix Summary

After selecting tungsten as the foam material having best potential and optimizing the catalyst processing technique, a parametric test matrix was conducted. The parameters varied were:

a. Tungsten foam pore size – 10 and 20 mil

b. Catalyst bed length – nominal length (2 centimeters) and twice nominal length (4 centimeters).

c. Iridium content – high (15% of total catalyst weight) and nominal (9% of total catalyst weight)

d. Bed loading – 3 to 4 kg/m^2 sec, 5 to 6 kg/m^2 sec, and 8 to 9 kg/m^2 sec.

The tests included 60-second steady-state firings, and 100 pulses having a duty cycle of 0.100 second on, 0.900 second off. The pulse trains and the steady-state firings were started with the reactor at ambient temperatures ranging from 290 to 300°K (60 to 80°F).

The parametric evaluation test results are summarized in Table 4-2.

Table 4-2
TASK 10 TEST MATRIX PERFORMANCE RATINGS

	Bed Loading, kg/m^2 sec					
	3–4		5–6		8–9	
	Bed Length		Bed Length		Bed Length	
	L	2L	L	2L	L	2L
20-mil tungsten, 9% Ir	1. Fair 2. Fair 3. Fair 4. Fair 5. Good	NA	1. Good 2. Good 3. Good 4. Excellent 5. Good (Rating: #1)	1. Poor 2. Poor 3. Poor 4. Fair 5. Good	1. Poor 2. Good 3. Good 4. Good 5. Good	1. NA 2. Fair 3. Poor 4. Good 5. Good
20-mil tungsten, 15% Ir	1. Fair 2. Good 3. Poor 4. Fair 5. Fair	NA	1. Good 2. Good 3. Good 4. Good 5. Fair (Rating: #3)	NA	1. Good 2. Good 3. Poor 4. Fair 5. Fair	NA
10-mil tungsten, 9% Ir	1. Poor 2. Good 3. Poor 4. Poor 5. Poor	NA	1. NA 2. Good 3. Poor 4. Excellent 5. Poor	NA	1. Excellent 2. Good 3. Good 4. Excellent 5. Poor (Rating: #2)	NA

Key:

1. Pulse mode performance (0.10 sec on/0.90 sec off duty cycle)
2. Response times (startup and tailoff times)
3. Chamber pressure roughness (poor: >10%; fair: 10%–7%; good: 6%–3%; excellent: 2% or less)
4. c* performance during steady-state firing (poor: <1,100 m/sec; fair: 1,100–1,190 m/sec; good: 1,191–1,239 m/sec; excellent: >1,240 m/sec
5. Catalyst reproducibility (fabrication and processing repeatability)

"Excellent" rating: equal to, or better than, Shell 405 catalyst performance

The performance ratings for each catalyst were based on pulse-mode performance, startup and tailoff response times, steady-state chamber pressure roughness (which indicates the life potential of the catalyst bed), steady-state c*, and the reproducibility of the particular type of catalyst from the standpoint of fabrication and processing prior to testing. The rating of "excellent" in Table 4-2 was given only if that performance parameter equalled or exceeded the performance of Shell 405 catalyst in the reactor. The best performing catalysts and operating conditions were:

Number 1	20-mil tungsten foam with 9% iridium using a bed loading of 5 to 6 kg/m^2 sec in the nominal length reactor
Number 2	10-mil tungsten foam with 9% iridium using a bed loading of 8 to 9 kg/m^2 sec in the nominal length reactor
Number 3	20-mil tungsten foam with 15% iridium using a bed loading of 5 to 6 kg/m^2 sec in the nominal length reactor.

Figures 4-2 and 4-3 show traces of oscillograph chamber pressure data from the number 1 rated monolithic catalyst. The pressure trace at steady-state shutdown shows typical chamber pressure oscillations and tailoff response time. The pulse-mode chamber pressure trace overlays, Figure 4-3, show the pulse shape transient as the reactor warms up during a firing. The pressure spiking that appears after pulse number 70 is typical of most catalysts tested, including Shell 405.

Figure 4-4 shows the excellent pulse shapes obtained with 10-mil tungsten foam, the second-ranked catalyst. No pressure spikes appeared during the pulses, apparently due to the thermal balances obtained with this bed. These pulses compare favorably with the Shell 405 catalyst pulses described in paragraph 4.3.2. The tungsten foam catalyst pulses had a slightly slower rise time than the Shell 405 pulses, probably due to the smaller percentage of iridium in the tungsten foam bed. This 10-mil tungsten foam was rated lower overall than the 20-mil tungsten foam because of two difficulties: 1) obtaining reproducibly high crush strength 10-mil tungsten foam from the foam supplier, and b) obtaining reproducible in-house ceramic coating. The three steady-state firings that were conducted on the 10-mil foam sample (runs number 168, 170, and 172) showed slowly increasing chamber pressure roughnesses with a maximum roughness of approximately 7%.

The third-rated foam sample, 20-mil tungsten with 15% iridium at a bed loading of 5 to 6 kg/m^2 sec, showed high overall performance characteristics. The disadvantage of this foam is in applying the higher iridium content coating. Microscopic cracking frequently appears in the higher percent metal coating, giving a high probability that the active metal will flake off, thereby deactivating the catalyst and limiting its life. Also, when more metal coating is applied to the ceramic base, more ceramic pores become plugged, reducing the surface area of the catalyst. Because of these processing complications, the higher iridium content catalyst was rated "fair" in the reproducibility category, and third overall.

4.3.2 Shell 405 Comparison Tests

During the parametric evaluation tests, 25- to 30-mesh Shell 405 catalyst was packed into the 5 kg/m^2 sec bed loading test reactor and fired under the same conditions as the monolithic foams. The following results were obtained:

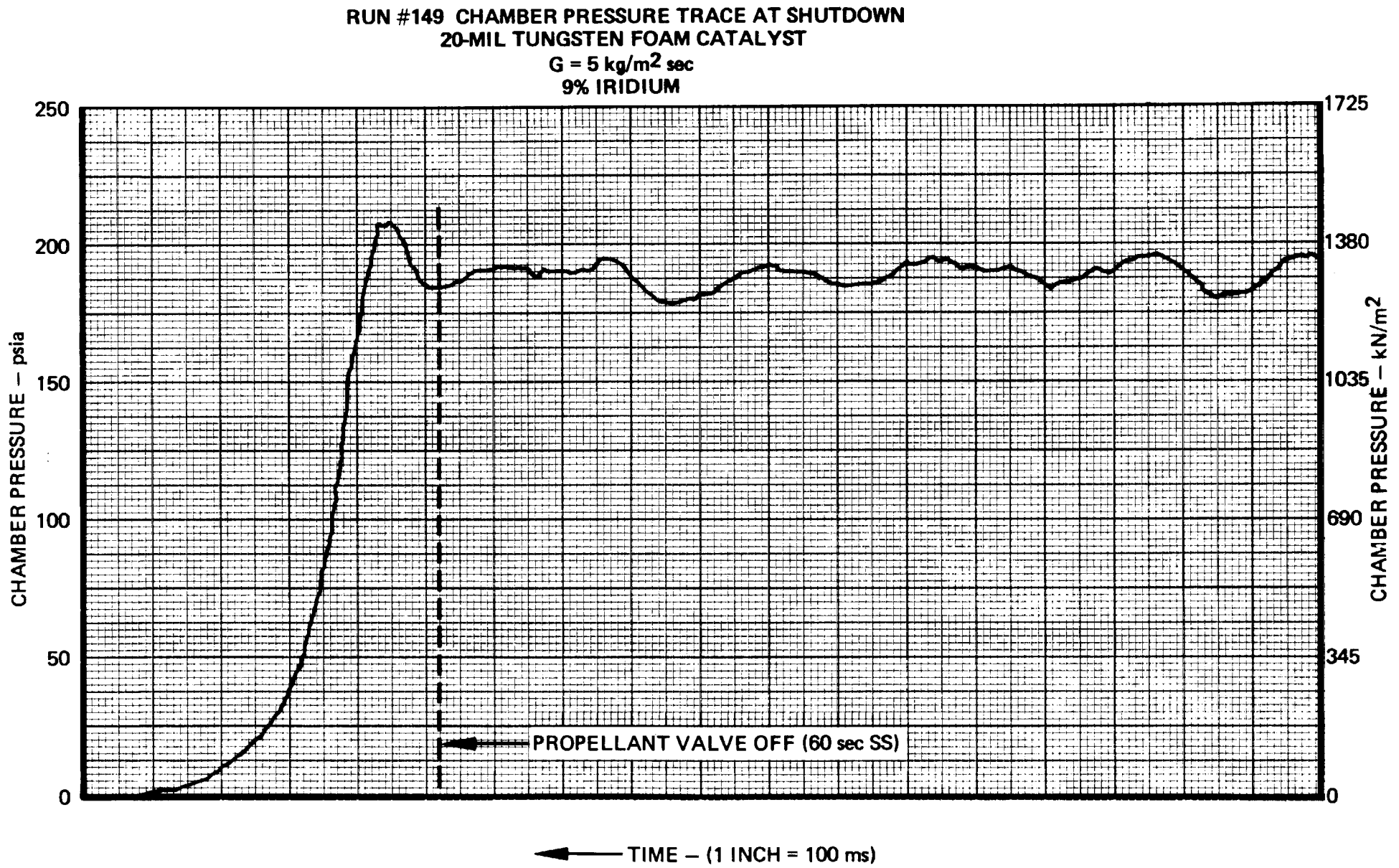
RUN #149 CHAMBER PRESSURE TRACE AT SHUTDOWN
20-MIL TUNGSTEN FOAM CATALYST
G = 5 kg/m2 sec
9% IRIDIUM
CHAMBER PRESSURE – psia
250
200
150
100
50
0
1725
1380
1035
690
345
0
CHAMBER PRESSURE – kN/m2
PROPELLANT VALVE OFF (60 sec SS)
TIME – (1 INCH = 100 ms)

Figure 4-2

CHAMBER PRESSURE PULSE SHAPES FOR RUN #150

20 MIL TUNGSTEN FOAM
G = 5 kg/m^2 sec
9% IRIDIUM
0.10 SEC ON/0.90 SEC OFF DUTY CYCLE

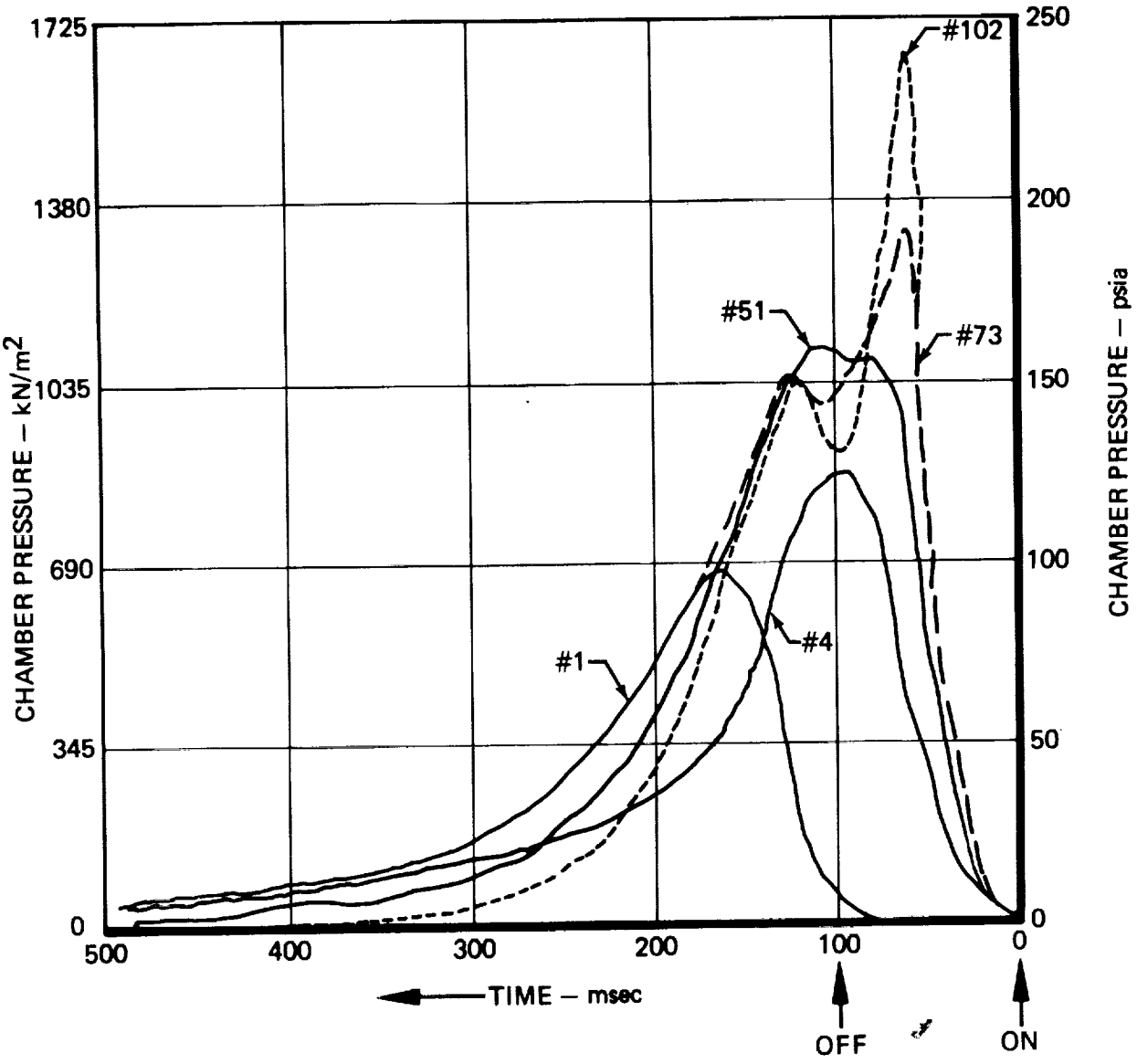

Figure 4-3

CHAMBER PRESSURE PULSE SHAPES FOR RUN #171

10 MIL TUNGSTEN FOAM
G = 7.4 kg/m^2 sec.
9% IRIDIUM

.10 SEC ON/.90 SEC OFF DUTY CYCLE

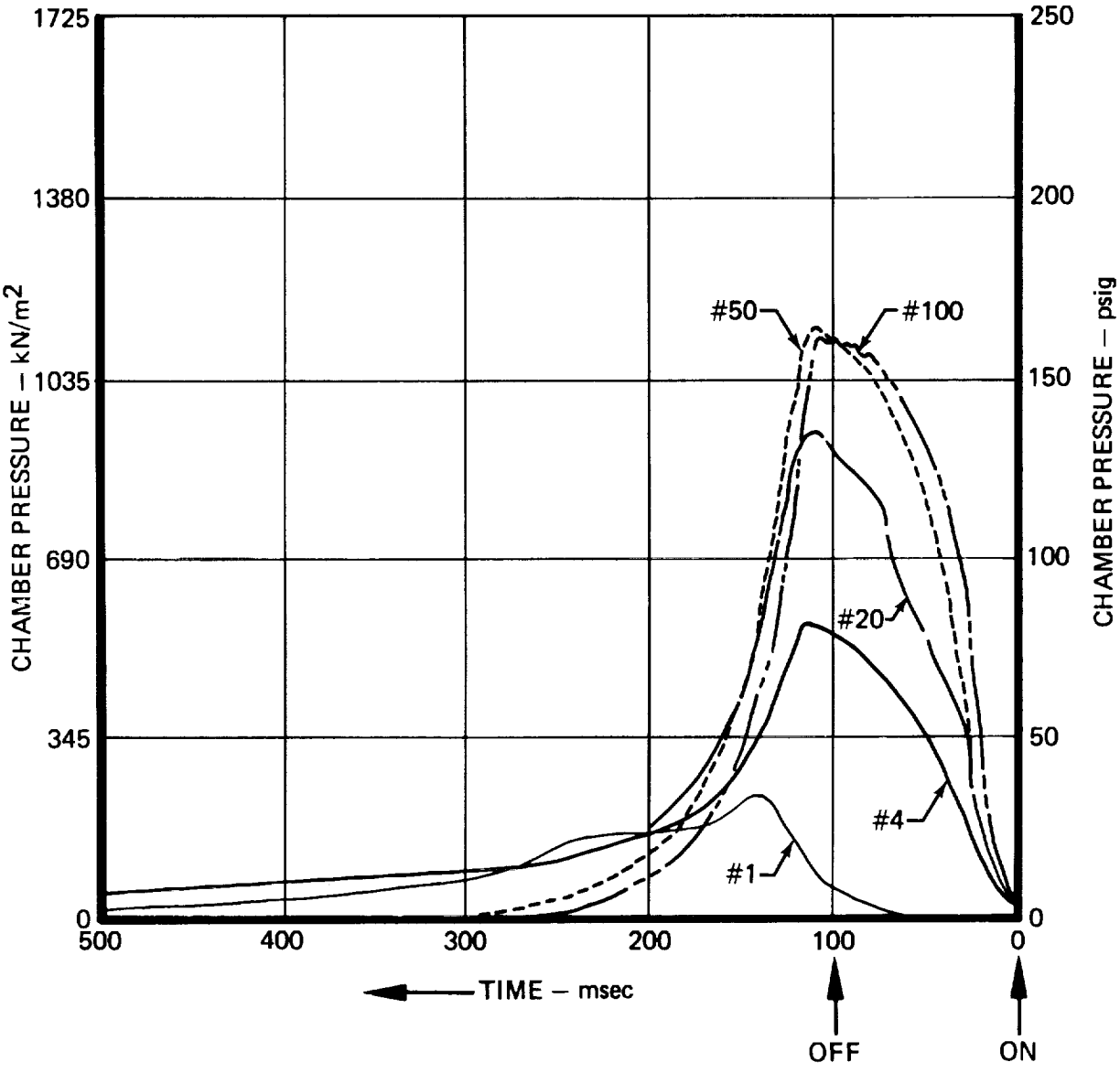

a. *Pulse mode test*: Figure 4-5 shows Shell 405 catalyst chamber pressure pulse overlays taken from oscillograph data. The pressure traces rise faster than the monolithic foam traces because of the higher active metal content in the catalyst. Pressure spiking occurs, then disappears by pulse number 100. Early pulses are better formed and give higher impulse values than the monolithic foam catalyst. Impulse bit data obtained with the number 1 rated monolithic catalyst are plotted with those obtained with the Shell 405 catalyst in Figure 4-6. The early Shell 405 impulse bit values are up to 10% higher than those for the monolithic foam; after 60 pulses, the impulse values are nearly equal.

b. *Steady-state firing*: Figure 4-7 shows the chamber pressure trace from an oscillograph at shutdown of a Shell 405 steady-state firing. Chamber pressure oscillations are slightly lower than those of the 20-mil monolithic catalyst. The Shell 405 chamber pressure tailoff time after shutdown is shorter (85 milliseconds vs. 160 milliseconds) than the foam catalyst times. Figure 4-8 shows startup plots from the steady-state firings of both Shell 405 and the 20-mil foam catalyst. This plot shows that the Shell 405 chamber pressure responds faster during the first 0.5 second of a steady-state firing. After that, however, the chamber pressure of the tungsten foam responds faster. The tungsten foam reaches 90% maximum pressure 1 second sooner than the Shell 405 catalyst. The slower rise time of the Shell 405 catalyst may be attributed to the difference in thermal properties between tungsten and aluminum oxide; the thermal conductivity of tungsten is about 40 times as great as that of aluminum oxide.

Comparison of the 20-mil foam catalyst to the Shell 405 catalyst as loaded in the test firing reactor is shown in Figure 4-9. The monolithic catalyst, with only 27% of the iridium weight used by Shell 405 catalyst, performs as well as or better than the Shell 405 except in pulse-mode performance, chamber pressure oscillations (neither of these is shown in Figure 4-9), and tailoff time. The Shell 405 catalyst, however, will also perform well at higher bed loadings (8 to 9 kg/m^2 sec) for which the reactor was originally designed. Therefore, at the lower bed loadings of 5 to 6 kg/m^2 sec used in these comparison tests, the quantity of Shell 405 catalyst could probably be reduced by shortening the catalyst bed length without any performance degradation. This would reduce the quantity of iridium required for a Shell 405 filled reactor.

4.3.3 Bed Loading

Early monolithic catalyst test firings were conducted at bed loadings of 8 to 12 kg/m^2 sec. This bed loading was used because the test firing reactor had performed well during previous programs when filled with Shell 405 catalyst. Because of the reduced amount of active metal present in a monolithic catalyst bed, it was postulated that reduced bed loadings would improve the performance of the monolithic bed. Consequently, additional chambers with smaller nozzles were made and tested which maintained the same test firing chamber pressure at lower propellant flow rates.

Table 4-3 summarizes the effects of the three bed loadings on various performance parameters. Included in this table is test data from the Shell 405 test firings. In general, the middle value bed

RUN #154 10-5-72
SHELL 405 (25–30 MESH)
.10 SEC ON/.90 SEC OFF DUTY CYCLE
G = 5 kg/m^2 sec

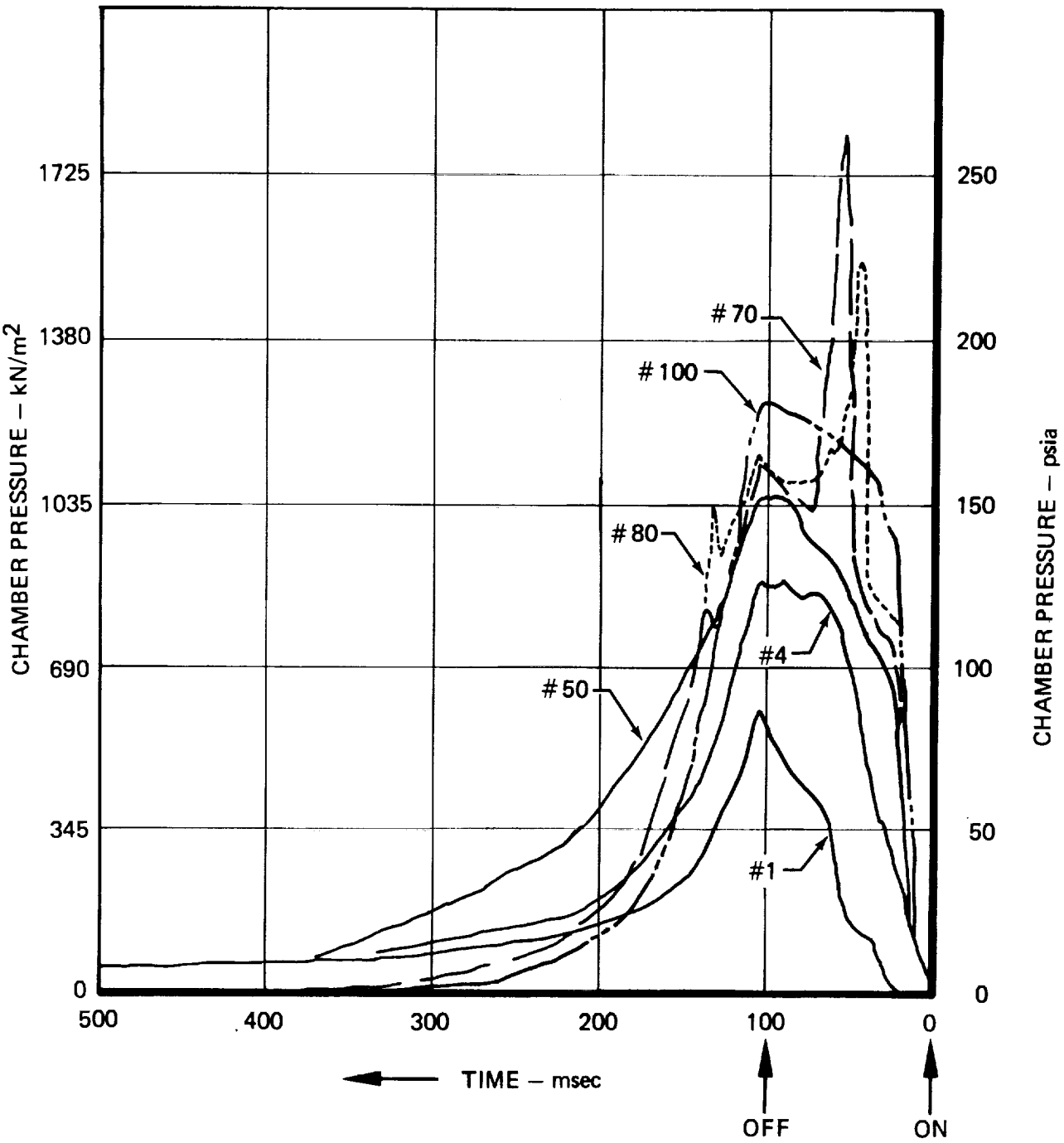

Figure 4-5

PULSE MODE PERFORMANCE OF SHELL 405 CATALYST
AND TUNGSTEN FOAM CATALYST
DUTY CYCLE 0.10 SEC. ON/0.90 SEC. OFF

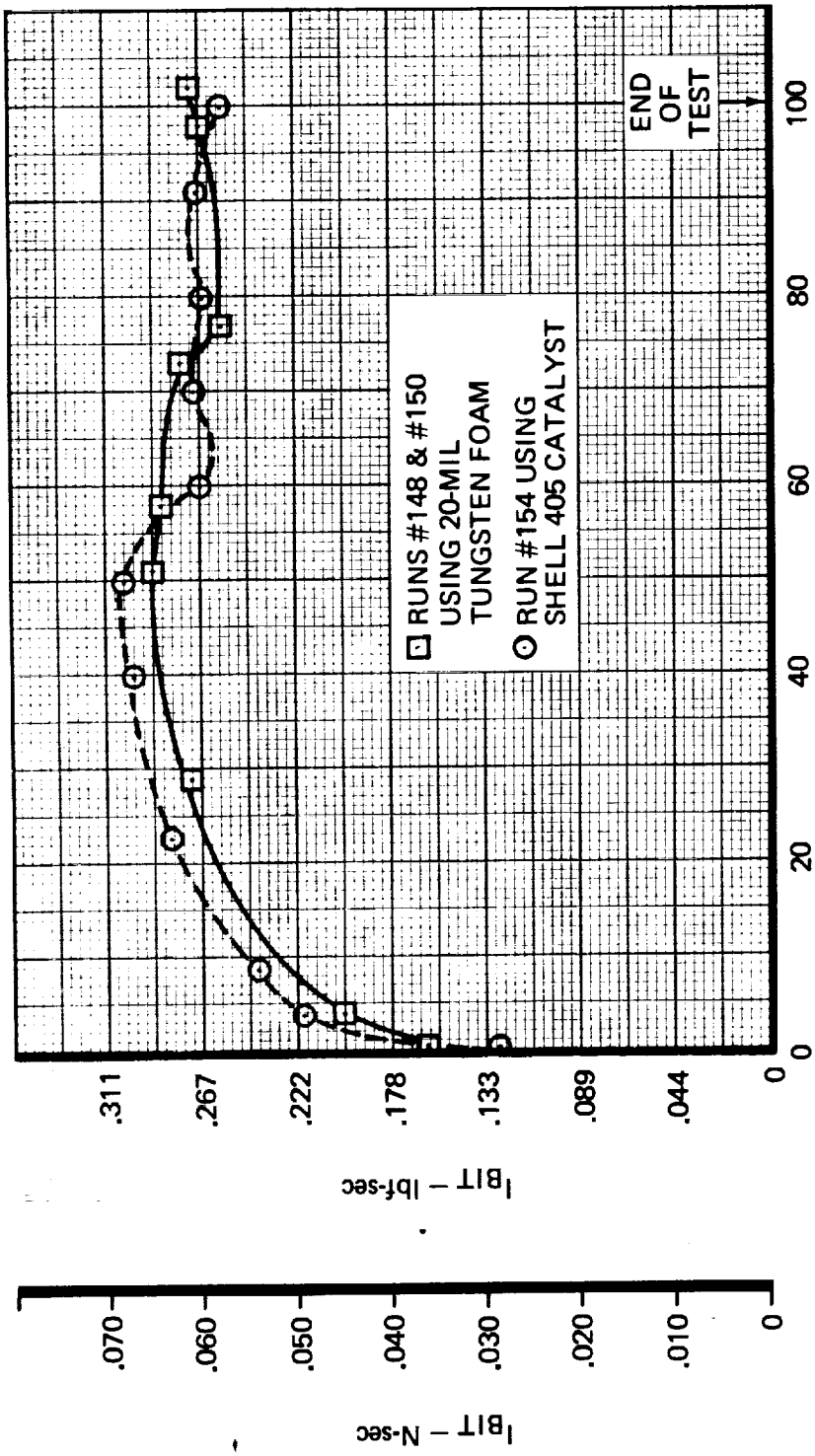

Figure 4-6

11062-52

RUN #155 CHAMBER PRESSURE TRACE AT SHUTDOWN
USING SHELL 405 CATALYST

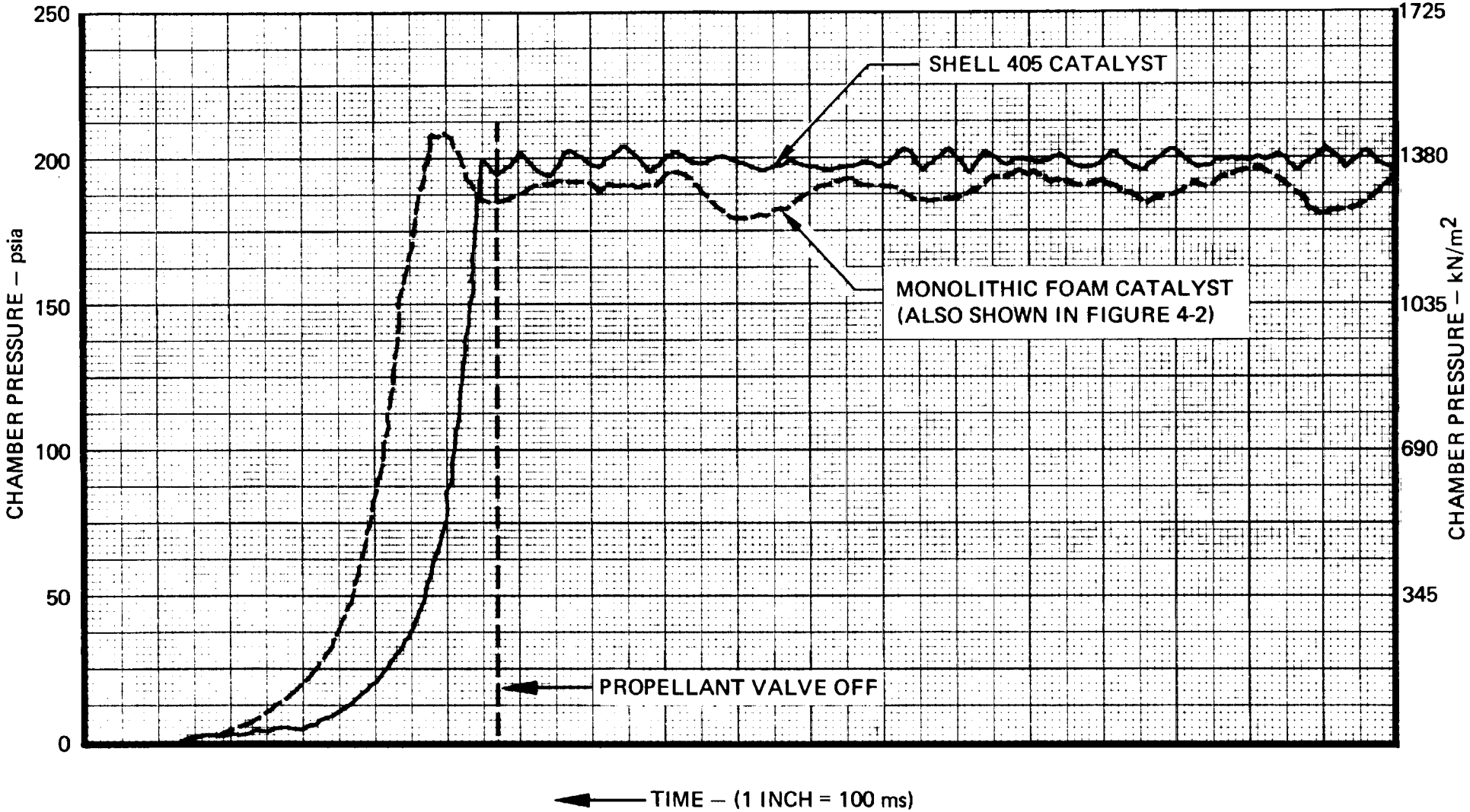

Figure 4-7

COMPARISON OF STARTUP BEHAVIOR OF MONOLITHIC VS.
SHELL 405 CATALYST

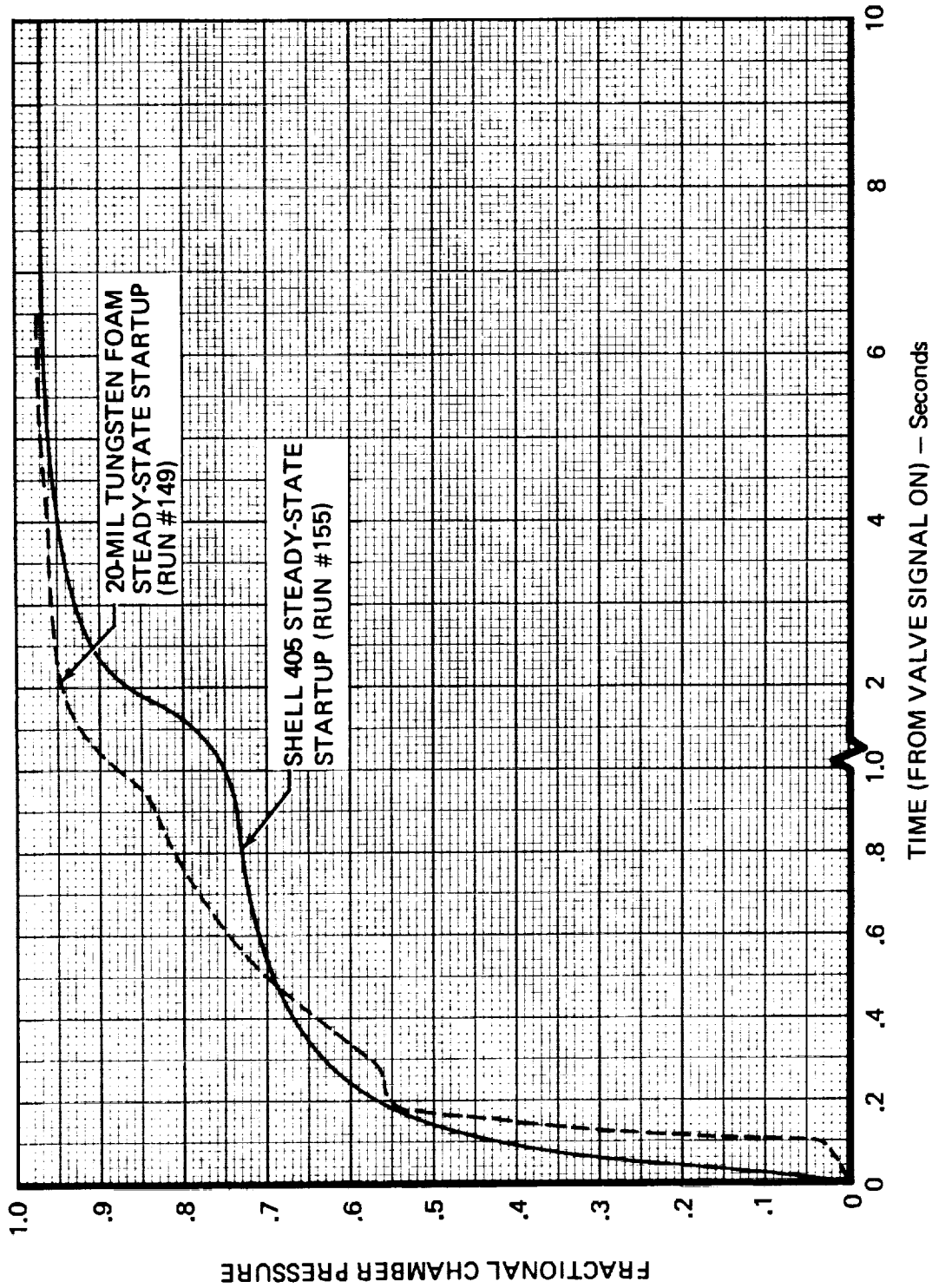

COMPARISON OF SHELL 405 CATALYST (TEST FIRING #154) TO #1 RATED MONOLITHIC CATALYST (TEST FIRING #149)

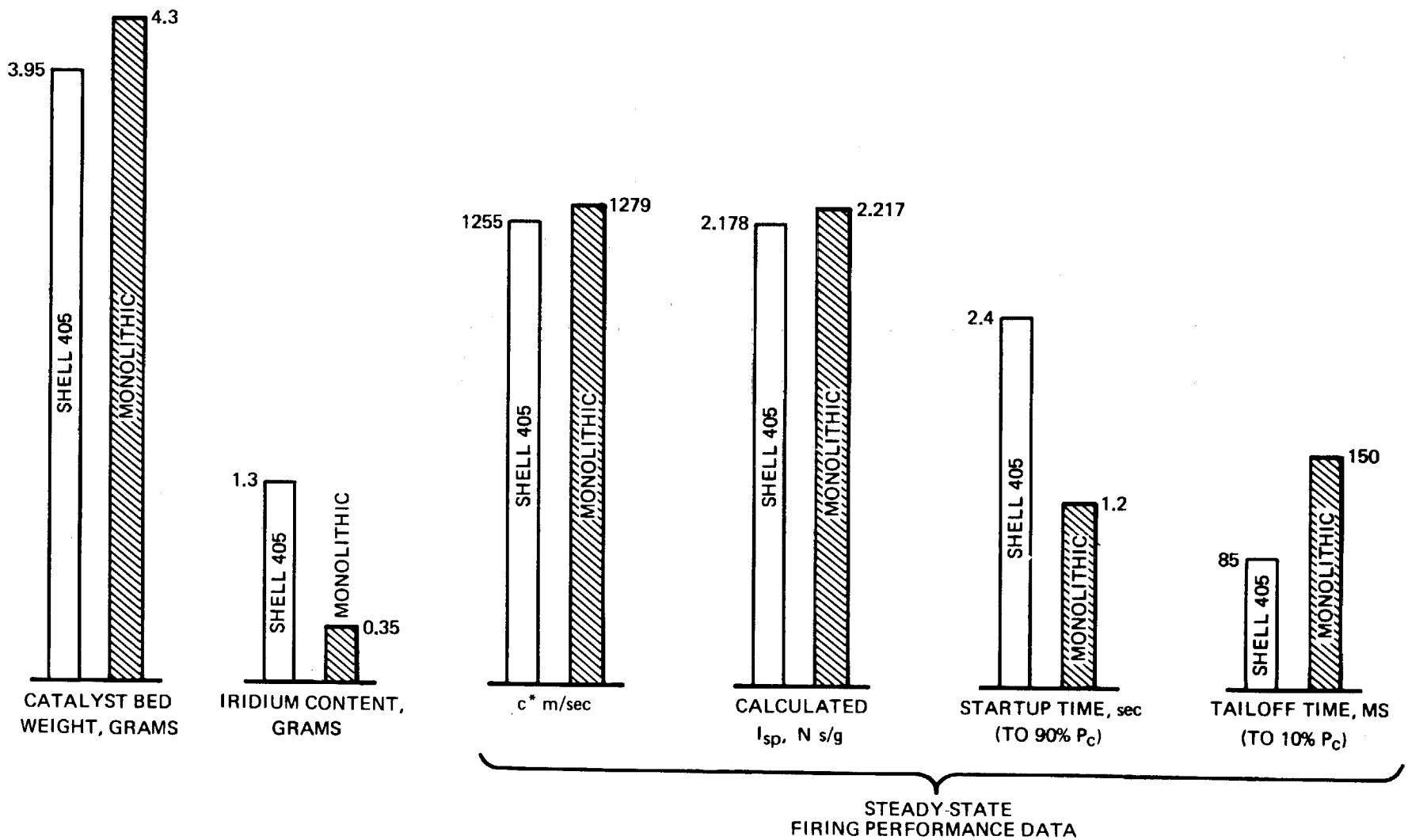

Figure 4-9

loading of 5 to 6 kg/m^2 sec gave higher performance than the higher or lower bed loadings. The exception occurred with the smaller pore size 10-mil tungsten foam catalyst, which performed better at the highest bed loading. The performance of none of the monolithic foam catalysts improved at the bed loading of 3 to 4 kg/m^2 sec.

Table 4-3
THE EFFECT OF BED LOADING ON TUNGSTEN FOAM CATALYST PERFORMANCE
(2 cm Bed Length Only)

	Bed Loading, kg/m^2 sec			
	3-4	5-6	8-9	
Pulse mode Performance	Fair Fair Poor N.A.	Good Good N.A. Excellent	Poor Good Excellent N.A.	20 mil, 9% Ir foam 20 mil, 15% Ir foam 10 mil, 9% Ir foam Shell 405 25-30 mesh
90% P_c response time, sec.	3.5 1.9 2.2 N.A.	1.1 1.2 1.7 2.4	1.3 1.7 5.6 N.A.	20 mil, 9% Ir foam 20 mil, 15% Ir foam 10 mil, 9% Ir foam Shell 405 25-30 mesh
10% P_c tailoff time, ms	270 225 140 N.A.	160 120 60 85	1170 1043 114 N.A.	20 mil, 9% Ir foam 20 mil, 15% Ir foam 10 mil, 9% Ir foam Shell 405 25-30 mesh
Steady-state c* m/sec	1152 1143 904 N.A.	1240 1230 1240 1255	1195 1161 1255 N.A.	20 mil, 9% Ir foam 20 mil, 15% Ir foam 10 mil, 9% Ir foam Shell 405 25-30 mesh
Average chamber pressure roughness ±% P_c	10% 13% 78% N.A.	4% 4% 63% 2%	5% 11% 6% N.A.	20 mil, 9% Ir foam 20 mil, 15% Ir foam 10 mil, 9% Ir foam Shell 405 25-30 mesh

4.3.4 Foam Pore Size

The effect of changing the monolithic catalyst pore size on various performance parameters is shown in Figure 4-10. The plots show that performance is closely related to bed loading as well as pore size; the improvement in performance gained by increasing pore size from 250 to 500 μm (10 to 20 mils) at one bed loading can be offset by a decrease in the same performance parameter at

THE EFFECT OF PORE SIZE ON TUNGSTEN FOAM CATALYST PERFORMANCE (USING 2 CM BED LENGTH REACTOR)

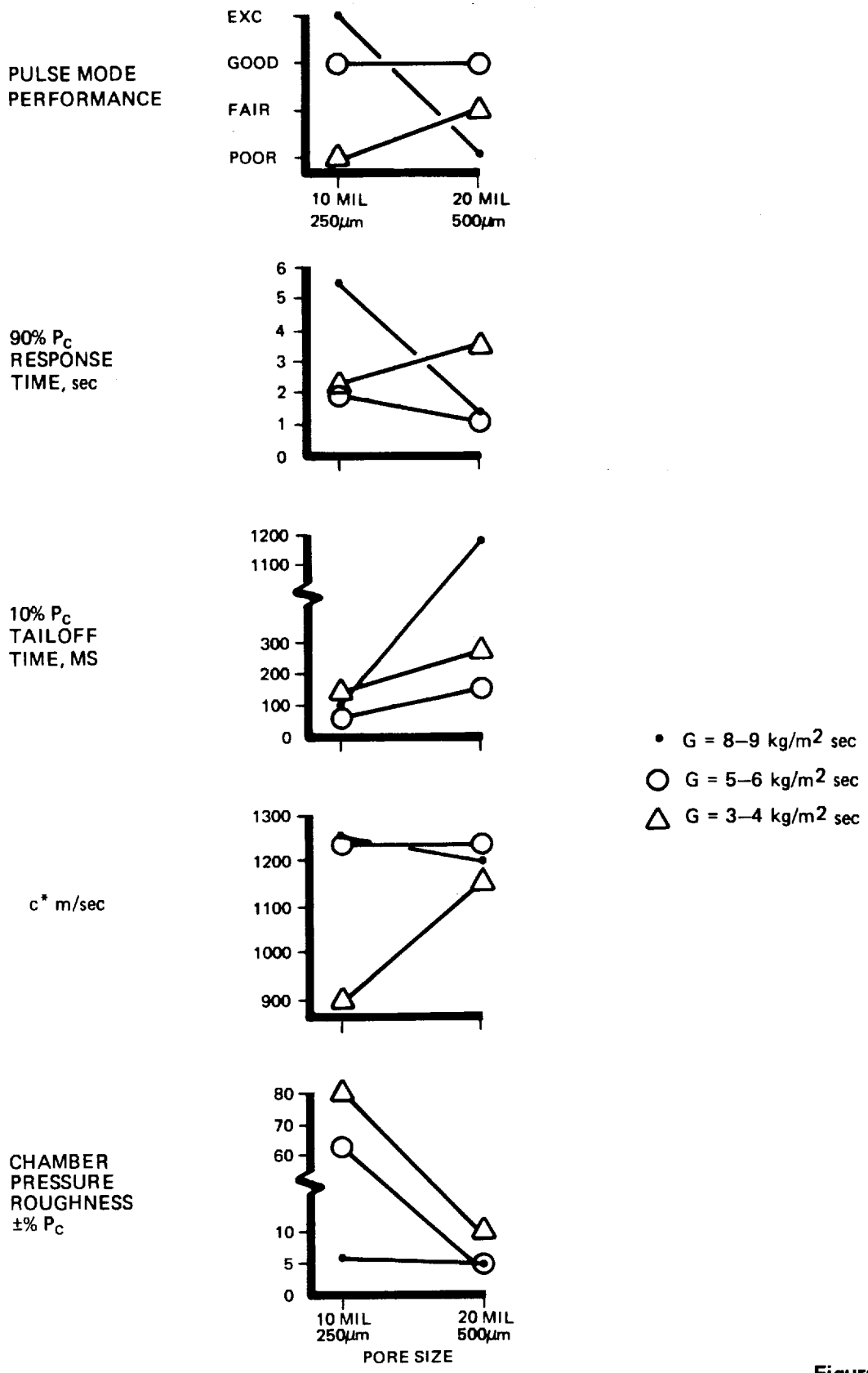

11062-74

Figure 4-10

another bed loading. For example, c* performance can be increased by increasing the pore size if the bed loading is 3 to 4 kg/m^2 sec. However, if the bed loading is 8 to 9 kg/m^2 sec, the c* performance will be decreased by increasing the pore size. In general, the smaller, 10-mil pore size catalyst performs better at higher bed loadings than the 20-mil pore size catalyst. The smaller pore size catalysts had shorter tailoff times but longer startup response times at a given bed loading. The results of these comparisons suggest that foam pore size would be an important factor in designing a reactor used primarily for pulse mode operation. The smaller pore, 10-mil foam with shorter tailoff times, may be more suitable for pulse-mode operation than the 20-mil foam.

4.3.5 Active Metal Content

The effect of increasing the iridium content of the monolithic catalyst from 9 to 15% of the total catalyst weight is shown in Figure 4-11. The higher percentage iridium was applied only to the 20-mil pore size tungsten foam. The improvements in performance gained by increasing the active metal content were 1) higher pulse-mode performance at high bed loadings, 2) a decrease in response time at low bed loadings, and 3) a slight decrease in tailoff times at all bed loadings. None of these slight increases in performance justified the 50% increase in active metal content. The optimum monolithic catalyst iridium content appears to be about 9% of the total catalyst weight (or 33% of the ceramic coating plus the active metal weight).

4.3.6 Bed Length

During the parametric evaluation test series, two test firings were conducted using a reactor having a 4-centimeter bed length instead of the regular 2 centimeter bed length. It was anticipated that the longer bed would decrease steady-state chamber pressure oscillations by increasing the propellant residence time in the bed. Figure 4-12 plots the effects of the longer bed and shows the chamber pressure oscillations increased with increased bed length. Other performance parameters were degraded or unimproved using the longer bed. The 2-centimeter bed length appears to be adequate for the bed loadings tested.

4.4 OPTIMUM CATALYST SELECTION

Based on the results of the parametric evaluation testing, the following catalyst and operating conditions were selected for the Task 11 useful life test firings:

Foam material: Tungsten

Foam pore size: 20 mil (500 μm)

Foam surface roughening procedure: dusted on tungsten powder

Ceramic loading: 0.3 g/cm^3

Iridium content: 9%

Reactor bed length: 2 centimeters

Reactor bed loading: 5 to 6 kg/m^2 sec

THE EFFECT OF ACTIVE METAL CONTENT ON TUNGSTEN FOAM CATALYST (USING 20 MIL FOAM ONLY)

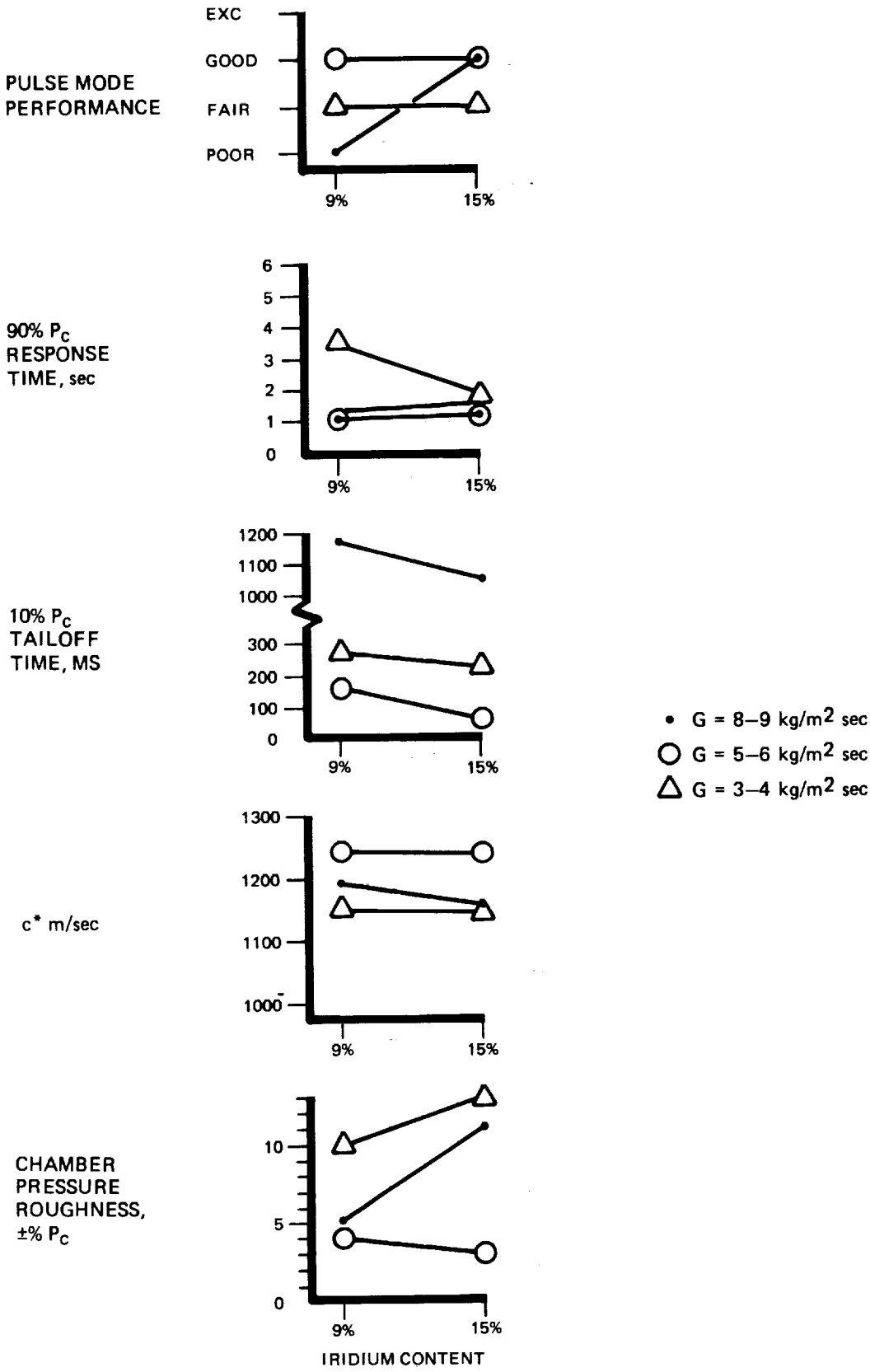

Figure 4-11

THE EFFECT OF BED LENGTH ON TUNGSTEN FOAM CATALYST PERFORMANCE (USING 20 MIL, 9% IRIDIUM CATALYST)

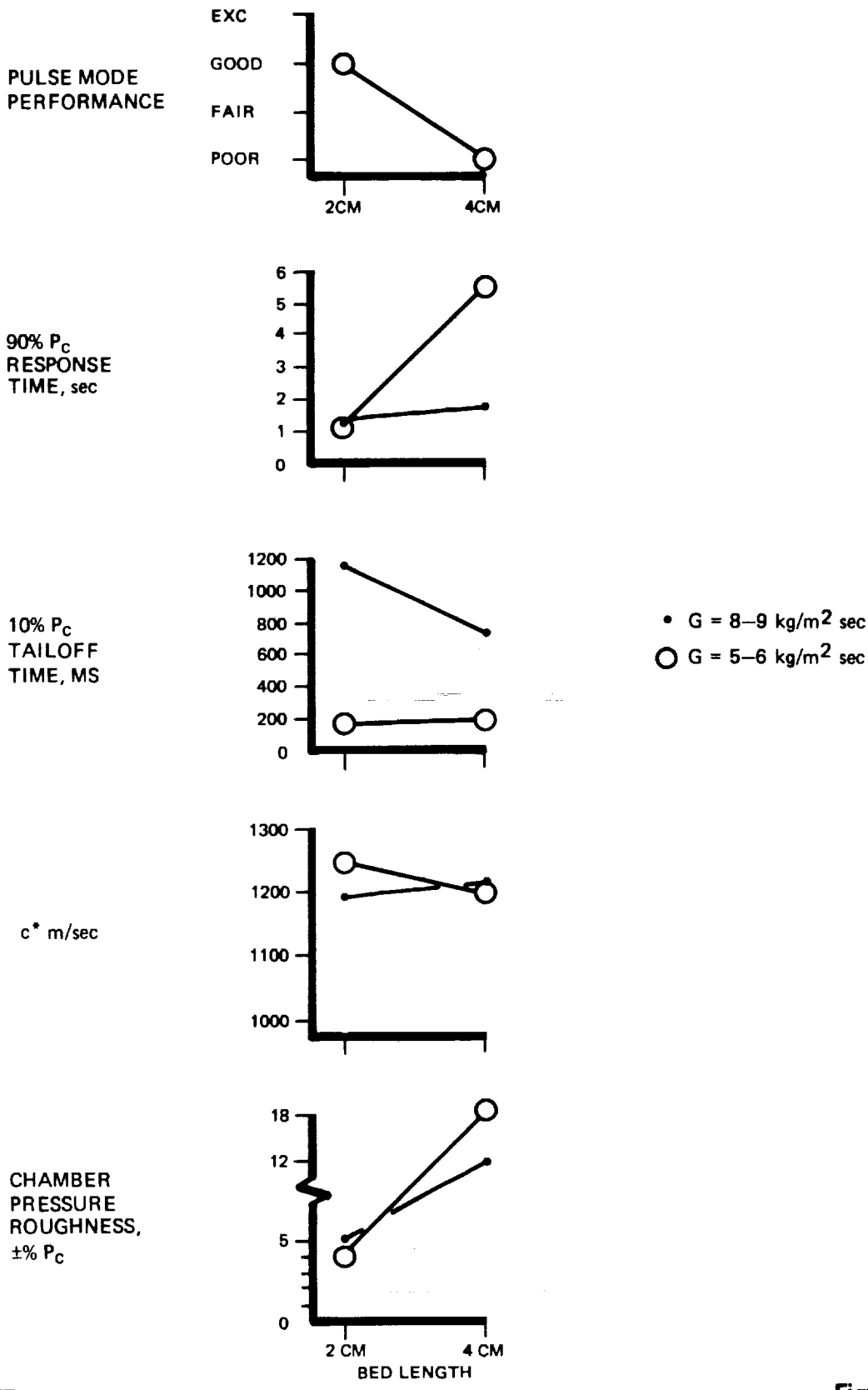

4.5 USEFUL LIFE EVALUATION

4.5.1 Test Procedure

The optimum monolithic foam catalyst described in the preceding paragraph was loaded into the same reactor used in the Task 10 test firings and subjected to the test firing duty cycle given in Table 4-4. The purpose of this life evaluation duty cycle was to accumulate a large number of cold starts on the monolithic catalyst and measure any performance degradation that occurred in both pulse-mode and steady-state duty cycles. The test firing duty cycle consisted of 60-second steady-state firings combined with pulse trains fired at a 10% duty cycle (100 milliseconds on/900 milliseconds off).

Table 4-4
USEFUL LIFE EVALUATION DUTY CYCLE

Sequence	Duty Cycle	Inlet Pressure
A-1	60 secs steady state	Maximum (2,860 kN/m^2)
A-2		90% maximum (2,575 kN/m^2)
A-3		80% maximum (2,290 kN/m^2)
A-4		70% maximum (2,000 kN/m^2)
A-5		50% maximum (1,430 kN/m^2)
A-6		35% maximum (1,000 kN/m^2)
A-7		25% maximum (715 kN/m^2)
A-8	60 secs steady state	10% maximum (286 kN/m^2)
B	50 pulses: 100 ms on, 900 ms off	Maximum
C	Repeat B 9 times	
D	60 secs steady state	
E	Repeat B, C, & D 9 times	
F	Repeat A	

The useful life evaluation tests were started with a series of eight 60-second steady-state firings at various propellant inlet pressures. These firings were followed by groups of 10 pulse trains with each group followed by one steady-state firing. The useful life tests were concluded with a repeat of the initial eight 60-second steady states.

The following test conditions were imposed during useful life evaluation test firings:

Maximum fuel inlet pressure:	2,860 kN/m^2 (400 psig)
Maximum reactor startup temperature:	311^{o}K (100^{o}F)
Maximum fuel inlet temperature:	305^{o}K (90^{o}F)

The reactor was fired in a 24-cubic-meter vacuum chamber at simulated altitude conditions (initial pressure equivalent to 73 km altitude). Following the completion of each test firing, the reactor was allowed to cool to 311°K (100°F) or less prior to firing the next sequence. The reactor cooloff time was reduced from 90 to 40 minutes by slowly bleeding gaseous nitrogen into the vacuum chamber following a firing. A maximum nitrogen pressure of 21 to 28 kN/m^2 (3 to 4 psia) was attained in the chamber during cooling periods. The nitrogen was pumped from the chamber before firing the reactor again.

4.5.2 Test Results

The monolithic foam catalyst bed completed the useful life evaluation test firing duty cycle without performance degradation. The catalyst bed accumulated the following test firing totals:

Cold-bed starts:	133
Firing time:	2,460 seconds
Pulses on bed:	5,132

Table 4-5 summarizes performance data from each of the 26 steady-state firings of the useful life test. These steady-state firings served as performance baseline checks between the pulsing duty cycles throughout the life test. The monolithic catalyst bed's various performance parameters are discussed below:

a. *C* Performance* – As shown in Table 4-5, the steady-state C* values did not decrease during the life test. This indicates no change in hydrazine decomposition products or exhaust gas temperatures during the test firings.

b. *Ignition Delay* – Figure 4-13 presents ambient temperature ignition delays obtained during the life test. The initial delay time of 50 milliseconds increased to 90 to 100 milliseconds at the end of the life tests. The gradual increase in ignition delay times noted indicates some loss of catalyst bed activity as the test progressed. However, the rate of increase leveled off and ignition delay remained constant after 40 cold starts.

c. *Response Time* – Figure 4-14 plots the times required for the reactor to achieve 90% of the final chamber pressure as obtained during each high-pressure, steady-state firing. The response times did not change appreciably during the life test after the initial steady-state firing. Figure 4-15 presents the steady-state startup transients of the first and last life test high-pressure steady-state firings. The roughness occurring in both startups did not exceed the final chamber pressure values and are not considered damaging to the bed.

   The oscillograph trace from the last steady-state firing is presented in Figure 4-16. This pressure trace shows that what appears to be sharp pressure spikes in Figure 4-15 are slower pressure excursions possibly caused by delayed propellant decomposition. These startup pressure excursions were not typical of the monolithic foam beds tested in Task 9 or Task 10; startups of these previous foam beds were similar to the pressure trace shown in Figure 4-8 for Run No. 149. The startup characteristics of the foam sample used for life testing were unique and appear to be the result of foam processing variables and/or variables associated with assembling the reactor.

Table 4-5

LIFE EVALUATION TEST STEADY-STATE FIRING SUMMARY

Sequence No.	Cold Start No.	Accumulated Firing Time (sec)	Accumulated Pulses	Inlet Pressure (% Max)	Bed Loading $\frac{Kg}{(m^2\text{-sec})}$	Response Time		Tailoff Time	Hardness Ratio $\frac{P_f - P_c}{P_c}$	Nominal Pressure Oscillations $\pm\%$ P_c	c* (m/sec)
						Start P_c Rise (ms)	90% P_c (sec)	10% P_c (ms)			
A-1	5	280	104	100	5.5	50	1.3	110	0.99	3.5	1,235
A-2	6	340	105	90	5.0	60	1.2	110	0.94	3.5	1,240
A-3	7	400	106	80	4.7	50	1.0	110	0.88	3	1,230
A-4	9	520	108	71	4.3	60	1.4	115	0.81	3	1,230
A-5	10	580	109	51	NA	70	1.6	125	0.68	4.5	NA
A-6	11	640	110	38	NA	NA	1.7	145	0.57	5	NA
A-7	12	700	111	28	NA	70	2.3	400	0.49	2.5	NA
A-8	13	760	112	13	NA	60	2.5	1,500	0.40	1	NA
D	24	870	613	100	5.4	90	0.95	110	1.00	3.5	1,220
E-11	35	980	1,114	↕	↕	90	0.80	110	1.00	3.5	1,230
E-22	46	1,090	1,615			100	0.95	110	1.01	3	1,220
E-33	57	1,200	2,116			85	0.85	115	1.05	3	1,210
E-44	68	1,310	2,617			90	0.90	105	1.00	3.5	1,220
E-55	79	1,420	3,118			95	0.90	115	0.99	3.5	1,230
E-66	90	1,530	3,619			95	0.90	110	0.99	3.5	1,230
E-77	101	1,640	4,120			115	0.90	115	1.00	4	1,230
E-88	112	1,750	4,621			110	0.80	110	0.99	3.5	1,240
E-99	123	1,860	5,122			95	1.00	110	1.01	3.5	1,225
F-1	124	1,920	5,123	100	5.4	90	1.00	110	1.01	4	1,225
F-2	125	1,980	5,124	90	5.1	80	0.95	190	0.94	5	1,220
F-3	126	2,040	5,125	81	4.7	90	1.10	290	0.89	4	1,220
F-4	127	2,100	5,126	71	4.2	60	1.30	270	0.82	6	1,230
F-6	129	2,220	5,128	37	NA	60	1.70	470	0.61	16	NA
F-7	130	2,280	5,129	28	NA	80	2.70	600	0.56	7	NA
F-9	132	2,400	5,131	51	NA	90	1.40	125	0.70	6	NA
F-10	133	2,460	5,132	13	NA	120	3.10	2,000	0.47	1.5	NA

NOTE: Several test firings were conducted on the catalyst prior to life testing.

NA indicates propellant flow rate was too low to register on flowmeters.

REACTOR IGNITION CHARACTERISTICS DURING LIFE EVALUATION TEST

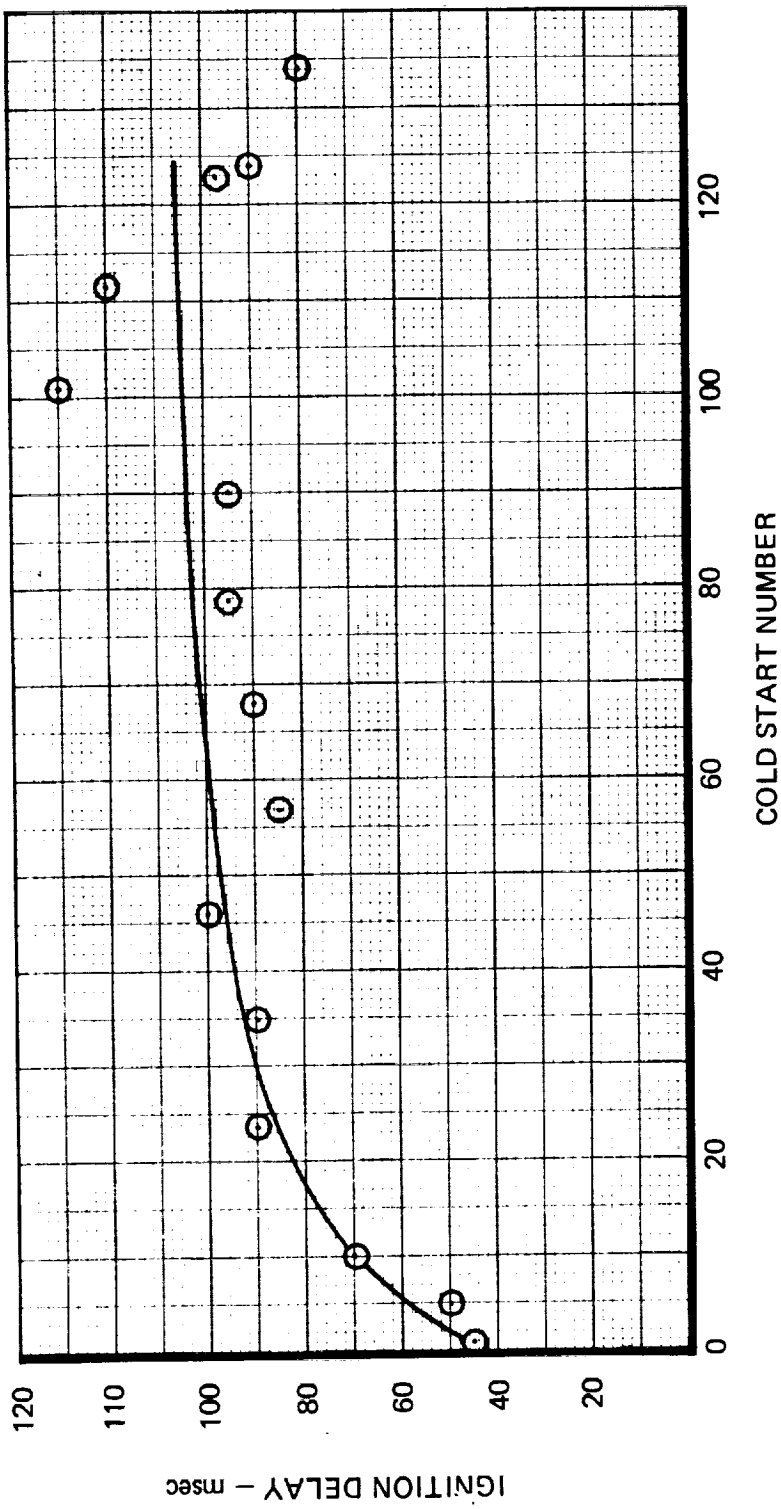

NOTE: IGNITION TIMES SHOWN ARE FROM
MAXIMUM INLET PRESSURE
STEADY-STATE FIRINGS

REACTOR RESPONSE TIMES TO 90% MAXIMUM CHAMBER PRESSURE
DURING LIFE EVALUATION TESTS

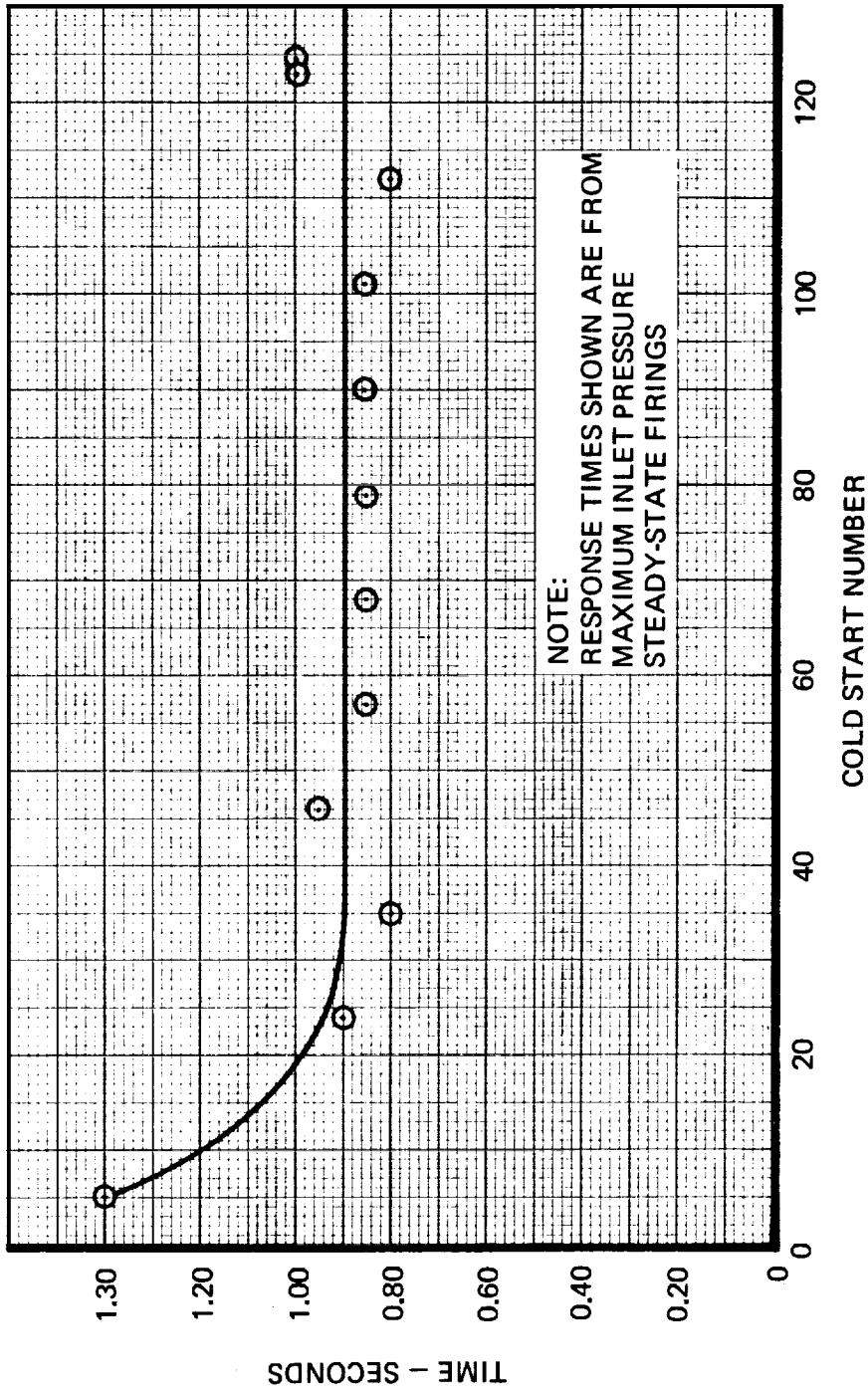

REACTOR RESPONSE CHARACTERISTICS – LIFE EVALUATION FIRINGS

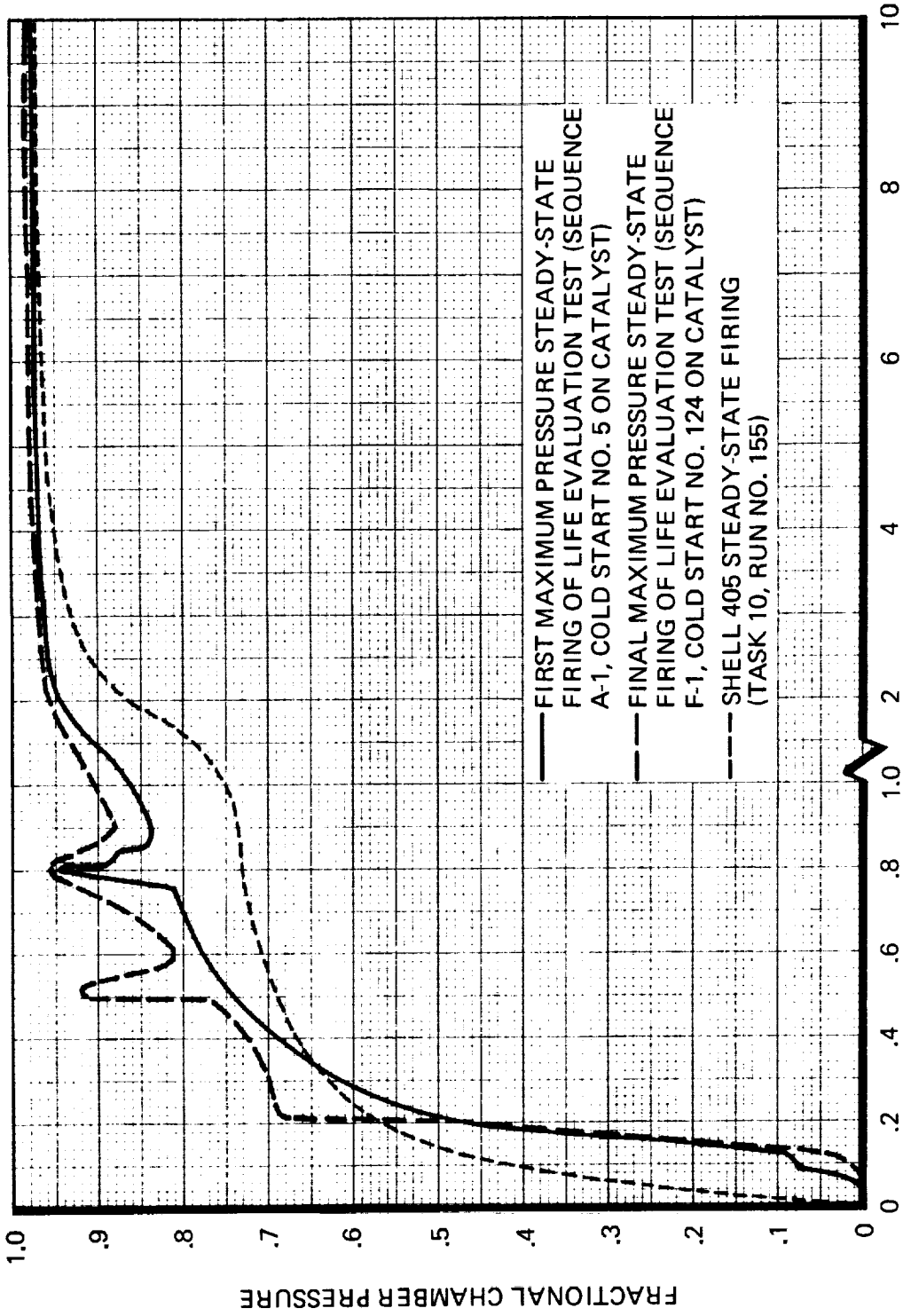

Figure 4-15

11064-92

REACTOR STARTUP PRESSURE TRACE FROM FINAL MAXIMUM PRESSURE STEADY-STATE FIRING OF LIFE EVALUATION TEST (OSCILLOGRAPH DATA TRACE)

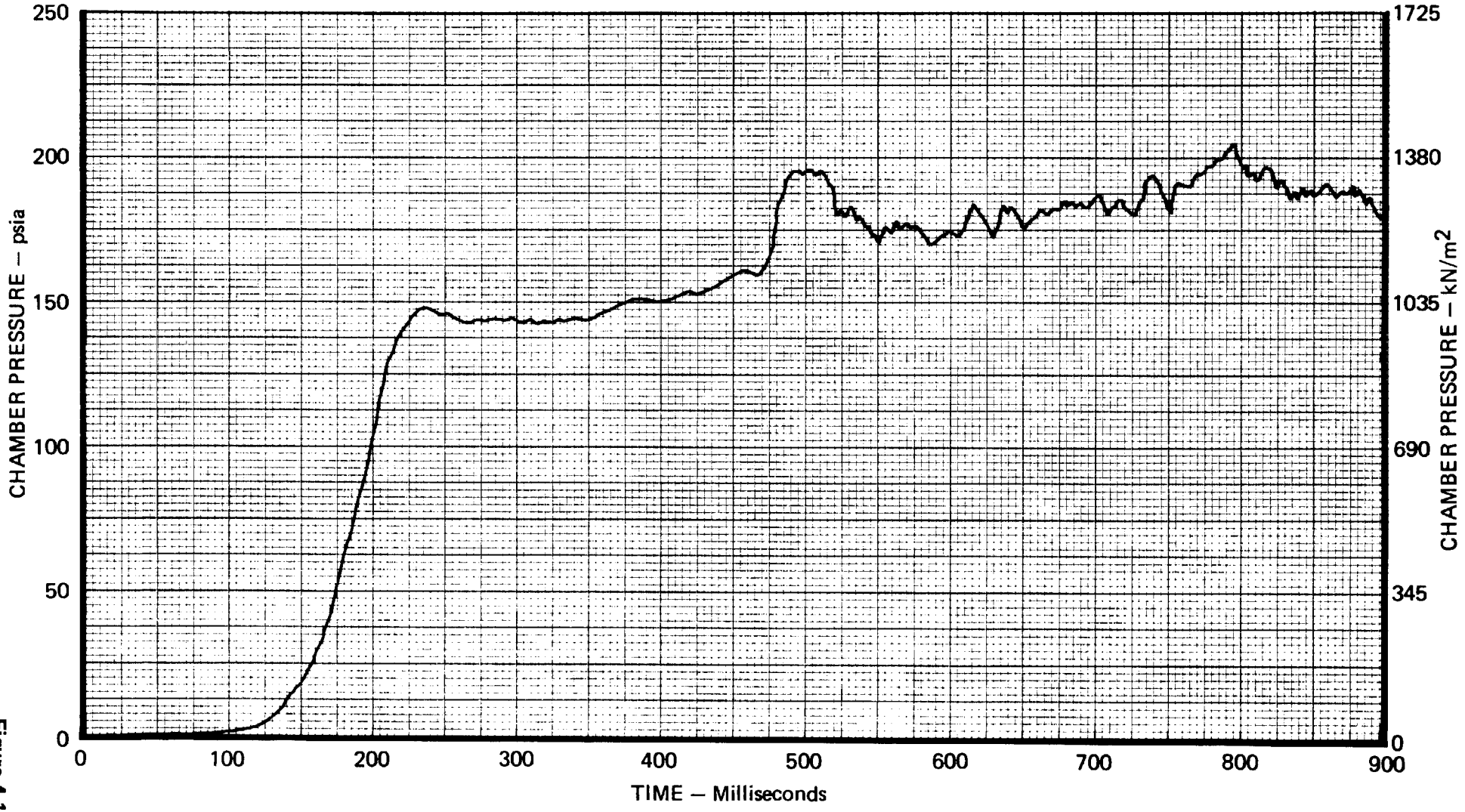

Figure 4-16

d. *Chamber Pressure Oscillations* – Figure 4-17 shows the variation in reactor chamber pressure oscillations during all steady-state firings. The oscillations during the maximum pressure firings did not increase throughout the life test. At lower than maximum inlet pressures, however, the oscillations increased appreciably, as indicated by the two series of test firings at each lower feed pressure. The two lowest feed pressure steady-state firings (10% maximum P_F nominal, 13% maximum P_F actual) ran very smooth during both test firings.

e. *Tailoff Time* – As shown in Table 4-5, the tailoff response times to 10% of final chamber pressure remained constant at about 110 milliseconds throughout the life test for the high-pressure steady-state firings. The tailoff times increased only when the feed pressures were decreased. The constant tailoff response times indicate the catalyst bed did not form a significant void volume during the life test.

f. *Pulse-Mode Performance* – Chamber pressure transients from the first life evaluation pulse train of 50 pulses are shown in Figure 4-18. They may be compared with the transients obtained during the last pulse train fired, shown in Figure 4-19. Some decrease in catalyst bed activity is evident from the slower responding number 1 pulse; however, subsequent pulses responded well as the reactor warmed.

   The impulse bit values obtained from individual pulses during the first, middle, and last pulse trains are presented in Figure 4-20. The maximum loss in impulse bit per pulse during the life evaluation is approximately 10%. Very little decrease in the impulse bit characteristics occurred during the last half of the life test series. It is postulated that the monolithic bed could have sustained many more cold-start pulse trains at the same level of activity.

4.5.3 Exhaust Gas Analysis

Following the life evaluation test duty cycle, a maximum-pressure steady-state firing was made using the same monolithic catalyst bed. A sample of the exhaust gas was taken and analyzed. The gas sample showed that 59% of the ammonia was dissociated. This amount of dissociation is typical of Shell 405 catalyst performance in this reactor.

REACTOR PRESSURE OSCILLATIONS AT VARYING FEED PRESSURES
DURING LIFE EVALUATION TESTS

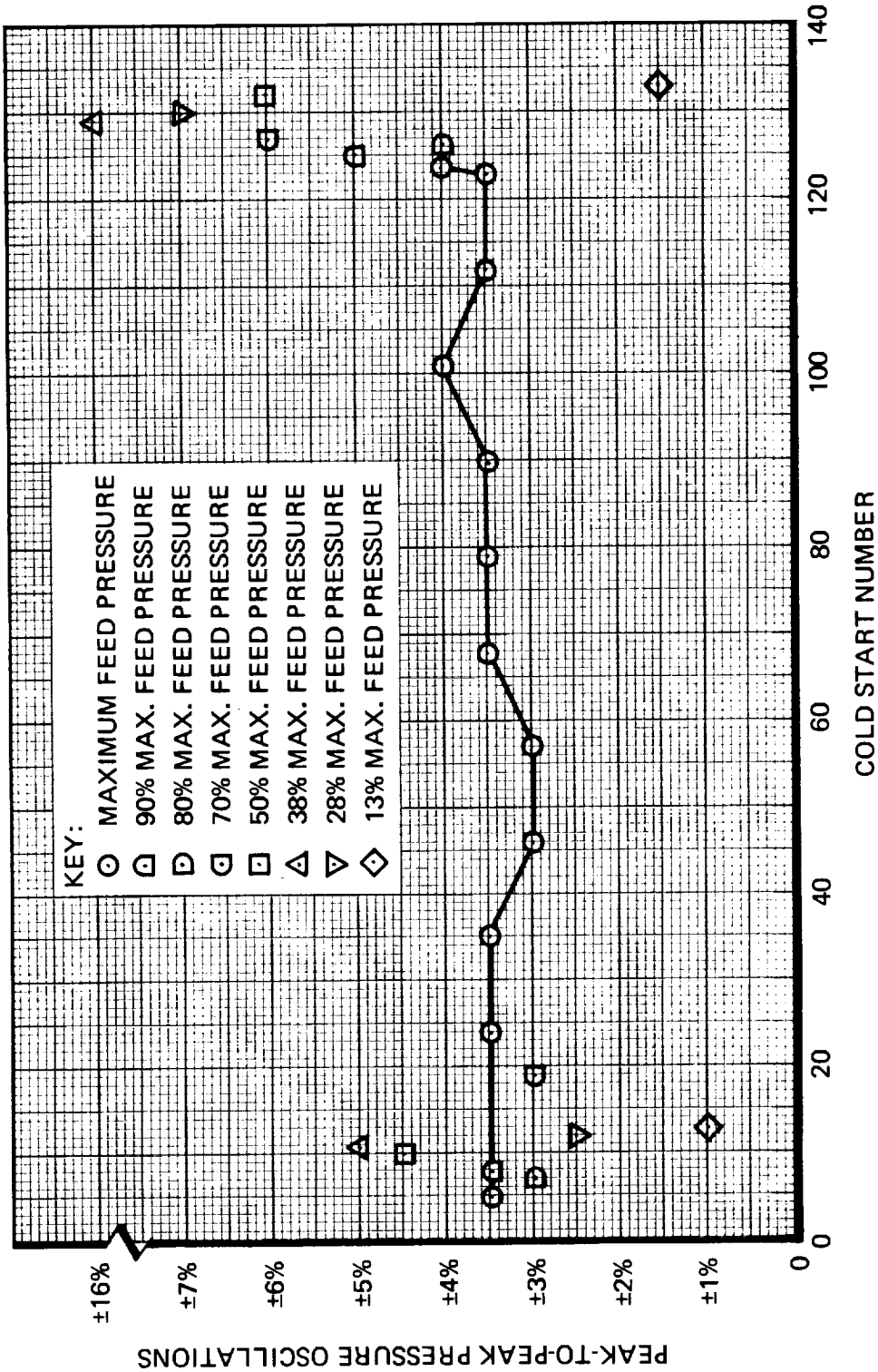

Figure 4-17

FIRST PULSE TRAIN (14th COLD START ON CATALYST BED)
TRANSIENT DURING LIFE EVALUATION TESTS

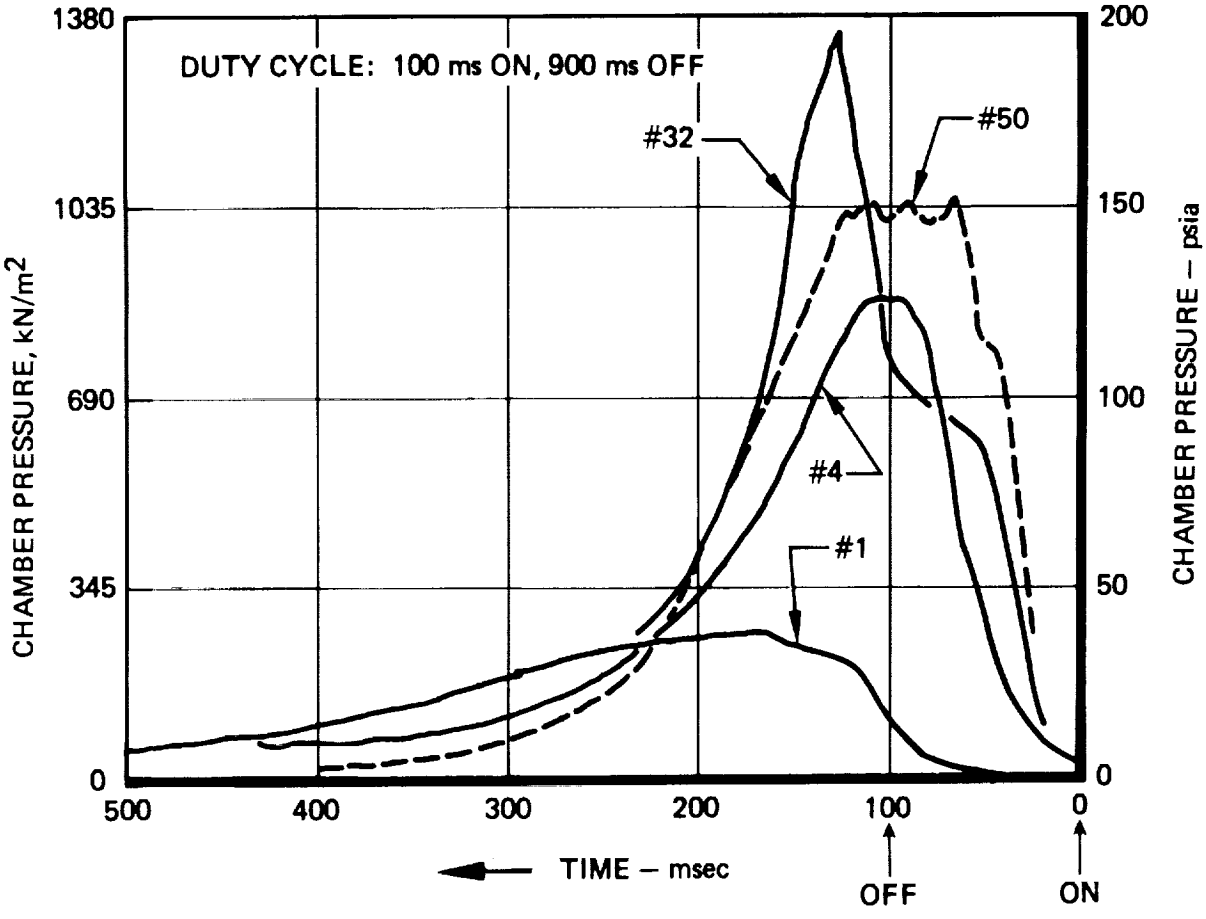

FINAL PULSE TRAIN (122nd COLD START ON CATALYST BED)
TRANSIENTS DURING LIFE EVALUATION TESTS

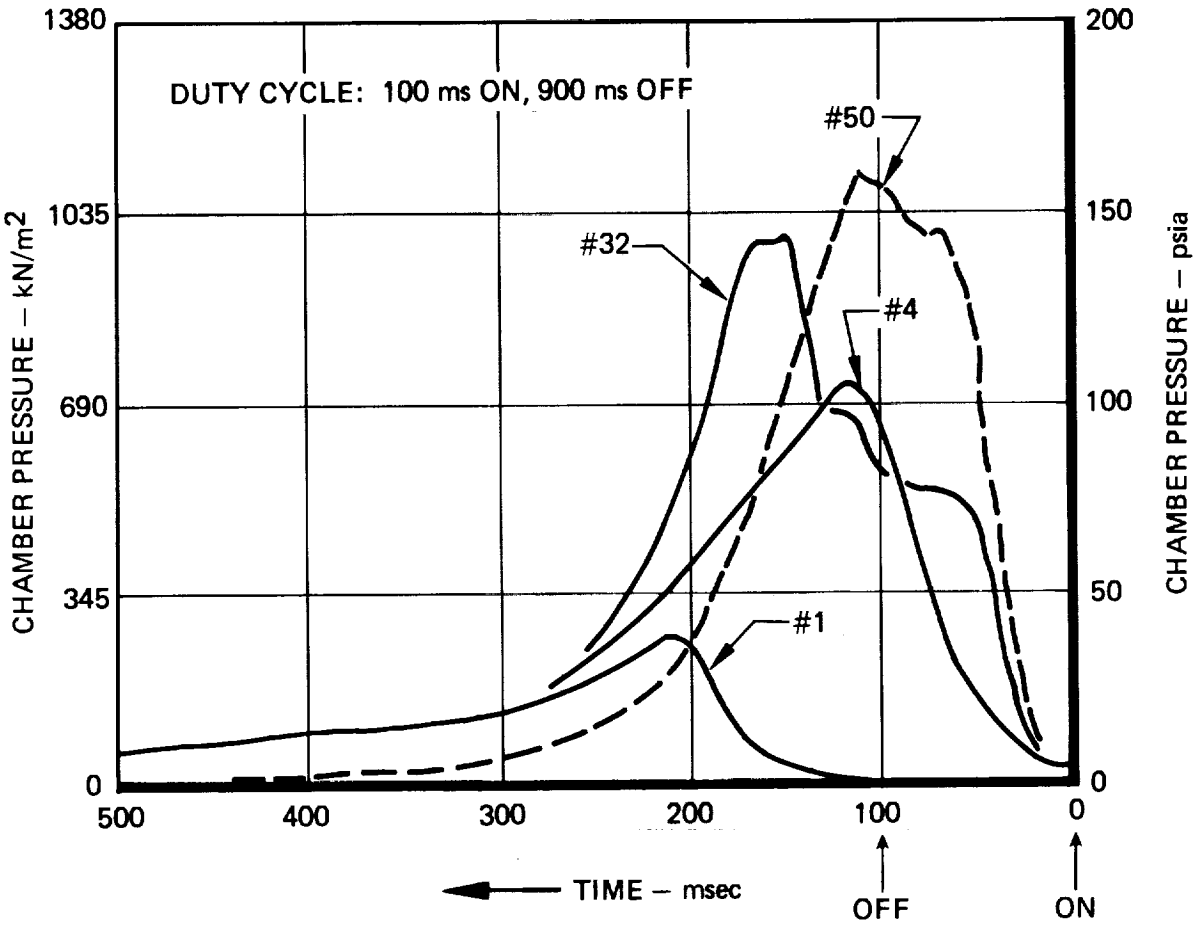

PULSE MODE PERFORMANCE DURING LIFE EVALUATION TEST

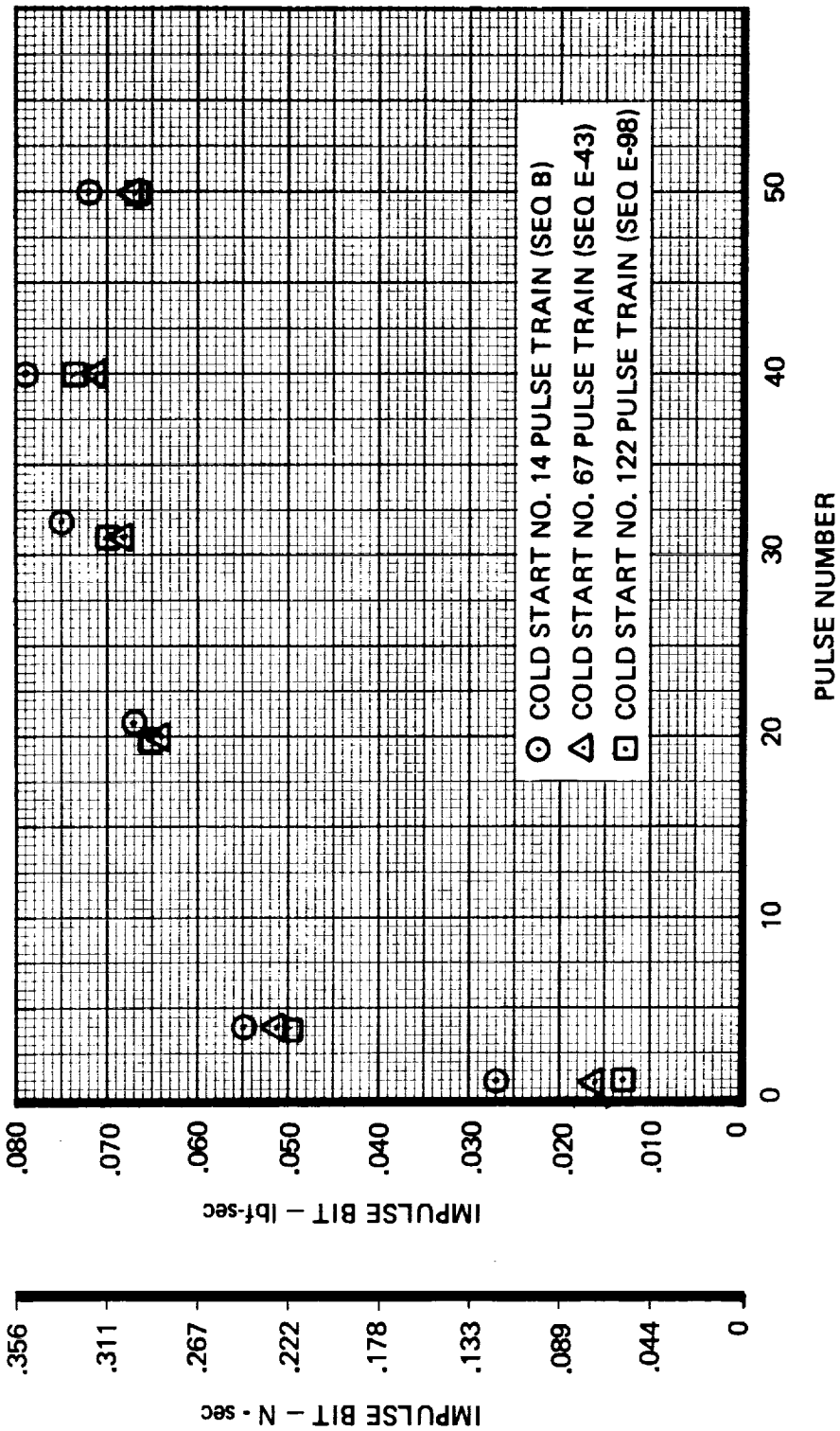

5.0 CONCLUSIONS AND RECOMMENDATIONS

The feasibility of developing a monolithic catalyst bed for hydrazine reactors which has catalytic activity comparable to Shell 405 catalyst has been demonstrated during this program. The monolithic catalyst uses only about one-third the amount of the expensive active metal, iridium, compared to an equivalent volume of Shell 405 catalyst, yet the monolithic catalyst has many performance characteristics equivalent to Shell 405 catalyst.

From the results of the life test it is postulated that the catalyst would have performed beyond the 133 cold starts, 5,132 pulses, and 2,460 seconds accumulated burn time without significant deterioration. It appears that in a monolithic catalyst the active metal is located where it is actually needed, namely on the surface of the catalyst support, whereas in Shell 405 a significant fraction of the active metal is in the core of the granules or pellets and does not contribute much to hydrazine decomposition. The results of this program are very encouraging and indicate that monolithic foam catalyst is a practical hydrazine reactor catalyst with performance characteristics comparable to Shell 405.

Additional developmental work with the monolithic catalyst is recommended in several areas to demonstrate the full potential of this unique catalyst. The major objectives of additional work are:

a. Develop an alternate source for tungsten foam material to avoid undesirable sole source procurement.

b. Develop foam fabrication process controls, so that different production lots of foams will have similar physical properties, including crush strength and surface finish.

c. Conduct further performance tests using a larger 5-lbf (22 N) reactor which uses a more sophisticated injector design giving improved propellant flow distribution. Preliminary test results showed that the performance of monolithic catalyst beds can be improved by using improved injection techniques. The 5-lbf reactor is a common size, available reactor for which much Shell 405 performance data already exists.

d. Study the potential logistic advantages of monolithic catalyst grains for on-site (on the space vehicle) refurbishment of flanged reactors. This may be particularly attractive for Space Shuttle and other reusable vehicles.

APPENDIX A

OPEN-CELL METAL FOAM MATERIAL SPECIFICATION

1.0 SCOPE

This specification defines the requirements for open-cell metal foams to be used in catalytic reactors.

2.0 APPLICABLE DOCUMENTS

None.

3.0 REQUIREMENTS

3.1 Foam Structure

The foam shall have a reticulated structure made up by a continuous network of ligaments. Each cell is surrounded by 8 to 24 windows (nominal 12).

3.1.1 Cell Structure

The foam shall be an open-cell foam; i.e., the windows of the cells shall not be closed by membranes. The number of closed windows shall not exceed two (2) percent of all windows present.

3.1.2 Ligament Structure

The ligaments making up the foam structure may be hollow. The ligament walls may have holes up to 1/10 of the diameter of the ligament, up to a maximum of three (3) holes per ligament between nodes. The foam shall be a continuous network of ligaments; i.e., the ligaments may not have cracks, but must interconnect all junctions. No more than five (5) percent of the ligaments on a machined surface and no more than one (1) percent of the ligaments present at a depth of more than one (1) cell diameter inside the foam may fail to connect neighboring junctions. To be regarded as a crack, the imperfection does not have to run all around the ligament. No more than one (1) percent of the ligaments present at a depth of more than one (1) cell diameter inside the foam shall be split lengthwise.

3.1.3 Ligament Thickness

Unless otherwise specified on the purchase order, the ligament thickness shall be within five (5) to thirty (30) percent of the cell diameter.

3.1.4 Cell Diameter

The nominal cell diameters shall be specified on the purchase order. If the term "pore size" is used instead it shall refer to the cell diameter, not to the cell window diameter.

The cell diameter shall be determined under the microscope with a reticle, measuring the inside distance of two (2) opposing ligaments or junctions.

3.1.5 Cell Diameter Uniformity

Within one (1) sample, the cell diameter shall not vary by more than $\pm$ 20 percent from the nominal diameter. The cell diameter shall be the same in all three (3) perpendicular directions. The mechanical properties shall be isotropic. Foams which have been compacted to increase the density shall not be acceptable.

3.2 Bulk Density

The bulk density of each individual sample prior to the application of eventual additional coatings shall be within $\pm$ 10 percent of the density specified on the purchase order.

3.3 Dimensional Tolerances

If tolerances of machined samples are not specified by the purchase order, the following standard tolerances shall apply:

Diameter Width or Thickness (inches)	Tolerance (inches)
Up to 1, inclusive	± 0.030
Over 1 to 10, inclusive	± 0.050
Over 10	± 0.100

Length (inches)	Tolerance (inches)
Up to 1, inclusive	± 0.030
Over 1 to 10, inclusive	± 0.050
Over 10	± 0.100

3.4 Coating

Foams which are to receive coatings of additional materials, as specified on the purchase order, shall be identified by lot and sample number prior to application of the coating. The coating pickup weight shall be reported for each individual sample. The coating procedure and the calcining temperature-time data shall be recorded in the manufacturer's notebooks, along with the sample identification numbers for future reference.

The coating material shall not plug more than five (5) percent of the pores nor shall it form membranes across more than five (5) percent of the windows present. The coating shall be uniform throughout the sample. Accumulation of coating material on the perimeter or in the center of the sample must be avoided.

Samples shall under no circumstances be exposed to oil or organic vapors after deposition of the coating.

3.5 Cleanliness

Foam samples shall not be contaminated by oil or loose particles after machining them to size.

4.0 QUALITY PROVISIONS

4.1 Identification and Packaging

The samples shall be individually bagged and identified by lot and sample number for delivery. The samples shall be carefully wrapped and packaged to prevent damage in transport.

4.2 Certification

Each shipment shall be accompanied by a certificate listing the lot and sample number and the required and the actual properties of the samples.

APPENDIX B
TEST RESULTS OF STEADY-STATE REACTOR FIRINGS

REACTOR STEADY-STATE FIRING SUMMARY

Test No.	Foam Type		Ceramic Loading (g/cm^3)	Active Metal in Coating (%)	Test Time (sec)	Bed Loading $\frac{kg}{m^2\text{-sec}}$	Response Time		Tailoff Time	Hardness Ratio $\frac{P_f - P_c}{P_c}$	Nominal Pressure Oscillations $\pm\%$ P_c	c* (m/sec)
	Material	Pore Size (Mils)					Start P_c Rise (ms)	90% P_c (sec)	10% P_c (ms)			
1	Hastelloy X	30	0.059	55.9	500	7.0	150					
2	Hastelloy X	30	0.059	55.9	500	7.0	80					
3	Hastelloy X	30	0.071		500	7.0	40					
4	Hastelloy X	30	0.071		500	7.0	200					
5	Molybdenum	20	0.149		500	7.0	35					
6	Molybdenum	20	0.149		500	7.0	80					
7	Tungsten	30	0.067	46.6	5	N.A.	360					
8	Tungsten	30	0.067	46.6	0	N.A.						
9	Tungsten	20	0.711	17.01	300	7.0	60					
10	Tungsten	30	0.13	26.3	15	N.A.	80					
11	Tungsten	30	0.318	22.1	500	6.3	40					
12	↓	↓	↓	↓	100	7.0	80					
13	↓	↓	↓	↓	100	6.3	100					
14	↓	↓	↓	↓	35	7.0	200					
15	Tungsten	30	0.318	22.1	35	6.3	200					
16	Hastelloy X	20	0.375	31.95	200	N.A.	47	44.85		1.5	7	1,254
17	Hastelloy X	20	0.36	31.30	150	7.0	59	3.75	143	1.6	5	1,224
18	Hastelloy X	20	0.36	31.30	100	7.0	72	23.00	157	1.7	2	1,213
21	Hastelloy X	20	0.19	28.99	100	7.0	82	.71	375	1.6	2	1,185
22	Hastelloy X	20	0.23	19.23	100	7.0	60	.95	233	1.8	7	1,148
23	Hastelloy X	20	0.25	29.28	100	7.0	82	.83	190	1.6	1	1,227
24	↓	↓	↓	↓	100	7.0	63	.75	164	1.6	2	1,233
25	↓	↓	↓	↓	500	7.0	67	.70	202	1.6	3	1,230
26	↓	↓	↓	↓	500	7.0	48	.81	219	1.6	3	1,251
27	Hastelloy X	20	0.25	29.28	500	6.3	55	.84	215	1.6	2	1,269
28	Hastelloy X	20	0.22	37.84	100	13.7	30	.34	153	0.7	1	1,186
29	↓	↓	↓	↓	100	N.A.	47	.84	227	1.4	2	1,181
30	↓	↓	↓	↓	100	9.7	61	.77	190	1.6	2	1,182
31	↓	↓	↓	↓	100	9.5	79	.84	207	1.5	2	1,180
32	↓	↓	↓	↓	100	9.3	67	.67	244	1.6	1	1,159

Brackets after test number indicate repeat firings using same catalyst sample.

REACTOR STEADY-STATE FIRING SUMMARY

Test No.	Foam Type: Material	Foam Type: Pore Size (Mils)	Ceramic Loading (g/cm^3)	Active Metal in Coating (%)	Test Time (sec)	Bed Loading $\frac{kg}{m^2\text{-sec}}$	Response Time: Start P_c Rise (ms)	Response Time: 90% P_c (sec)	Tailoff Time: 10% P_c (ms)	Hardness Ratio $\frac{P_f - P_c}{P_c}$	Nominal Pressure Oscillations ±% P_c	c* (m/sec)
33	Hastelloy X	20	0.22	37.84	100	9.3	67	.64	206	1.6	2	1,183
34	↓	↓	↓	↓	100	9.2	77	.82	188	1.5	2	1,226
35	↓	↓	↓	↓	100	9.2	94	.78	196	1.4	0.5	1,228
36	↓	↓	↓	↓	100	9.0	53	.95	174	1.4	1	1,185
37	Hastelloy X	20	0.22	37.84	100	7.4	88	1.07	87	1.9	1	1,202
38	Tungsten	20	0.27	28.75	100	14.3	50	1.17	603	0.7	6	1,224
39	↓	↓	↓	↓	500	12.9	207	.81	1,360	0.5	19	1,238
40	↓	↓	↓	↓	100	N.A.	65	.93	--	0.5	26	1,225
42	Hastelloy X	10	0.41	36.13	500	N.A.	24	1.11	1,133	0.7	2	1,198
43	(Composite	20	0.23	37.10	500	N.A.	38	.71	560	↓	1	1,207
44	Bed) ↓	↓	↓	↓	515	N.A.	63	.64	737	↓	1	1,203
45	↓	↓	↓	↓	500	N.A.	50	.77	640	↓	1	1,237
46	↓	↓	↓	↓	500	N.A.	45	.75	698	↓	1	1,156
47	↓	↓	↓	↓	500	13.0	45	.83	570	↓	1	1,194
48	↓	↓	↓	↓	500	13.0	46	.90	1,274	0.7	2	1,193
49	Hastelloy X	20	0.23	37.10	500	13.0	62	.96	1,070	0.8	2	1,185
50	Tungsten	20	0.26	29.53	500	13.2	55	2.74	1,748	0.7	3	1,159
51	Tungsten	20	0.26	29.53	55	13.7	48	1.81	1,614	0.8	23	1,052
52	Tungsten	30	0.21	34.04	150	N.A.	62	1,840	--	0.71	33	1,157
53	Hastelloy X	20	0.30	34.03	500	13.2	243	.47	245	1.1	2	916
54	↓	↓	↓	↓	100	12.7	122	.81	795	1.2	2	915
55	↓	↓	↓	↓	100	12.7	170	.77	870	1.2	2	908
56	↓	↓	↓	↓	100	N.A.	428	.67	710	0.6	1	--
57	Hastelloy X	10	0.446	33.10	100	N.A.	36	.96	693	0.7	1	1,198
58	Hastelloy X	10	0.535	35.85	100	12.8	30	1.12	--	0.7	2	1,226
59	Tungsten	20	0.261	35.79	100	13.2	31	1.00	830	0.6	2	1,225
60	Tungsten	20	0.261	35.79	100	12.8	51	.99	742	0.6	2	1,246

Brackets after test number indicate repeat firings using same catalyst sample.

REACTOR STEADY-STATE FIRING SUMMARY

Test No.	Foam Type		Ceramic Loading (g/cm^3)	Active Metal in Coating (%)	Test Time (sec)	Bed Loading $\frac{kg}{m^2 sec}$	Response Time		Tailoff Time	Hardness Ratio $\frac{P_f - P_c}{P_c}$	Nominal Pressure Oscillations ±% P_c	c* (m/sec)
	Material	Pore Size (Mils)					Start P_c Rise (ms)	90% P_c (sec)	10% P_c (ms)			
61	Tungsten	20	0.292	34.02	500	N.A.	37	2.00	1,780	0.9	1	--
62					500	11.3	18	1.42	--	0.8	1	1,257
63					500	10.6	38	1.72	1,270	1.0	1	1,193
64					500	11.1	18	1.51	--	0.9	1	1,255
65					500	10.5	20	1.57	--	0.9	1	1,206
66					500	10.5	30	1.46	790	0.9	1	1,244
67					500	10.5	32	1.35	1,130	0.9	1	1,179
68					500	10.9	70	1.41	920	0.9	2	1,250
69					500	10.9	60	1.32	--	0.9	3	1,250
70					500	10.9	49	1.18	775	0.9	3	1,233
71					100	10.9	50	1.20	--	0.9	3	1,241
72					500	9.1	62	1.18	965	1.3	3	1,260
73					500	9.2	45	1.60	1,370	1.3	3	1,250
74					500	9.2	49	1.50	--	1.2	3	1,255
75					500	9.2	50	1.79	152	1.2	2	1,259
76					500	9.5	82	1.95	910	1.2	2	1,256
77	Tungsten	20	0.292	34.02	100	7.6	79	1.15	--	1.8	2	1,215
78	Tungsten	10	0.366	36.4	200	5.1	65	3.75	N.A.	2.1	3	1,191
79		10	0.366	36.4	200	4.9	60	2.90	1,702	2.1	1	1,170
80		10	0.366	36.4	073.9	10.7	50	0.62	1,040	0.3	11	1,161
81		10	0.272	39.9	120	9.1	100	1.33	655	0.9	8	1,200
82		10	0.504	35.1	500	6.2	110	2.02	1,128	1.2	5	1,255
83		10	0.504	35.1	430	8.2	N.A.	N.A.	N.A.	0.9	37	1,240
84	Tungsten	20	0.517	34.0	500	N.A.	50	1.75	560	1.4	6	N.A.
85			0.517	34.0	500	8.7	153	5.13	1,008	0.8	7	1,223
86			0.517	34.0	500	8.7	43	2.69	919	0.8	5	1,170
87			0.517	34.0	500	8.6	61	3.28	777	0.8	9	1,201
88			0.517	34.0	500	8.7	69	2.83	1,700	0.8	6	1,205
89			0.517	34.0	500	8.6	104	3.29	1,547	0.8	6	1,200

Brackets after test number indicate repeat firings using same catalyst sample.

REACTOR STEADY-STATE FIRING SUMMARY

Test No.	Foam Type: Material	Foam Type: Pore Size (Mils)	Ceramic Loading (g/cm^3)	Active Metal in Coating (%)	Test Time (sec)	Bed Loading kg / (m^2-sec)	Response Time: Start P_c Rise (ms)	Response Time: 90% P_c (sec)	Tailoff Time: 10% P_c (ms)	Hardness Ratio $\frac{P_f - P_c}{P_c}$	Nominal Pressure Oscillations ±% P_c	c* (m/sec)
90	Tungsten	20	0.517	34.0	N.A.	N.A.	N.A.	N.A.	N.A.	N.A.	N.A.	N.A.
91	↓	↓	0.517	34.0	50	N.A.	N.A.	3.414	624	4.4	N.A.	N.A.
92	↓	↓	0.517	34.0	200	8.6	46	3.12	1,908	0.8	10	1,259
93	↓	↓	0.517	34.0	100	8.6	29	1.69	6,196	0.8	6	1,217
94	↓	↓	0.517	34.0	100	8.7	46	2.00	750	0.8	4	1,197
95	↓	20	0.517	34.0	100	8.7	38	6.21	1,254	0.8	6	1,227
100	Tungsten	20	0.446	34.6	500	8.7	34	1.56	2,010	0.7	5	1,278
101	↓	↓	0.446	34.6	500	8.8	38	2.59	1,770	0.7	4	1,283
102	↓	↓	0.446	34.6	500	8.8	33	3.17	N.A.	0.7	4	1,286
103	↓	↓	0.446	34.6	500	8.8	30	2.52	1,195	0.7	4	1,284
104	↓	↓	0.446	34.6	500	8.8	35	2.45	537	0.7	5	1,272
110	↓	20	0.446	34.6	100	8.8	33	1.91	745	0.7	4	1,230
111	Tungsten	10	0.446	33.4	500	9.2	35	N.A.	70	0.6	8	1,037
112	↓	10	0.446	33.4	232	9.2	36	N.A.	1,200	1.2	7	1,040
113	Tungsten	10	0.446	33.4	255	9.5	40	N.A.	1,250	1.2	5	944
114	Tungsten	10	0.456	33.0	197	8.7	32	N.A.	1,100	N.A.	4	1,188
116	↓	↓	0.456	33.0	500	9.4	36	5,667	880	1.2	2	903
117	↓	↓	0.456	33.0	500	8.6	41	11,498.00	1,013	1.2	9	950
118	↓	↓	0.456	33.0	500	9.2	40	N.A.	819	1.2	2	920
121	↓	↓	0.456	33.0	500	9.5	43	2,250	780	1.5	4	900
122	Tungsten	10	0.456	33.0	200	8.7	75	7,350	814	1.0	4	1,030
126	Hastelloy	10	0.40	35.7	100	10.2	160	2,028	1,038	1.0	2	1,204
	(Composite	20	0.22	38.6								
127	Bed)				100	10.4	101	1,388	1,351	1.2	6	1,107
129	Tungsten	20	0.27	34.8	100	10.6	43	1.44	598	0.6	33	1,151
130	Tungsten	20	0.27	34.8	40	9.8	47	.97	373	0.8	21	1,198
131	Tungsten	20	0.343	32.3	300	8.4	29	1.29	1,242	0.3	5	1,186
132	↓	↓	↓	↓	100	7.7	44	1.18	1,099	0.5	4	1,164
133	↓	↓	↓	↓	200	8.4	29	1.32	1,173	1.1	5	1,195
134	↓	↓	↓	↓	200	7.0	54	.51	174	1.0	5	1,323
135	Tungsten	20	0.27	47.9	300	8.8	18	1.69	1,043	1.0	11	1,161

Brackets after test number indicate repeat firings using same catalyst sample.

REACTOR STEADY-STATE FIRING SUMMARY

Test No.	Foam Type: Material	Foam Type: Pore Size (Mils)	Ceramic Loading (g/cm^3)	Active Metal in Coating (%)	Test Time (sec)	Bed Loading $\frac{kg}{m^2 sec}$	Response Time: Start P_c Rise (ms)	Response Time: 90% P_c (sec)	Tailoff Time: 10% P_c (ms)	Hardness Ratio $\frac{P_f - P_c}{P_c}$	Nominal Pressure Oscillations ±% P_c	c* (m/sec)
136	Tungsten	20	0.343	32.3	250	8.4	27	.25	85	0.4	25	1,282
137	Tungsten	20	0.343	32.3	120	8.4	30	.95	68	0.8	30	1,166
139**	Tungsten	20	0.316	33.2	500	8.5	36	1.74	736	0.6	12	1,213
140	↓		0.315	31.1	140	8.3	90	.88	1,600	0.6	10	1,237
141					170	8.3	60	N.D.	720	0.7	5	1,204
142					400	8.3	20	N.D.	850	0.6	6	1,201
143	Tungsten	20	0.17	31.7	300	5.7	N.A.	N.A.	100	0.3	9	1,252
147	Tungsten	20	0.304	30.7	60	5.0	60	1.13	160	1.1	2	1,240
149	Tungsten	20	0.304	30.7	60	4.9	80	1.20	150	1.1	3	1,279
155	Shell 405	COMPARISON TEST			100	5.1	25	2.30	90	1.0	3	1,255
156	Tungsten	20	0.328	48	60	5.1	30	1.20	120	0.97	4	1,230
158	Tungsten	10	0.352	30.1	43	5.0	50	1.70	60	0.98	64	1,240
159	Tungsten	20	0.350	32.3	60	3.4	60	3.50	270	0.91	10	1,152
161	Tungsten	20	0.326	49	60	3.3	50	1.90	225	1.01	13	1,143
163	Tungsten	20	0.326	49	100	3.4	60	4.70	160	0.96	7	1,165
164	Tungsten	10	0.334	29.9	60	3.5	50	2.20	140	1.56	78	904
167	Tungsten	10	0.334	29.9	100	3.5	70	1.50	160	1.04	25	1,115
168	Tungsten	10	0.332	32.9	60	7.5	50	4.30	130	1.28	2	1,230
170	Tungsten	10	0.332	32.9	500	7.5	60	5.60	114	1.18	6	1,255
172	Tungsten	10	0.332	32.9	60	7.4	60	5.00	138	1.28	7	1,245
173**	Tungsten	20	0.341	33.5	60	5.3	140	5.50	180	0.98	18	1,190

Brackets after test number indicate repeat firings using same catalyst sample.

**Double length catalyst bed used.

APPENDIX C
NOMENCLATURE

NOMENCLATURE

A_c	Chamber area
A_t	Throat area
BET area =	Active surface area determined by the Brunauer-Emmett-Teller method (J. Am. Chem. Soc. 60, 309-19 (1938))
c*	Characteristic velocity = $P_c A_t : \dot{m}$
cal	Calorie, 1 cal = 4.1868 Joule
$\bar{d}$	Mean pore diameter
g_c	Gravitational constant, 9.8066 m/s^2
G	Bed loading, $G = \dot{w}/A$, kg/m^2 s = 703 lb/in^2 s
I_{BIT}	Impulse bit, Ns
kN	Kilonewton, 1 lbf = 0.00448 kN
L_B	Bed length, m
$\dot{m}$	Mass flow rate, kg/s
mesh	Particle size per ASTM E11-61
mm Hg	Millimeter of mercury = $1.333 \cdot 10^2$ N/m^2
N	Newton 1 lbf = 4.448 N
N_{PD}	Pressure drop modules (dimensionless)
N_{Re}	Reynolds number (dimensionless)
mil	1/1000 of an inch = $2.54 \cdot 10^{-5}$ m
P	Pressure, kN/m^2 = 6.894 lbf/in^2 (psi)

P_c	Chamber pressure, kN/m^2
P_f	Feed pressure, kN/m^2
$\dot{w}$	Mass flow rate, kg/s
ζ	Density, g/cm^3 or kg/m^3
μ	Viscosity, Ns/m^2
μm	Micrometer = 10^{-6} m = $3.937 \cdot 10^{-5}$ inch
π	3.1415
ΔP	Pressure drop, kN/m^2

APPENDIX D

DISTRIBUTION LIST

DISTRIBUTION LIST FOR FINAL REPORT
CONTRACT

Copies	Recipient	Designee
	NASA Headquarters Washington, D. C. 20546	
1	Contracting Officer	X
1	Patent Office	X
	NASA Lewis Research Center 21000 Brookpark Rd. Cleveland, Ohio 44135	
1	Office of Technical Information	X
1	Contracting Officer	
1	Patent Office	
	NASA Manned Spacecraft Center Houston, Texas 77058	
1	Office of Technical Information	X
1	Contracting Officer	
1	Patent Office	
	NASA Marshall Space Flight Center Huntsville, Alabama 35812	
2	Office of Technical Information, MS-IP	X
1	Technical Library	X
1	Purchasing Office, PR-EC	
1	Patent Office, M-PAT	
1	Dale Burrows S+E-ASTN-PJ	
1	Technology Utilization Office, MS-T	X
	NASA Ames Research Center Moffet Field, Calif. 94035	
1	Patents and Contracts Management	X
	Jet Propulsion Laboratory 4800 Oak Grove Dr. Pasadena, Calif. 91103	
4	Technical Manager, Mr. W. W. Riebling, 125-224	X

DISTRIBUTION LIST FOR FINAL REPORT (Continued)

Copies	Recipient	Designee
3	Manager, Liquid Rocket Propulsion Tech., Code RPL	X
	or	
3	Manager, Propellant Chemistry and Combustion Technology, Code RPC	
	or	
3	Manager, Space Storage Propulsion Technology, Code RPI Office of Advanced Research and Technology NASA Headquarters Washington, D. C., 20546	
1	Director, Technology Utilization Division Office of Technology Utilization NASA Headquarters Washington, D. C. 20546	X
25	NASA Scientific and Technical Information Facility P. O. Box 33 College Park, Maryland 20740	X
1	Director, Launch Vehicles and Propulsion, SV Office of Space Science and Applications NASA Headquarters Washington, D. C. 20546	X
1	Director, Advanced Manned Missions, MT Office of Manned Space Flight NASA Headquarters Washington, D. C. 20546	X
1	Mission Analysis Division NASA Ames Research Center Moffett Field, California 24035	X
	NASA FIELD CENTERS	
2	Ames Research Center Moffett Field, California 94035	Hans M. Mark
1	Goddard Space Flight Center Greenbelt, Maryland 20771	Merland L. Moseson Code 620

DISTRIBUTION LIST FOR FINAL REPORT (Continued)

NASA FIELD CENTERS (Continued)

Copies	Recipient	Designee
2	Jet Propulsion Laboratory California Institute of Technology 4800 Oak Grove Drive Pasadena, California 91103	Henry Burlage, Jr. Propulsion Div. 38
2	John F. Kennedy Space Center, NASA Cocoa Beach, Florida 32931	Dr. Kurt H. Debus
2	Langley Research Center Langley Station Hampton, Virginia 23365	Ed Cortwright Director
2	Lewis Research Center 21000 Brookpark Road Cleveland, Ohio 44135	Director
2	Marshall Space Flight Center Huntsville, Alabama 35812	Hans G. Paul Code R-P+VED
2	Manned Spacecraft Center Houston, Texas 77058	J. G. Thibodaux, Jr. Chief, Prop. + Power Div. H. Pohl

GOVERNMENT INSTALLATIONS

1	Headquarters, U. S. Air Force Washington 25, D. C. 20546	Col. C. K. Stambaugh AFRST
1	Arnold Engineering Development Center Arnold Air Force Station Tullahoma, Tennessee 37388	Dr. H. K. Doetsch
2	Air Force Rocket Propulsion Laboratory Research and Technology Division Air Force Systems Command Edwards, California 93523	RPRPD/MR. H. Main

DISTRIBUTION LIST FOR FINAL REPORT (Continued)

GOVERNMENT INSTALLATIONS (Continued)

Copies	Recipient	Designee
1	Air Force Missile Test Center Holloman Air Force Base New Mexico 45433	Library
1	Air Force Missile Test Center Patrick Air Force Base, Florida	L. J. Ullian
1	Aeronautical Systems Division Air Force Systems Command Wright-Patterson Air Force Base Dayton, Ohio 45433	D. L. Schmidt Code ASRCNC-2
1	Space and Missile Systems Organization Air Force Unit Post Office Los Angeles 45, California 90045	Col. Clark Technical Data Center
1	Defense Documentation Center Headquarters Cameron Station, Building 5 5010 Duke Street Alexandria, Virginia 22314 Attn: TISIA	
1	Bureau of Naval Weapons Department of the Navy Washington, D. C. 20546	J. Kay RTMS-41
1	U. S. Naval Ordnance Test Station China Lake California 93557	Code 4562 Chief, Missile Propulsion Div.
1	Picatinny Arsenal Dover, New Jersey 07801	I. Forsten, Chief Liquid Propulsion Laboratory
1	U. S. Army Missile Command Redstone Arsenal Alabama 35809	Dr. Walter Wharton

DISTRIBUTION LIST FOR FINAL REPORT (Continued)

CPIA

Copies	Recipient	Designee
1	Chemical Propulsion Information Agency Applied Physics Laboratory 8621 Georgia Avenue Silver Spring, Maryland 20910	Tom Reedy

INDUSTRY CONTRACTORS

1	Aerojet-General Corporation P. O. Box 296 Azusa, California 91703	W. L. Rogers
1	Aerojet-General Corporation P. O. Box 1947 Technical Library, Bldg. 2015, Dept. 2410 Sacramento, California 95809	R. Stiff
1	Aerojet-General Corporation Space Division 9200 East Flair Dr. El Monte, California 91734	S. Machlawski
1	Aerospace Corporation 2400 East El Segundo Boulevard P. O. Box 95085 Los Angeles, California 90045	John G. Wilder MS-2293
1	AVCO Systems Division Wilmington, Massachusetts	Howard B. Winkler
1	Beech Aircraft Corporation Boulder Division Box 631 Boulder, Colorado	J. H. Rodgers
1	Bell Aerosystems Company P. O. Box 1 Buffalo, New York 14240	W. M. Smith

DISTRIBUTION LIST FOR FINAL REPORT (Continued)

INDUSTRY CONTRACTORS (Continued)

Copies	Recipient	Designee
1	Bendix Systems Division Bendix Corporation 3300 Plymouth Road Ann Arbor, Michigan 48105	John M. Brueger
1	Boeing Company P. O. Box 3999 Seattle, Washington 98124	Library
1	Boeing Company P. O. Box 1680 Huntsville, Alabama 35801	Ted Snow
1	Missile Division Chrysler Corporation P. O. Box 2628 Detroit, Michigan 48231	Mr. John Gates
1	Wright Aeronautical Division Curtiss-Wright Corporation Wood-Ridge, New Jersey 07075	G. Kelley
1	Research Center Fairchild Hiller Corporation Germantown, Maryland	Ralph Hall
1	Republic Aviation Corporation Fairchild Hiller Corporation Farmingdale, Long Island, New York	Library
1	General Dynamics, Convair Division P. O. Box 1128 San Diego, California	Library
1	Missile and Space Systems Center General Electric Company Valley Forge Space Technology Center P. O. Box 8555 Philadelphia, Pa.	F. Mezger F. E. Schultz

DISTRIBUTION LIST FOR FINAL REPORT (Continued)

INDUSTRY CONTRACTORS (Continued)

Copies	Recipient	Designee
1	Grumman Aircraft Engineering Corp. Bethpage, Long Island New York 11714	Joseph Gavin
1	Honeywell, Inc. Aerospace Division 2600 Ridgway Rd. Minneapolis, Minn.	Mr. Gordon Harms
1	Hughes Aircraft Co. Aerospace Group Centinela and Teale Streets Culver City, California 90230	E. H. Meier V. P. and Div. Mgr., Research + Dev. Div.
1	Walter Kidde and Company, Inc. Aerospace Operations 567 Main Street Belleville, New Jersey	R. J. Hanville Dir. of Research Engr.
1	Ling-Temco-Vought Corporation P. O. Box 5907 Dallas, Texas, 75222	Library
1	Arthur D. Little, Inc. 20 Acorn Park Cambridge, Massachusetts 02140	Library
1	Lockheed Missiles and Space Co. Attn. Technical Information Center P. O. Box 504 Sunnyvale, California 94088	J. Guill
1	Lockheed Propulsion Company P. O. Box 111 Redlands, California 92374	Library
1	The Marquardt Corporation 16555 Saticoy Street Van Nuys, Calif. 91409	Library

DISTRIBUTION LIST FOR FINAL REPORT (Continued)

INDUSTRY CONTRACTORS (Continued)

Copies	Recipient	Designee
1	Baltimore Division Martin Marietta Corporation Baltimore, Maryland 21203	Mr. John Calathes (3214)
1	Denver Division Martin Marietta Corporation P. O. Box 179 Denver, Colorado 80201	Dr. Morganthaler A. J. Kullas
1	Orlando Division Martin Marietta Corporation Box 5837 Orlando, Florida	J. Ferm
1	McDonnell-Douglas Corp. P. O. Box 516 Municipal Airport St. Louis, Missouri 63166	R. A. Herzmark
1	Space + Information Systems Division Rockwell International 12214 Lakewood Boulevard Downey, California 90241	Library
1	Rocketdyne (Library 586-306) 6633 Canoga Avenue Canoga Park, Calif. 91304	S. J. Domokos
1	Northrop Space Laboratories 3401 West Broadway Hawthorne, California 90250	Dr. William Howard
1	Aeroneutronic Corporation Philco Corporation Ford Road Newport Beach, California 92663	R. Hoffman

DISTRIBUTION LIST FOR FINAL REPORT (Continued)

INDUSTRY CONTRACTORS (Continued)

Copies	Recipient	Designee
1	Astro-Electronics Division Radio Corporation of America Princeton, New Jersey 08540	Y. Brill
1	Rocket Research York Center Redmond, Washington 98052	F. McCullough, Jr.
1	Scientific Service Bureau Inc. P. O. Box 375 Morrisplains, New Jersey 07950	T. F. Seamans
1	Stanford Research Institute 333 Ravenswood Avenue Menlo Park, California 94025	Dr. Gerald Marksman
1	Sundstrand Aviation 2421 11th Street Rockford, Ill. 61101	R. W. Reynolds
2	Shell Development Company P. O. Box 79090 Houston, Texas 77079	Dr. W. L. Petty
1	TRW Systems Group TRW Incorporated One Space Park Redondo Beach, Calif. 90278	G. W. Elverum
1	Tapco Division 23555 Euclid Avenue Cleveland, Ohio 44117	P. T. Angell
1	Thiokol Chemical Corp. Aerospace Services	Library

DISTRIBUTION LIST FOR FINAL REPORT (Concluded)

INDUSTRY CONTRACTORS (Concluded)

Copies	Recipient	Designee
1	Thiokol Chemical Corporation Huntsville Division Huntsville, Alabama 35807	John Goodloe
1	Research Laboratories United Aircraft Corp. 400 Main Street East Hartford, Conn. 06108	Erle Martin
1	Hamilton Standard Division United Aircraft Corp. Windsor Locks, Conn. 06096	Mr. R. Hatch
1	United Technology Center 587 Methilda Avenue P. O. Box 358 Sunnyvale, California 94088	Dr. David Altman
1	Florida Research And Development Pratt and Whitney Aircraft United Aircraft Corporation P. O. Box 2691 West Palm Beach, Florida 33402	R. J. Coar
1	Vickers, Inc. Box 302 Troy, Michigan Elkton Division Bristol, Pennsylvania	Library